DYNAMICS OF NEUTRALLY BUOYANT INFLATABLE STRUCTURES USED IN SUBMARINE DETECTION

by

ARUN KANTI MISRA

B.Tech. (Hons.), Indian Institute of Technology, Kharagpur, 1969

A THESIS SUBMITTED IN PARTIAL FULFILMENT OF

THE REQUIREMENTS FOR THE DEGREE OF

DOCTOR OF PHILOSOPHY

in the Department

of

Mechanical Engineering

We accept this thesis as conforming to the

required standard

THE UNIVERSITY OF BRITISH COLUMBIA

September, 1974

In presenting this thesis in partial fulfilment of the requirements for an advanced degree at the University of British Columbia, I agree that the Library shall make it freely available for reference and study. I further agree that permission for extensive copying of this thesis for scholarly purposes may be granted by the Head of my Department or by his representatives. It is understood that publication, in part or in whole, or the copying of this thesis for financial gain shall not be allowed without my written permission.

ARUN KANTI MISRA

Department of Mechanical Engineering

The University of British Columbia,
Vancouver, Canada, V6T1W5

Date 9th Oct. 1974

ABSTRACT

The dynamics of a submarine detection system using neutrally buoyant inflated structural members is investigated with mathematical models representing increasing order of complexity. An appreciation of the flexural deflections of a single inflated viscoelastic cylindrical cantilever is first gained using the three parameter solid model. This is followed by its free vibration analysis in the presence of hydrodynamic forces and axial tension arising due to the internal pressure. The approximate solutions of the governing nonlinear, partial differential equation are substantiated through numerical and experimental data. An analysis of dynamical response to the surface wave excitations provides useful design information.

Next, the coupled motion of an array consisting of three legs and a central head is studied. The inplane and out of plane motions, which essentially decouple for small oscillations, are considered separately. Effects of the inflation pressure and inertia parameters on the natural frequencies of the system are examined and the possibility of dynamic instability for certain parametric values established.

The vertical motion of a buoy-cable-array assembly is considered subsequently. The cable is replaced by a spring of equivalent stiffness and the flexural displacements of the legs are superposed on the motion of the central head. The free vibration of the system is studied first and the influence of the important system parameters on the natural frequencies evaluated. The motion excited by a sinusoidal

surface wave is also studied to explore the possibility of reducing the tip displacements.

The dynamics of a buoy-cable-array assembly drifting with a uniform velocity is then investigated. As the motion is rather complex because of the large number of degrees of freedom involved, a relatively simple model is considered to obtain some appreciation of the problem. The oscillations of the buoy and flexibility of the legs are ignored and the cable is represented by two straight lines. The steady state configurations of this system and their dependence on various parameters are examined. The double pendulum type motion of the cable along with the rotational oscillations of the array around the equilibrium positions are studied to obtain preliminary information regarding the stability of the motion. Reduction in the length or diameter of the arms appears to improve the damping rates of the system.

Finally, some of the restrictions inherent in the simplified model are removed. The flexibility of the legs and the tangential drag which were neglected earlier, are taken into account. A more accurate cable configuration is considered to make the model closer to the reality. However, the oscillations of the buoy are again ignored. With this, the steady state configurations of the system are determined around which a linearized perturbation analysis is carried out. Longitudinal and lateral motions essentially decouple for small amplitude motions. Natural frequencies of the system are found by analyzing the resulting eigenvalue problem and the influence of various parameters on the damping of the disturbances examined. As noticed in the rigid array analysis, shorter arm lengths improve the decaying characteristics of the system. But the minimum acceptable length being governed by the signal processing considerations, a compromise is indicated in the design. For given cable and arm lengths, there appears to be an optimum diameter from the stability considerations.

TABLE OF CONTENTS

LIST OF TABLES

LIST OF FIGURES

Figure Page

ACKNOWLEDGEMENT

The author wishes to express his deep gratitude to Dr. V.J. Modi for the guidance given throughout the preparation of this thesis. His help and encouragement have been invaluable.

The investigation reported here was supported by the Defence Research Board of Canada, Grant No. 9550-38.

LIST OF SYMBOLS

$A(\xi,\tau)$	amplitude of vibration of the leg, Equation (2.23)
A_k, B_k	constants, Equation(2.46)
A_{ij}, B_{ij}	coefficients in the eigenvalue expansion of v_i and w_i, respectively, Equation (3.4)
$\bar{A}_i$	equivalent relative velocity, $[\bar{W}_{\ell i} - (\bar{W}_{\ell i} \cdot \bar{e}_{ti})\bar{e}_{ti}]$; $i = 1,2,3$
$C_d, C_{db}, C_{dc}, C_{dh}$	drag coefficients of the leg, buoy, cable and head, respectively
$C_m, C_{mb}, C_{mc}, C_{mh}$	added inertia coefficients of the leg, buoy, cable and head, respectively
C_N, C_T	normal and tangential drag coefficients of the leg, respectively
C_{Nc}, C_{Tc}	normal and tangential drag coefficients of the cable, respectively
C_N^*	equivalent normal drag coefficient of the array, Equation (6.19h)
C_{ki}	coefficients in the eigenfunction expansion of $\frac{d^2\Phi_k}{d\xi^2}$, Equation (2.47)
E	Young's modulus
E_1, E_2, ν_2	three parameters of viscoelastic solid
$E^*(\omega)$	complex modulus
F	tip load
F_H	total hydrodynamic force acting on an element of a cylinder, Equation (2.14b)

F_N, F_T	normal and tangential hydrodynamic forces
F_a	axial tension
F_b, F_h, F_i	total hydrodynamic forces on the buoy, head and i^{th} leg, respectively; i=1,2,3
$\bar{F}_{ia}$	axial force acting on an element of the i^{th} leg; i=1,2,3
$\bar{F}_{Nc}, \bar{F}_{Tc}$	normal and tangential components of the hydrodynamic drag on the cable, respectively
$\bar{F}_{Ncj}, \bar{F}_{Tcj}$	normal and tangential components of the hydrodynamic drag on the j^{th} part of the cable, respectively; j=1,2
$\bar{F}_{iN}, \bar{F}_{iT}$	normal and tangential components of the hydrodynamic drag on the i^{th} leg, respectively; i=1,2,3
H	depth of the central head below the water surface
I	moment of inertia of the cross-section of a leg
I_i	$2\pi(i-1)/3$; i=1,2,3
I_x^*, I_y^*, I_z^*	dimensionless apparent moments of inertia of the central head, Equation (3.15b)
$J(t), J_s(t)$	creep compliances in tension and shear, respectively
K_r	normalizing multiplier, Equation (2.18b)
L, L_c	lengths of the leg and cable, respectively
L_1, L_2	lengths of the two linear parts of the cable
P	pressure parameter, Equation (2.15)
$\bar{P}$	weighted pressure parameter, Equation (4.10)
Q_k	nonconservative generalized forces corresponding to the generalized coordinates q_k,($q_k \equiv \phi,\theta,\psi,A_{ij},B_{ij}$, $z_b,z_h,\beta_1,\beta_2,\beta_h,G_h,\varepsilon_h,k_h$)

Q'_k	contribution of the follower forces to Q_k
Q''_k	contribution of the hydrodynamic forces to Q_k
$\hat{Q}_k$	density of the nonconservative generalized forces, $q_k \equiv v_k, w_k$; $k = 1,2,3$
$\bar{Q}_k$	dimensionless generalized forces arising due to the nonconservative forces, $q_k \equiv \beta_1, \beta_2$
Q^*_k	dimensionless generalized forces arising due to both the conservative and nonconservative forces, $q_k \equiv \beta_h$, $G_h, \varepsilon_h, k_h, \eta_i, \zeta_i, \psi, \theta$
R	length to diameter ratio of each leg, L/d
R_d	ratio of the diameters of the cable and leg, d_c/d
R_j	ratio of the length of the j^{th} portion of the cable to that of the leg, L_j/L; $j = 1,2$
R_ℓ	ratio of the lengths of the cable and leg, L_c/L
R_ρ	density ratio, ρ_c/ρ_w
Re	Reynold's number
S, S_b, S_h	areas of cross-section of the leg, buoy and head, respectively
T	kinetic energy
T_a, T_c, T_h	kinetic energy of the array, cable and head, respectively
$\hat{T}$	kinetic energy density
$\bar{T}$	period of the wave
U	potential energy
U_e, U_g	elastic and gravitational potential energy, respectively
$\hat{U}$	potential energy density

V	velocity of drifting
V_h	velocity of the head
$V_{hx_0}, V_{hy_0}, V_{hz_0}$	components of V_h along x_0, y_0, z_0 axes, respectively
V_m	maximum velocity
$\bar{W}_c, \bar{W}_{cj}, \bar{W}_{\ell i}$	relative velocity of the cable, j^{th} portion of the cable and i^{th} leg, with respect to the fluid, respectively
a, a_b, a_h	added inertia of the leg, buoy and head, respectively
a_{ij}, b_{ij}	coefficients in the eigenfunction expansion of η_i and ζ_i, respectively
$\bar{a}_i$	dimensionless equivalent relative velocity, $\bar{A}_i/V$
$b_r(\xi)$	coefficient of α^r, Equation (2.27)
c	equivalent stiffness due to the buoyancy
d, d_c	diameter of each leg and the cable, respectively
$\bar{e}_{tc}, \bar{e}_{tcj}, \bar{e}_{ti}$	unit tangential vector of an element of the cable, j^{th} part of the cable and i^{th} leg, respectively
$\bar{e}_{nc}, \bar{e}_{pc}$	unit normal and binormal vector of an element of the cable, respectively
f, f_b, f_h	coefficients of forcing functions in the vertical motion of the system, Equation (4.10)
g	acceleration due to gravity
h	wall thickness of each leg
$\bar{i}, \bar{j}, \bar{k}$	unit vectors along x_0, y_0, z_0 axes, respectively
k	equivalent spring stiffness of the cable

m, m_b, m_c, m_{cj}, m_h	mass of each leg, the buoy, cable, j^{th} portion of the cable and head, respectively
m_T, m_{ca}	apparent mass of the array and cable, respectively
p	internal pressure
q_k	generalized coordinate
δq_k	perturbations of q_k, ($q_k \equiv \psi, \theta, \beta_h, G_h, \varepsilon_h, k_h, \eta_i, \zeta_i$)
r_1	$2\{(R_1+R_2)/10\}^2/\pi(1+C_m)$
$r_{h\ell}, r_{b\ell}, r_{c\ell}, r_{ch}$	inertia parameters, Equations (3.15a), (4.10), (5.12e)
r_{hd}	dimensionless weight of the head, $2m_h g/\rho_w V^2 Ld$
$\bar{r}_c, \bar{r}_h, \bar{r}_i$	position vector of an element of the cable, centre of mass of the head and an element of the i^{th} leg, with respect to the inertial co-ordinate system, respectively
s	distance of an element along the cable from the centre of mass of the head
s_j	distance of an element of the j^{th} portion of the cable from the hinge
t	time
$\tilde{t}$	dimensionless time, Equation (2.27)
$u_{hx_0}, u_{hy_0}, u_{hz_0}$	components of the dimensionless velocity of the central head along x_0, y_0, z_0 axes, respectively, $u_{hj} = V_{hj}/V$; $j \equiv x_0, y_0, z_0$
$\bar{u}_x, \bar{u}_y, \bar{u}_z$	unit vectors along x, y, z axes, respectively
v_i, w_i	inplane and out of plane flexural displacements of an element of the i^{th} leg
w	flexural displacement of an element of a cylindrical cantilever
$w_{v.e.}$	viscoelastic displacement

x, y, z	body co-ordinate axes
x_0, y_0, z_0	inertial co-ordinate axes
x_1, y_1, z_1	co-ordinate axes with the origin located at the centre of the head, parallel to the inertial system
x_{1b}, y_{1b}, z_{1b}	co-ordinates of the buoy in x_1, y_1, z_1 system
z_b, z_h	vertical displacements of the buoy and head, respectively
z_w, z_{wh}, z_{wi}	displacement of a water particle at the buoy, central head and a point on the i^{th} leg, due to the ocean waves, respectively
$\Phi_i(\xi)$	eigenfunctions of a cantilever without axial force
$\Psi_i(\xi)$	eigenfunctions of a cantilever with axial force, Equation (2.18)
Ω_j	dimensionless j^{th} natural frequency of each leg, $j=1,2,\cdots\infty$
$\bar{\Omega}$	square root of the ratio of the stiffness of the spring to that due to the buoyancy, $\sqrt{k/c}$
$\alpha, \alpha_b, \alpha_h$	damping parameter of each leg, the buoy and head, respectively, Equations (2.16b), (4.10)
β, ε	angles defining the orientation of a cable element, Figure 6-1
β_1, β_2	inclinations of the double pendulum to the vertical, Figure 5-1
$\beta_h, G_h, \varepsilon_h, k_h$	variables defining the orientation of the cable, Equation (6.10)
β_{irs}	constant, Equation (2.33b)

$\gamma(\omega)$	nondimensional viscoelastic damping coefficient, measure of energy loss in the structure
δ_ℓ	tip deflection
δ_m	constant, $2\sigma_m/\mu_m$; $m = 1,2,\cdots\infty$
δ_{ij}	deflection at station i due to the load at station j
η	dimensionless displacement, w/d
η_0	amplitude of η
η_b,η_h	dimensionless vertical displacements of the buoy and head, respectively
η_s,η_c,η_{bs} $\eta_{bc},\eta_{hs},\eta_{hc}$	sine and cosine components of η,η_b and η_h, respectively
η_i,ζ_i	dimensionless inplane and out of plane flexural displacements of an element of the i^{th} leg, respectively
$\eta_w,\eta_{wh},\eta_{wi}$	dimensionless displacements of a water particle at the buoy, central head and a point on the i^{th} leg, due to the ocean waves, respectively
λ_j	j^{th} eigenvalue
λ_i^*	principal stretches, i=1,2,3
μ	modulus of rigidity
μ_r	eigenvalues of a cantilever
μ_r',μ_r''	functions of μ_r, Equation (2.19)
ξ	dimensionless distance from the fixed end of a cantilever
ρ_w,ρ_c	densities of water and the cable, respectively
σ_r	functions of μ_r,μ_r' and μ_r'', Equation (2.19c)

σ_{ij}	stress tensor
τ	dimensionless time
ϕ, θ, ψ	Eulerian rotations
$\phi_0, \phi_1, \phi_{-1}$	scalar functions of principal stretches, Equation (2.3)
ψ_i	inclination of the i^{th} leg to the projected direction of flow in the plane of the array
ω	frequency

Dots and primes indicate differentiation with respect to t and τ, respectively. The subscript 0 indicates steady state configurations.

1. INTRODUCTION

1.1 Preliminary Remarks

In recent years foldable or inflatable structures have gained much prominence because of their compactness and light weight. They find a variety of applications primarily requiring transportation of deployable systems, in a concise form, to their destinations. Inflated cylindrical structures have been suggested for fuselage and satellite appendages while inflated plates may form the wings of re-entry gliders and control surfaces of satellites. An interesting discussion on applications of inflatable structures for space explorations is given by Brauer[1]. As regards the underwater applications, neutrally buoyant inflated structures have been proposed for several missions like submarine detection, oceanographic survey, lifting surfaces of hydrofoil type vehicles, etc. Consider, for example, the problem of patrolling of submarines. It is currently undertaken in various ways, such as:

(i) long range patrol aircraft equipped with radar which can detect the surfaced or snorkeling subs;

(ii) turnstiles placed across the various gateways to the major ocean basins;

(iii) fixed site or towed sonar systems;

(iv) sonobuoys providing platforms for hydrophones and telemetering systems; etc.

Of particular interest is the last option. Sonobuoys are passive listening devices housed usually in a cylindrical container about 3 ft.long and 5 to 6 in. in diameter. The containers are dropped from an aircraft in the area of interest. On hitting the water surface, a hydrophone attached by a cable to the floating container is released. The system transmits all the signals received by the hydrophone back to the aircraft. Theoretically, at least three or four hydrophones are needed to locate an object in two or three dimensions, respectively.

The sonobuoy has a certain lifetime after which it ceases to function and is allowed to sink. It has been established that the efficiency of this operation can be improved considerably by using an array of inflatable tubes, each carrying a hydrophone at one end and joined to a central head, equipped with a pump, at the other (Figure 1-1). The pump pressurizes the tubes with water making them neutrally buoyant. An object can then be located through processing of signals received by the array, provided the position and orientation of the array are known.

As the system under normal operating conditions will be subjected to the ocean currents, waves and other local disturbances, the knowledge of its dynamics is of fundamental importance for evolving suitable design procedures. The analysis of statics and dynamics of such systems employing neutrally buoyant inflated structural members forms the main objective of this thesis.

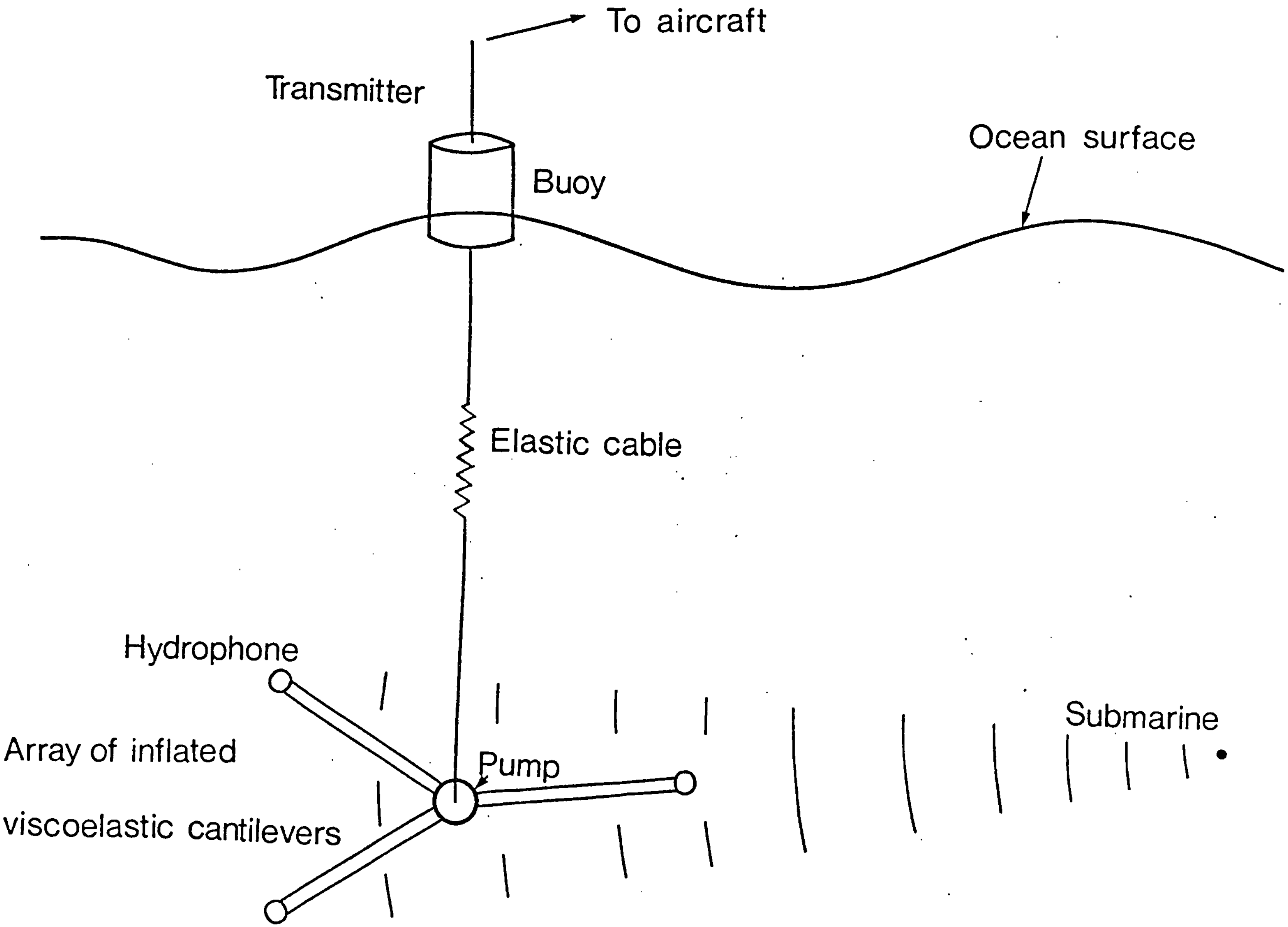

Figure 1-1 Schematic diagram of a submarine detection system using an array of inflated structural members

1.2 Literature Review

The possibility of numerous applications have led to investigations aimed at better understanding the structural behaviour of an inflatable member. A review of the available literature suggests that the interest in the field is of relatively recent origin. There are several studies dealing with inflated membranes having different geometries: plate-like structures, bodies of revolution having cylindrical, spherical or toroidal shapes, etc. The works concerning inflated cylindrical structures are of interest in the present investigation. The buckling and collapse loads for inflated cylindrical cantilever beams were calculated by Leonard, Brooks and McComb[2] using a simple analysis. It was observed that the local buckling starts at the extreme fiber when the compressive stress due to a bending moment just cancels the tensile stress due to the internal pressure. As the load is increased, the wrinkle progresses around the cross-section and the collapse occurs when the wrinkle has progressed all the way to the other extreme. At this point, the resisting "plastic hinge moment" is just exceeded by the moment due to the load. Stein and Hedgepeth[3] considered an inflated circular cylindrical tube carrying a constant moment and obtained a relation between the beam curvature and the moment. Comer and Levy[4] studied the deflection of an inflated elastic cylindrical cantilever beam when the load exceeded the buckling value and obtained the tip deflection and maximum stress. The relation between the shearing stiffness and inflation pressure, accounting for the beam edge effect, has been determined by Topping[5], who concluded that the inflation pressure can be treated as an effective shear modulus. All these investigators observed that the flexural stiffness is essentially independent of the internal pressure. This is true only if the deformations are reasonably small.

Corneliussen and Shield[6] formulated a theory for the finite inflation of a thin membrane composed of homogeneous elastic material and extended it to the case of a small bending deformation superposed on the known finite deformation. Small flexural deformations of a circular cylindrical tube which has been subjected to a finite homogeneous extension and inflation were considered as an example. Later Douglas[7] using a similar theory of incremental deformations, showed how the structural stiffness of an inflated cylindrical cantilever is influenced by large deformations which occur during inflation. The analysis covers a rather wide range of inflation pressures leading to a change in diameter as high as 400%. It was observed that the inflation pressure has a linear relationship with the stretch in diameter only in the early stages of inflation (up to about 40% stretch in diameter or $pd_0/2\mu h_0 \simeq 0.6$). The pure bending deformation of an inflated circular cylindrical membrane of initially isotropic rubbery materials was analyzed by Koga[8]. It was assumed that the cylindrical membrane is inflated into another circular cylinder which is then subjected to small pure bending. The wrinkling of the membrane was also taken into account. All these investigations are limited to the materials which do not exhibit time dependent properties.

The knowledge of the hydrodynamic forces acting on a vibrating cylinder is essential to the study of its dynamics. The forces on cylinders in an oscillating fluid have been measured by Morison et al.[9] and Keulegan and Carpenter[10] while that on a cylinder vibrating in a fluid have been obtained by Laird et al.[11], Bishop and Hassan[12], Toebes and Ramamurthy[13] and Protos et al.[14] All the above investigators measured the total force on the cylinder but followed different procedures for the analysis of the data. For example, Keulegan and Carpenter separated the total resistance into a drag force which is due to the velocity effects and an inertia force caused by the acceleration of the surrounding water and the cylinder, and studied the variation of both inertia coefficient C_m and drag coefficient C_d with period parameter $V_m\bar{T}/d$. On the other hand, Laird et al. assumed C_m to remain constant and included its deviation from the theoretical value in the variation of C_d with Reynold's number. Toebes, Protos and their associates also considered a fixed apparent mass but studied the distribution of the remaining force with the frequency ratio (ratio of the natural frequency of the cylinder to the Strouhal frequency).

Although there is a vast amount of literature on the flexural vibration of a rigid circular cylinder in a fluid, corresponding studies for a flexible cylinder are relatively scarce. Landweber[15,16] and Warnock[17] investigated the dynamics of an elastic cylinder in an incompressible, inviscid fluid to determine the apparent mass effects. But the hydrodynamic damping forces were absent as the flow was considered potential. The flexural vibration of an inflated cylindrical cantilever has been studied by Douglas[18] and Corneliussen and Shield[6] taking into account the change in the flexural rigidity due to inflation. But both the components of the resultant fluid dynamic force, i.e., added inertia and drag were neglected probably because the structure was oscillating in air. The general case of a dissipative system with axial tension arising due to the inflation pressure is yet to be studied.

Under the normal operating conditions the system may drift because of the presence of a current. The equilibrium configurations and dynamical behaviour will be similar to those of a towed vehicle system although the drifting velocity is usually much lower. The towed vehicle problem has been a subject of considerable interest over the last half century. Applications of this system range over a broad spectrum, from the mooring of buoys to the towing of glider aircrafts. Similarly, there is a variety of techniques employed to study these systems -- method of characteristics, linearization procedures, equivalent lumped mass approach, finite element method, etc. A survey of these analytical methods for dynamic simulation of cable-body systems is given by Choo and Casarella[19].

In many applications it is important not only to assess the dynamical stability but also the precise location of the towed body with respect to the towing vehicle and hence the steady state solution. For this, an accurate description of the fluid dynamic loading on a cable inclined to the flow direction is necessary. The forces on a cable element can be resolved into two components F_N and F_T, normal and tangential to the elements, respectively. These were first measured by Relf and Powell[20]. It was observed that the function F_N exhibited a sine square dependence on the angle of attack of the cable. On the other hand, no functional form was suggested by the data for F_T. It was apparent, however, that the magnitude of F_T is generally much smaller than the magnitude of F_N. Subsequent investigators have generally agreed upon the sine square variation for F_N, but have used widely varying forms to describe F_T. Hoerner[21] and Whicker[22] derived theoretical expressions for F_T, the former obtaining a cosine form while the latter, a combination of cosine and cosine square functions. Mustert[23] and Schneider and Nickels[24] have fitted experimental data to a cosine square term. Apparently, no single form for F_T has been universally accepted by researchers working in the area of towed vehicle systems.

Among the early studies of the towing problem, the contribution of Glauert[25,26] is the most significant one. The first of Glauert's papers dealt with the equilibrium configurations and the stability of a towed vehicle system in a uniform flow field. For simplicity, it was assumed that the tangential drag and the mass of the cable can be neglected. Three different problems were considered. The towed body in the first problem was a sphere. The cable was assumed to be in a plane but the entire system underwent a rigid body rotation about the longitudinal axis of the towing vehicle. By considering small oscillations about the equilibrium configuration, it was shown that both longitudinal (in plane) and lateral (side to side) motions were always asymptotically stable. The second problem focused attention on the aerodynamics of the towed body.

Only longitudinal motion in the plane of the cable was considered but the towed body was allowed translational motion as well as rotation about its pitch axis. It was observed that a short towed body and a short towing cable tended to be unstable. The third problem dealt with the lateral stability of the towed body. Glauert's second paper on the subject provided tables and graphs for the computation of two dimensional equilibrium configurations of a heavy flexible cable for specified towed body forces.

During and after the World War II, attention was focused on ways of stabilizing gliders being towed by military aircrafts. Bryant et al.[27], Mitchell and Beach[28], O'Hara[29], Söhne[30] and Shanks[31] represent a few of the numerous investigators who explored the natural frequencies, damping rates and stability criteria for various glider models. The lateral instability observed in the motion of a towed bucket used in the transportation of construction materials by helicopters, was explained by Etkin and Mackworth[32]. While these investigators were interested mainly in the dynamics of towed systems, some others were concerned with obtaining a more accurate description of the steady state configuration. Landweber and Protter[33], including the tangential drag for the first time, gave a series of equations and curves for equilibrium shapes and tensions. However, they neglected the mass of the cable, which was subsequently taken into account by Pode[34].

Recently, attempts have been made to incorporate cable inertia into the dynamical studies of the system. Some of the analyses use the finite element method. In one case, all the forces and masses along the cable were assumed to be concentrated at the nodes, sections between the nodes being considered either inextensible straight lines (Dominguez[35]) or extensible straight springs (Hicks and Clark[36]). In another approach, the segments were taken to be straight, rigid cylinders with universal joints at the junctions (Strandhagen and Thomas[37], Morgan[38], Paul and Soler[39]). Studies by Phillips[40], Whicker[22], Schram[41] and Huffman and Genin[42] have incorporated a continuously distributed cable mass into the dynamical analysis of the towed vehicle system. Phillips analyzed the propagation of disturbances along an inextensible, infinitely long, originally straight cable, and noticed that waves propagating upward from the point of disturbance were always damped while those propagating downward could either be amplified or damped depending on the relative magnitudes of wave velocity and towing speed. As the equations were hyperbolic in nature, Whicker used the method of characteristics to study the two dimensional cable dynamics. Schram extended it to three dimensions. Huffmann and Genin included elasticity into the model to obtain the frequencies of oscillation and damping rates of a heavy elastic cable as functions of towing speeds and cable lengths. The cable was assumed to lie in a plane. While the above investigations, accounting for cable inertia, resorted to numerical techniques, Cannon[43] developed several approximate analytical solutions for three dimensional towing vehicle systems, which gave a better insight into the problem. The vibrational frequencies and damping rates for both lateral and longitudinal motions were determined by using the principle of angular momentum and later by an averaging technique applied to the differential equations.

The emphasis in the above investigations was more on the cable dynamics and not so much on the dynamics of the towed body which was most of the times a rigid body and sometimes even a sphere. The configuration of the towed body, in the submarine detection system under consideration, is not only more complicated than earlier studies but also flexible in character. Thus flexibility of the leg forms an important parameter in the analysis and can affect the stability of the system to a great extent.

1.3 Purpose and Scope of the Investigation

The precise knowledge of stiffness and dynamical characteristics of the inflatable members is a prerequisite to any attempt at a structural design using them. The inflatable members in the present case are generally made of plastic films like polyethylene, mylar, etc., or sandwich materials formed out of them, which exhibit time dependent deformations. This fact has received little attention in the past while studying the flexural deflection of inflated structures. Hence, at first, the static solutions for cylindrical cantilevers are extended to the viscoelastic case for moderately large inflation. This is followed by a free vibration analysis of the cantilevered member in the presence of hydrodynamic drag and a tensile follower force arising due to the internal pressure. The effect of added inertia is also accounted for. The governing equation is studied using two approximate analytical procedures:

mode approximation method and perturbation technique. Subsequently, the dynamical response of a viscoelastic, inflated cantilever to surface wave excitation is investigated.

Next, the coupled motion of the array consisting of three legs and a central head is considered. The effect of the various system parameters on the natural frequencies of the system is studied and the possibility of any dynamic instability examined.

This is followed by the dynamical analysis of the cable-buoy-array assembly. Two situations are considered:

(a) the system at one station undergoing vertical motion;

(b) dynamics of drifting assembly.

For the first case the natural frequencies of free vibration and their dependence on the different system parameters are determined. The steady state response to the surface wave excitation is also investigated. The drifting motion of the system adds to the complexity of the problem because of the large number of degrees of freedom: the spatial motion of the buoy, three dimensional oscillations of the cable, the motion of the array in its own plane and the motion of the plane of the array itself, etc. So to start with, a simplified model is considered where the cable is approximated by two straight lines and the flexural displacements of the legs are ignored. The buoy is assumed to move with a constant velocity and the double pendulum type motion of the system along with the rotational motion of the array investigated. Later, the above assumptions are removed to make the analysis more general. The equilibrium configurations are determined and small oscillations around these equilibrium positions studied. Furthermore, the effects of system parameters on the natural frequencies and damping rates are evaluated.

Figure 1-2 schematically illustrates the plan of study.

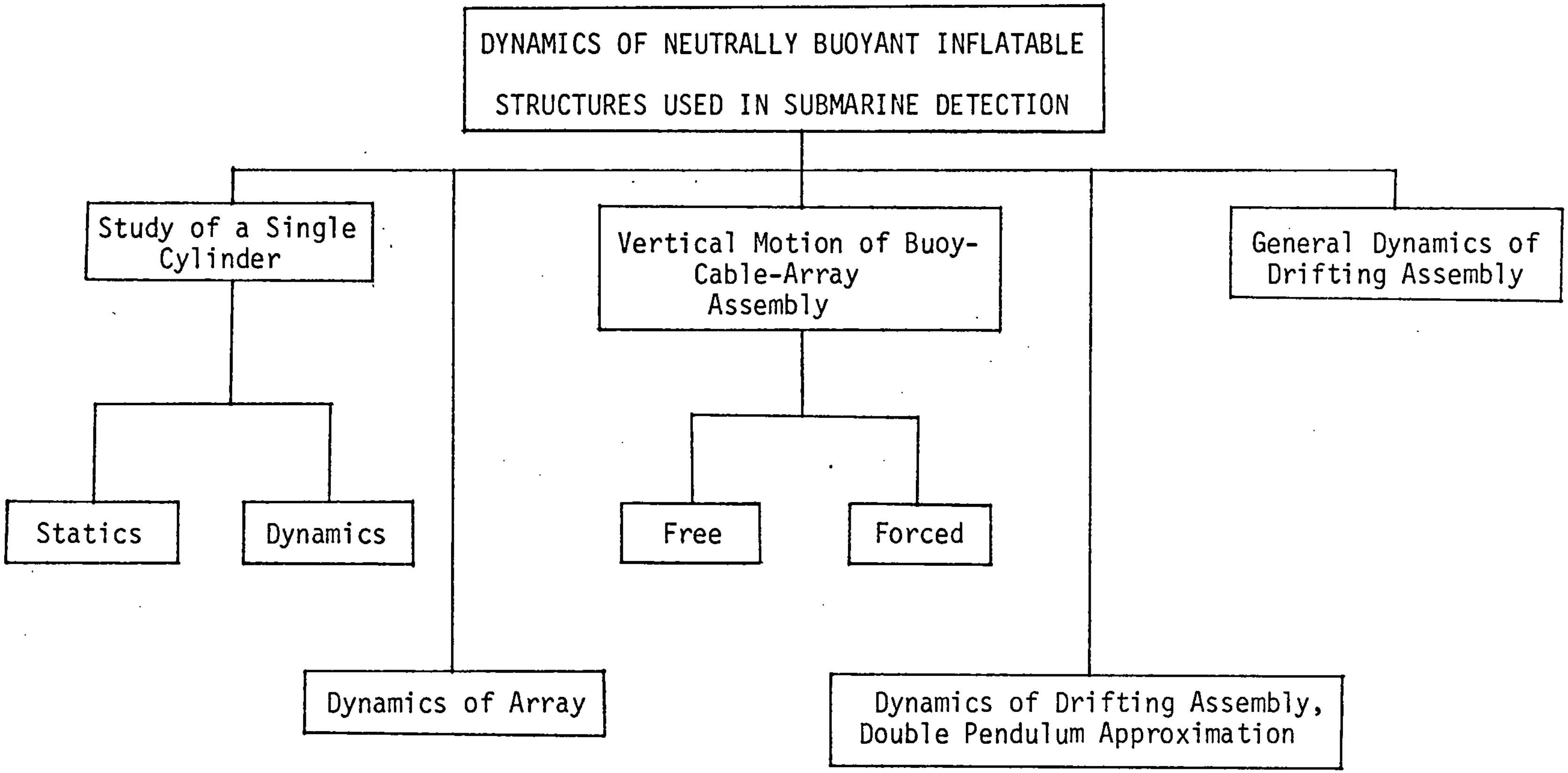

Figure 1-2 Schematic diagram of the proposed plan of study

2. STATICS AND DYNAMICS OF A NEUTRALLY BUOYANT INFLATED VISCOELASTIC CIRCULAR CYLINDRICAL CANTILEVER

This chapter investigates the flexural deformations and vibrations of a neutrally buoyant inflated circular cylindrical cantilever made of materials exhibiting time dependent properties. First, the flexural deflection of the structure is studied using the three parameter solid model in conjunction with the correspondence principle[44]. The analytical procedure is substantiated through an experimental program employing several polyethylene models.

The flexural free vibration of the cylindrical cantilever in the presence of hydrodynamic forces and a tensile follower force due to the inflation pressure is considered next. The governing nonlinear, partial differential equation is studied using two approximate analytical procedures:

(a) mode approximation in conjunction with the Krylov and Bogoliubov method[45], which yields essentially the same results as the first order perturbation;
(b) more precise second order perturbation technique[46].

The validity of the approximate methods is examined by comparing the results with numerical and experimental data.

This is followed by the steady state response analysis of the beam to the surface wave excitation, with the motion of a water particle due to the waves approximated to a sinusoidal function. The information concerning the statics and dynamics of a single cylinder so generated should prove useful during the dynamical study of a more complex submarine detection system.

2.1 Statics

Consider a neutrally buoyant inflated cylindrical cantilever (Figure 2-1a) of initial length L_0, diameter d_0, wall thickness h_0 and internal pressure p. Let the initial dimensions of the cylinder and those at any instant during inflation be related by the principal stretches as follows,

$$L = \overset{*}{\lambda}_1 L_0 \ , \quad d = \overset{*}{\lambda}_2 d_0 \ \text{ and } \ h = \overset{*}{\lambda}_3 h_0 \quad . \tag{2.1}$$

The bulk modulus of most of the materials under consideration is relatively large. The material, therefore, can be assumed to be more or less incompressible. Hence,

$$\overset{*}{\lambda}_1 \overset{*}{\lambda}_2 \overset{*}{\lambda}_3 = 1 \ . \tag{2.2}$$

It can be shown that the principal stresses are given by[7]

$$\sigma_{11} = \phi_0 + \phi_1 \overset{*}{\lambda}{}_1^{2} + \phi_{-1} \overset{*}{\lambda}{}_1^{-2} = pd/4h \ , \tag{2.3a}$$

$$\sigma_{22} = \phi_0 + \phi_1 \overset{*}{\lambda}{}_2^{2} + \phi_{-1} \overset{*}{\lambda}{}_2^{-2} = pd/2h \ , \tag{2.3b}$$

$$\sigma_{33} = \phi_0 + \phi_1 \overset{*}{\lambda}{}_3^{2} + \phi_{-1} \overset{*}{\lambda}{}_3^{-2} = O(p) \ , \tag{2.3c}$$

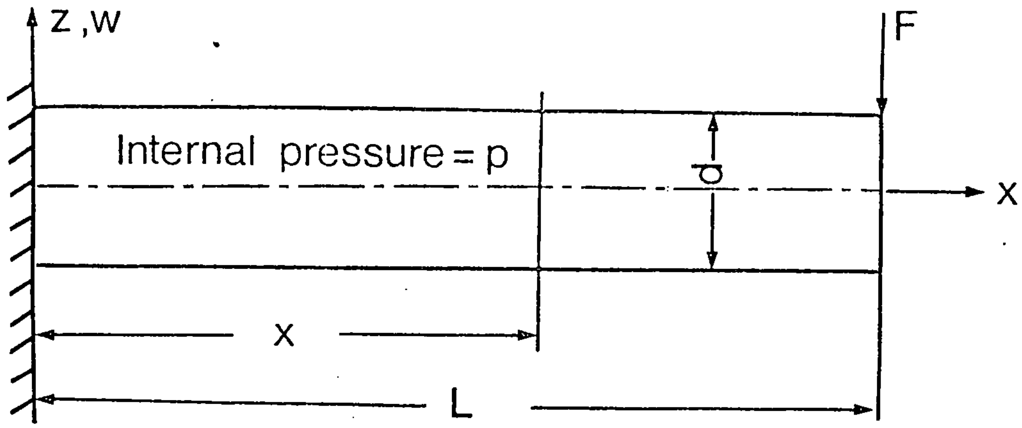

(a)

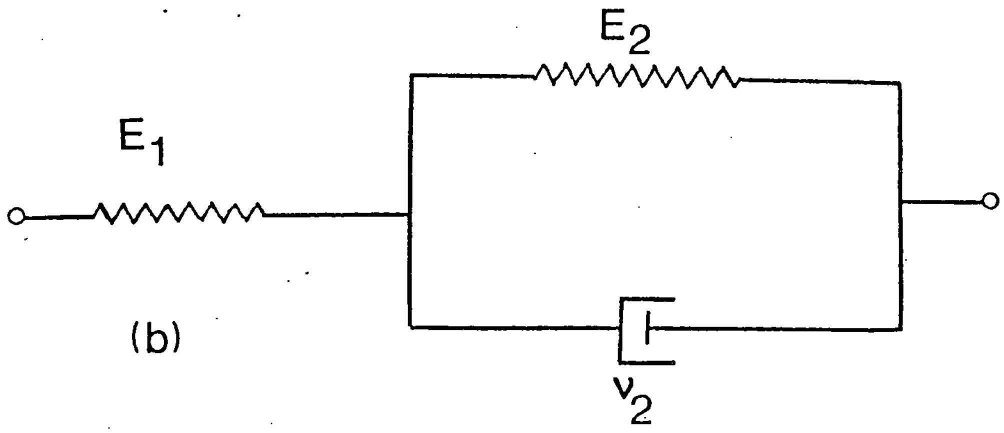

(b)

Figure 2-1 (a) Geometry of flexure of a single cylinder;
(b) Three parameter viscoelastic solid

where ϕ_i are scalar functions of the diagonal stretch matrix. Since σ_{33} is small compared to σ_{11} or σ_{22} (the ratio being of the order of h/d), it may be neglected. With this approximation, one obtains from Equations (2.2) and (2.3),

$$(\lambda_1^{*2}\lambda_2^{*4}-1)(\phi_1-\lambda_1^{*2}\phi_{-1}) = 2(\lambda_1^{*4}\lambda_2^{*2}-1)(\phi_1-\lambda_2^{*2}\phi_{-1}) . \tag{2.4}$$

For a material obeying the Mooney-Rivlin constitutive equations, ϕ_1 and ϕ_{-1} are constants:

$$\phi_1 = \mu(\tfrac{1}{2}+\beta_e) , \tag{2.5a}$$

$$\phi_{-1} = -\mu(\tfrac{1}{2}-\beta_e) , \tag{2.5b}$$

where μ is the shear modulus of the underformed material and β_e is the Mooney-Rivlin elastic coefficient.

It has been found that inflation is independent of β_e for moderate stretches (upto about 40% increase in diameter)[7]. Since in the present case inflation lies within this range, an arbitrary β_e may be assumed to obtain a relation between p and λ_i^* . Choosing $\beta_e = 0$, Equation (2.4) yields

$$\lambda_1^{*2} = 1 , \tag{2.6a}$$

and (2.2) reduces to

$$\lambda_2^* \lambda_3^* = 1 . \tag{2.6b}$$

Above relations together with Equation (2.3) lead to

$$\lambda_2^* = (1-pd_0/2\mu h_0)^{-1/4}$$

$$\simeq 1+pd_0/8\mu h_0 \quad ,$$

since $pd_0/2\mu h_0$ is small compared to unity in the present case. Thus ,

$$d = d_0(1+pd_0/8\mu h_0) \quad . \tag{2.7}$$

In the actual practice, a change in length is small compared to the changes in the diameter and thickness. Hence $\lambda_1^* = 1$, i.e. $\beta_e = 0$, represents a good approximation in evaluating changes in the dimensions due to inflation.

Equation (2.7) suggests that the variation in diameter is proportional to the internal pressure. To account for the time dependent properties of the material, the equation can be modified, approximately, using a concept similar to the correspondence principle to

$$d(t) = d_0[1+pd_0J_s(t)/8h_0] \quad ,$$

where $J_s(t)$ is the creep compliance in shear and p the step pressure applied at t = 0. The diameter after a long time is thus given by

$$d_f = d_0[1+pd_0J_s(\infty)/8h_0] \quad , \tag{2.8a}$$

with the final thickness as

$$h_f = h_0[1-pd_0J_s(\infty)/8h_0] \quad . \tag{2.8b}$$

The cantilever beam is now allowed to undergo bending deformations. It is assumed that there are no wrinkles in the structure. Wrinkles appear as soon as the stress at any point becomes compressive. This implies that the internal pressure is sufficiently large to make the resultant stress tensile everywhere. The elastic solution must be obtained before the viscoelastic one, which is then realized by the correspondence principle. The resultant stress on an element with coordinates (x,y,z) is given by superposing the stresses due to bending and inflation pressure, i.e.,

$$\sigma_{11} = pd_f/4h_f+F(L-x)z/I \quad , \tag{2.9}$$

where F is the load and I the moment of inertia of the cross-section about a transverse axis,

$$I = \pi d_f^3 h_f/8 \ .$$

The curvature is approximately given by

$$\frac{d^2w}{dx^2} = -F(L-x)/EI \quad . \tag{2.10}$$

Integrating and using the boundary conditions at x = 0, lead to

$$w(x) = -(FL^3/6EI)[(x/L)^2(3-x/L)] = W(x)/E \quad . \tag{2.11}$$

If the stress level is not too high, the materials used for inflatable structures behave like a linear viscoelastic solid. In that case a three parameter solid (Figure 2-1b) can represent the material behaviour fairly well since the long time creep is very small. But this is not true if the stress level is high. However, even in that case the creep in the initial stages can be represented fairly well by the above mentioned model.

Applying the correspondence principle,

$$\bar{w}_{v.e.}(x,s) = \bar{w}(x,s)E/s\bar{E}(s) \quad , \tag{2.12}$$

where $\bar{w}_{v.e.}(x,s)$, $\bar{w}(x,s)$ and $\bar{E}(s)$ are the Laplace transforms of the viscoelastic solution, elastic solution and the relaxation modulus of the material, respectively. For a three parameter solid,

$$s\bar{E}(s) = E_1(E_2+\nu_2 s)/(E_1+E_2+\nu_2 s) \quad ,$$

where E_1, E_2 and ν_2 are the three parameters defining the material behaviour. Noting that

$$\bar{w}(x,s) = W(x)/sE \quad ,$$

from (2.12) one obtains

$$\bar{w}_{v.e.}(x,s) \;=\; W(x)(E_1+E_2+\nu_2 s)/E_1(E_2+\nu_2 s)s \quad ,$$

and on inverting,

$$\begin{aligned}\bar{w}_{v.e.}(x,t) \;&=\; W(x)[(1/E_1)+(1/E_2)\{1-\exp\,(-E_2 t/\nu_2)\}] \\ &=\; W(x)J(t) \quad ,\end{aligned} \tag{2.13}$$

where W(x) is given by Equation (2.11) and

$$J(t) \;=\; (1/E_1)+(1/E_2)\{1-\exp(-E_2 t/\nu_2)\} \quad .$$

2.2 Dynamics

2.2.1 Free vibration of an inflated elastic cylindrical cantilever under water

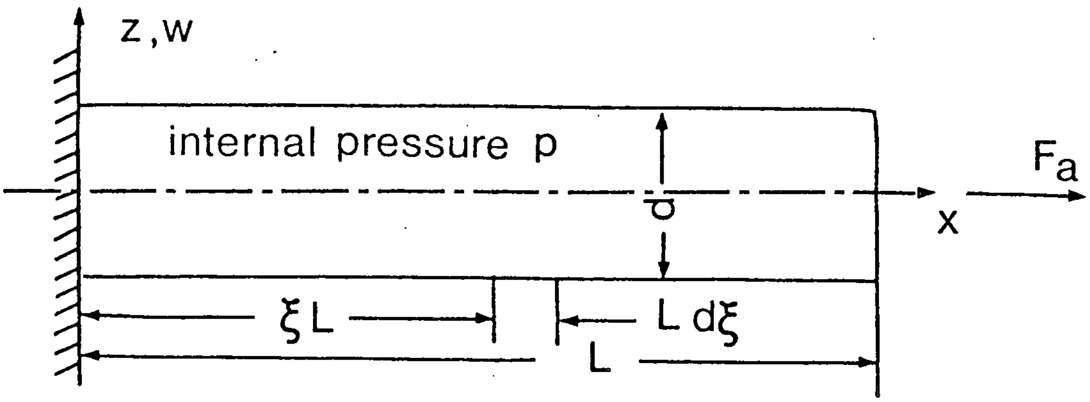

Figure 2-2 Geometry of motion of a single cylinder

Equilibrium of the forces acting on an element of an inflated elastic cylinder (Figure 2-2) oscillating in water leads to

$$EI \frac{\partial^4 w}{\partial x^4} + S\rho_w \frac{\partial^2 w}{\partial t^2} - F_a \frac{\partial^2 w}{\partial x^2} + F_H = 0 \quad , \tag{2.14a}$$

where F_H is the total hydrodynamic force on the element and F_a the axial force due to the inflation pressure. Note that existence of the pressure term is not quite apparent from the elementary beam theory, however, its presence can be explained by the membrane shell theory. It may be noted that the second term representing the inertia force of the element is primarily due to the water inside the structure since the mass of the wall material is very small. The resistance F_H is often separated into a drag force proportional to the square of the velocity and an added inertia force caused by the acceleration of the surrounding water, i.e.,

$$F_H = (1/2)C_d d\rho_w V_{rel}|V_{rel}| + C_m S\rho_w \frac{dV_{rel}}{dt} \quad , \tag{2.14b}$$

where C_d and C_m are the drag and added inertia coefficients, respectively, and V_{rel} the velocity of the element relative to the fluid. This assumes that the drag and the inertia effects are free of appreciable mutual interference. Thus any dynamical study requires the knowledge of the variation of C_d and C_m with flow conditions. The value of C_m as predicted by simple hydrodynamic theory is 1.0 while C_d in the subcritical region is approximately 1.18. More precisely, Keulegan et al.[10] have correlated the variation of C_d and C_m with the period parameter $V_m\bar{T}/d$ where V_m and $\bar{T}$ are the maximum velocity and period of the motion, respectively. (The coefficient C_m in their investigation corresponds to the total inertia force, not the added inertia force, i.e. it exceeds the present coefficient by unity). It was observed that as the period parameter is increased the total inertia coefficient first falls from the theoretical value to a minimum around $V_m\bar{T}/d = 15$ and then gradually increases to a value of 2.5 at $V_m\bar{T}/d = 120$. On the other hand, C_d shows exactly the opposite behaviour. Hence, in general the sum of the two forces deviates relatively less from the theoretical value.

Laird et al.[11] and Toebes et al.[13] assumed a constant C_m thereby including all its deviations from unity in the variation of C_d. The forces on cylinders having constant acceleration or deceleration have been measured by Laird et al. Although C_d was found to change, the variations were not substantial. On the other hand, Toebes et al. determined the hydrodynamic forces on an oscillating cylinder with its axis perpendicular to the mean flow direction. C_d was observed to deviate substantially from the theoretical value if the frequency of vibration was close to the Strouhal frequency. However, the deviations were small for frequencies far from the Strouhal frequency.

In the present analysis, these coefficients C_d and C_m are assumed to be constant and equal to 1.18 and 1.0, respectively.

From Equations (2.14a) and (2.14b),

$$EI\,\frac{\partial^4 w}{\partial x^4} + S\rho_w(1+C_m)\,\frac{\partial^2 w}{\partial t^2} - F_a\,\frac{\partial^2 w}{\partial x^2} + \frac{1}{2}\,C_d d\rho_w\,\frac{\partial w}{\partial t}\left|\frac{\partial w}{\partial t}\right| = 0 \,. \quad (2.14c)$$

Defining

$$\eta = w/d, \qquad \xi = x/L \quad ,$$

$$\tau = [EI/S\rho_w(1+C_m)L^4]^{1/2}t, \quad P = F_a L^2/EI \ , \qquad (2.15)$$

Equation (2.14c) can be nondimensionalized as

$$\frac{\partial^4 \eta}{\partial \xi^4} - P\frac{\partial^2 \eta}{\partial \xi^2} + \frac{\partial^2 \eta}{\partial \tau^2} + \alpha\frac{\partial \eta}{\partial \tau}\left|\frac{\partial \eta}{\partial \tau}\right| = 0 \ , \qquad (2.16a)$$

where

$$\alpha = 2C_d/\pi(C_m + 1) \ . \qquad (2.16b)$$

It may be noticed that the damping parameter α is independent of the geometrical dimensions of the cylinder. The boundary conditions are given by

$$\begin{aligned} \eta(0,\tau) &= \frac{\partial \eta(0,\tau)}{\partial \xi} = \frac{\partial^2 \eta(1,\tau)}{\partial \xi^2} \\ &= \frac{\partial^3 \eta(1,\tau)}{\partial \xi^3} = 0 \ . \end{aligned} \qquad (2.16c)$$

Let the initial conditions be

$$\eta(\xi,0) = A_0(\xi) \quad \text{and} \quad \frac{\partial \eta(\xi,0)}{\partial \tau} = 0 \ . \qquad (2.16d)$$

This is a nonlinear partial differential equation with no known exact solution. Hence one is forced to resort to approximate or numerical analysis. Two distinct approaches have been attempted. Since the equation is moderately nonlinear and the displacement-time relation is usually more important than the displacement variation along the length, it may be assumed that the mode shape does not deviate substantially from the linear case. This approximation yields a non-linear ordinary differential equation which can be solved by the Krylov-Bogoliubov method. An alternate approach would be the perturbation technique which yields relatively more accurate results but leads to complicated expressions.

(a) Mode approximation method

The nondimensionalized equation of motion in the absence of hydrodynamic drag is given by

$$\frac{\partial^4\eta}{\partial\xi^4} - P\,\frac{\partial^2\eta}{\partial\xi^2} + \frac{\partial^2\eta}{\partial\tau^2} = 0 \;. \tag{2.17}$$

The above equation can easily be solved by the separation of variables[47] and the solution can be shown to be

$$\eta(\xi,\tau) = \sum_{r=1}^{\infty} \Psi_r(\xi) f_r(\tau) \;, \tag{2.18a}$$

where

$$\Psi_r(\xi) = K_r[(\cosh\mu_r''\xi - \cos\mu_r'\xi) - \sigma_r\{\sinh\mu_r''\xi - (\mu_r''/\mu_r')\sin\mu_r'\xi\}] \;, \tag{2.18b}$$

and

$$f_r(\tau) = A_r\cos\mu_r^2\tau + B_r\sin\mu_r^2\tau \;. \tag{2.18c}$$

Here

$$\mu_r''^2 = (\mu_r^4 + P^2/4)^{1/2} + P/2 \quad , \tag{2.19a}$$

$$\mu_r'^2 = (\mu_r^4 + P^2/4)^{1/2} - P/2 \quad , \tag{2.19b}$$

$$\sigma_r = [\cosh\mu_r'' + (\mu_r'^2/\mu_r''^2)\cos\mu_r']/[\sinh\mu_r'' + (\mu_r'/\mu_r'')\sin\mu_r'] \quad , \tag{2.19c}$$

and μ_r are the roots of the frequency equation

$$P^2 + 2\mu^4(1 + \cosh\mu''\cos\mu') - \mu^2 P\sinh\mu''\sin\mu' = 0 \; . \tag{2.20}$$

The coefficients K_r are so chosen as to normalize $\Psi_r(\xi)$, i.e.,

$$\int_0^1 \Psi_r^2(\xi)d\xi = (1/4)[\Psi_r^2(1) + (P/\mu_r^4)\left\{\frac{d\Psi_r(1)}{d\xi}\right\}^2] = 1 \; . \tag{2.21a}$$

From Equation (2.18b), with the help of (2.20) one obtains

$$\Psi_r^2(1) = K_r^2[(\mu_r'^2 + \mu_r''^2)^2/\mu_r'^3\mu_r''^3][(\mu_r'^3\sinh\mu_r'' + \mu_r''^3\sin\mu_r')/(\mu_r''\sinh\mu_r'' + \mu_r'\sin\mu_r')] \quad , \tag{2.21b}$$

and

$$\left\{\frac{d\Psi_r(1)}{d\xi}\right\}^2 = K_r^2[(\mu_r'^2 + \mu_r''^2)^4/4\mu_r'^4\mu_r''^4] \; *$$

$$[\{(\mu_r'^2-\mu_r''^2)+\mu_r'\mu_r''\sinh\mu_r''\sin\mu_r'\}/(\mu_r''\sinh\mu_r''+\mu_r'\sin\mu_r')]^2 \ . \tag{2.21c}$$

Substitution of the above relations in (2.21a) yields K_r. Then A_r and B_r may be evaluated from the initial conditions. The objective here is to employ these modes in the analysis of the nonlinear Equation (2.16).

If the modes of oscillation are close to the ones given by Equation (2.18b) ,

$$\frac{\partial^4\eta}{\partial\xi^4} - P\frac{\partial^2\eta}{\partial\xi^2} \simeq \mu^4\eta \ .$$

Equation (2.16a) now yields a nonlinear differential equation

$$\frac{\partial^2\eta}{\partial\tau^2} + \mu^4\eta + \alpha\left(\frac{\partial\eta}{\partial\tau}\right)\left|\frac{\partial\eta}{\partial\tau}\right| = 0 \ . \tag{2.22}$$

As the nonlinearity is not too strong ($\alpha \simeq 0.35$), Krylov-Bogoliubov method[45] may be used to yield the solution of the form,

$$\eta = A(\xi,\tau)\cos[\mu^2\tau+\theta(\tau)] \ , \tag{2.23}$$

where $A(\xi,\tau)$ and $\theta(\tau)$ are slowly varying functions of τ and can be obtained from the following averaging relations:

$$\dot{A} = -(\alpha/\mu^4)(\mu^2/2\pi)\int_0^{2\pi}\mu^4 A\sin\zeta|A\sin\zeta|\sin\zeta d\zeta = -4\alpha\mu^2A^2/3\pi \quad , \tag{2.24a}$$

and

$$\dot{\theta} = -(\alpha/\mu^4)(\mu^2/2\pi A)\int_0^{2\pi}\mu^4 A\sin\zeta|A\sin\zeta|\cos\zeta d\zeta = 0 \quad . \tag{2.24b}$$

Evaluation of A and θ from the above equations and substitution in (2.23) lead to

$$\eta = [A(\xi,0)/\{1+4\alpha\mu^2A(\xi,0)\tau/3\pi\}]\cos[\mu^2\tau+\theta(0)] \quad . \tag{2.25}$$

Equation (2.25) shows a decay in the amplitude of the motion with time in the presence of hydrodynamic drag. On the other hand, the frequency of oscillation remains unaffected, at least up to the first order approximation. This approximate method can be applied only if the initial conditions correspond to one of the natural modes.

(b) Perturbation method

The governing Equation (2.16a) may be rewritten as

$$\frac{\partial^4\eta}{\partial\xi^4} - P\frac{\partial^2\eta}{\partial\xi^2} + \frac{\partial^2\eta}{\partial\tau^2} \pm \alpha\left(\frac{\partial\eta}{\partial\tau}\right)^2 = 0 \quad , \tag{2.16a'}$$

where the appropriate sign is chosen so as to oppose the motion. It is sufficient to solve (2.16a') either for positive or negative sign for half a cycle as the solution for the other half may be obtained simply by reversing the sign of α with the new initial conditions.

The solution for the negative sign is sought in the form

$$\eta(\xi,\tau) = \eta_0(\xi,\tau) + \alpha\eta_1(\xi,\tau) + \alpha^2\eta_2(\xi,\tau) + \cdots\cdot \quad . \qquad (2.26)$$

A new time variable $\tilde{t}$ is defined by

$$\tilde{t} = \tau[1 + \alpha b_1 + \alpha^2 b_2 + \cdots\cdot] \quad . \qquad (2.27)$$

Since the period of oscillation may vary slowly across the length, b_1 and b_2 are slowly varying functions of ξ. With (2.26) and (2.27), Equation (2.16a') becomes

$$\frac{\partial^4}{\partial\xi^4}(\eta_0+\alpha\eta_1+\alpha^2\eta_2+\cdots\cdot) - P\frac{\partial^2}{\partial\xi^2}(\eta_0+\alpha\eta_1+\alpha^2\eta_2+\cdots\cdot)+[1+\alpha b_1+\alpha^2 b_2+\cdots\cdot]^2 *$$

$$[\frac{\partial^2}{\partial\tilde{t}^2}(\eta_0+\alpha\eta_1+\alpha^2\eta_2+\cdots\cdot)-\alpha\{\frac{\partial}{\partial\tilde{t}}(\eta_0+\alpha\eta_1+\alpha^2\eta_2+\cdots\cdot)\}^2] = 0 \; .$$

Equating the coefficients of the different powers of α to zero separately, one obtains

$$\alpha^0: \quad \frac{\partial^4\eta_0}{\partial\xi^4} - P\frac{\partial^2\eta_0}{\partial\xi^2} + \frac{\partial^2\eta_0}{\partial\tilde{t}^2} = 0 \quad , \tag{2.28a}$$

$$\alpha^1: \quad \frac{\partial^4\eta_1}{\partial\xi^4} - P\frac{\partial^2\eta_1}{\partial\xi^2} + \frac{\partial^2\eta_1}{\partial\tilde{t}^2} = -2b_1(\xi)\frac{\partial^2\eta_0}{\partial\tilde{t}^2} + \left(\frac{\partial\eta_0}{\partial\tilde{t}}\right)^2 \quad , \tag{2.28b}$$

$$\alpha^2: \quad \frac{\partial^2\eta_2}{\partial\xi^4} - P\frac{\partial^2\eta_2}{\partial\xi^2} + \frac{\partial^2\eta_2}{\partial\tilde{t}^2} = -[2b_2(\xi) + b_1^2(\xi)]\frac{\partial^2\eta_0}{\partial\tilde{t}^2}$$

$$+ 2b_1(\xi)\left[\left(\frac{\partial\eta_0}{\partial\tilde{t}}\right)^2 - \frac{\partial^2\eta_1}{\partial\tilde{t}^2}\right] + 2\frac{\partial\eta_0}{\partial\tilde{t}}\frac{\partial\eta_1}{\partial\tilde{t}} \quad , \tag{2.28c}$$

etc.

The objective is to solve this system of equations such that all η_i's confirm to the boundary conditions (2.16c) with initial conditions (2.16d) satisfied by η_0 alone, while zero initial conditions are met by other η_i's.

Equation (2.28a) is identical to (2.17) and its solution for the given initial conditions can be written as

$$\eta_0(\xi,\tilde{t}) = \sum_{r=1}^{\infty} A_{0r}\Psi_r(\xi)\cos\mu_r^2\tilde{t} \quad , \tag{2.29a}$$

where $\Psi_r(\xi)$ and μ_r are defined by (2.18b) and (2.20), respectively and

$$A_{0r} = \int_0^1 A_0(\xi)\Psi_r(\xi)d\xi \quad . \tag{2.29b}$$

With this, Equation (2.28b) becomes

$$\frac{\partial^4 \eta_1}{\partial \xi^4} - P\frac{\partial^2 \eta_1}{\partial \xi^2} + \frac{\partial^2 \eta_1}{\partial \tilde{t}^2} = \frac{1}{2}\left[\sum_{r=1}^{\infty}\sum_{s=1}^{\infty} \Psi_r(\xi)*\right.$$

$$\Psi_s(\xi)\mu_r^2\mu_s^2 A_{0r}A_{0s}\{\cos(\mu_r^2-\mu_s^2)\tilde{t}-\cos(\mu_r^2+\mu_s^2)\tilde{t}\}]$$

$$+2b_1(\xi)\sum_{r=1}^{\infty} \mu_r^4\Psi_r(\xi)A_{0r}\cos\mu_r^2\tilde{t}$$

$$= q(\xi,\tilde{t}) \quad . \tag{2.30}$$

The solution to (2.30) can be taken in the form

$$\eta_1(\xi,\tilde{t}) = \sum_{j=1}^{\infty} \Psi_j(\xi)f_j(\tilde{t}) \quad . \tag{2.31}$$

Substitution of (2.31) in (2.30), multiplication by $\Psi_i(\xi)$, integration with respect to ξ over the length and the use of orthogonality condition lead to

$$\frac{d^2}{d\tilde{t}^2} f_i(\tilde{t}) + \mu_i^4 f_i(\tilde{t}) = Q_i(\tilde{t}),\ i = 1,2,\cdots\infty \quad , \tag{2.32}$$

where

$$Q_i(\tilde{t}) = [\int_0^1 q(\xi,\tilde{t})\Psi_i(\xi)d\xi] / [\int_0^1 \Psi_i^2(\xi)d\xi] .$$

Since $\Psi_i(\xi)$ are in the normalized form, the denominator is equal to unity (Equation 2.21a); hence

$$Q_i(\tilde{t}) = \frac{1}{2}\sum_{r=1}^{\infty}\sum_{s=1}^{\infty}\beta_{irs}\mu_r^2\mu_s^2 A_{0r}A_{0s}\{\cos(\mu_r^2-\mu_s^2)\tilde{t}$$

$$-\cos(\mu_r^2+\mu_s^2)\tilde{t}\} + 2\sum_{r=1}^{\infty}\int_0^1 b_1(\xi)\Psi_i(\xi)\Psi_r(\xi) *$$

$$A_{0r}\cos\mu_r^2\tilde{t}d\xi \quad , \tag{2.33a}$$

where

$$\beta_{irs} = \int_0^1 \Psi_i(\xi)\Psi_r(\xi)\Psi_s(\xi)d\xi \quad . \tag{2.33b}$$

As the last term in Equation (2.33a) gives rise to secular quantities, it must vanish for all i, hence

$$b_1(\xi) = 0 \quad , \tag{2.34}$$

i.e. the frequencies do not deviate from the linear case upto the first order. It may be noted that the mode approximation also led to the same conclusion.

The solution to (2.32) can now be written as

$$f_i(t) = \frac{1}{2}\sum_{r=1}^{\infty}\sum_{s=1}^{\infty}\beta_{irs}\mu_r^2\mu_s^2 A_{0r}A_{0s}[\cos(\mu_r^2-\mu_s^2)\tilde{t}/$$

$$\{\mu_i^4-(\mu_r^2-\mu_s^2)^2\}-\cos(\mu_r^2+\mu_s^2)\tilde{t}/\{\mu_i^4-(\mu_r^2+\mu_s^2)^2\}]$$

$$+C_{1r}\cos\mu_i^2\tilde{t} + D_{1r}\sin\mu_i^2 t \quad .$$

Evaluating C_{1r} and D_{1r} from zero initial conditions and substituting in (2.31) yield

$$\eta_1(\xi,\tilde{t}) = -\frac{1}{2}\sum_{i=1}^{\infty}\sum_{r=1}^{\infty}\sum_{s=1}^{\infty}\beta_{irs}\mu_r^2\mu_s^2 A_{0r}A_{0s}\Psi_i(\xi)*$$

$$[\{\cos\mu_i^2\tilde{t}-\cos(\mu_r^2-\mu_s^2)\tilde{t}\}/\{\mu_i^4-(\mu_r^2-\mu_s^2)^2\}$$

$$-\{\cos\mu_i^2\tilde{t}-\cos(\mu_r^2+\mu_s^2)\tilde{t}\}/\{\mu_i^4-(\mu_r^2+\mu_s^2)^2\}] \quad . \qquad (2.35)$$

Now the second order Equation (2.28c) becomes

$$\frac{\partial^2\eta_2}{\partial\xi^4} - P\,\frac{\partial^2\eta_2}{\partial\xi^2} + \frac{\partial^2\eta_2}{\partial\tilde{t}^2} = -\,2b_2(\xi)\,\frac{\partial^2\eta_0}{\partial\tilde{t}^2} + 2\,\frac{\partial\eta_0}{\partial\tilde{t}}\,\frac{\partial\eta_1}{\partial\tilde{t}}$$

$$= 2b_2(\xi)\sum_{j=1}^{\infty} A_{0j}\Psi_j(\xi)\mu_j^4\cos\mu_j^2\tilde{t}+(1/2) *$$

$$\sum_{i=j}^{\infty}\sum_{j=1}^{\infty}\sum_{r=1}^{\infty}\sum_{s=1}^{\infty} \beta_{irs}A_{0j}A_{0r}A_{0s}\mu_j^2\mu_r^2\mu_s^2\Psi_i(\xi)\Psi_j(\xi)$$

$$[[-\mu_i^2(1-\cos2\mu_i^2\tilde{t})+(\mu_r^2-\mu_s^2)\{\cos(\mu_r^2-\mu_s^2-\mu_j^2)\tilde{t}$$

$$-\cos(\mu_r^2-\mu_s^2+\mu_j^2)\tilde{t}\}]/\{\mu_i^4-(\mu_r^2-\mu_s^2)^2\}-[-\mu_i^2(1-\cos2\mu_i^2\tilde{t})$$

$$+(\mu_r^2+\mu_s^2)\{\cos(\mu_r^2+\mu_s^2-\mu_j^2)\tilde{t}-\cos(\mu_r^2+\mu_s^2+\mu_j^2)\tilde{t}\}]/$$

$$\{\mu_i^4-(\mu_r^2+\mu_s^2)^2\}] \quad . \tag{2.36}$$

To avoid secular quantities, sum of all the terms having frequency equal to one of the natural frequencies must vanish,

$$2b_2(\xi)\sum_{j=1}^{\infty} A_{0j}\Psi_j(\xi)\mu_j^4\cos\mu_j^2\tilde{t}+(1/2)\sum_{i=1}^{\infty}\sum_{j=1}^{\infty}\sum_{p=1}^{\infty}\beta_{ijp} *$$

$$A_{0j}^2A_{0p}\Psi_i(\xi)\Psi_j(\xi)\mu_j^4\mu_p^2 \quad [(\mu_j^2-\mu_p^2)/\{\mu_i^4-(\mu_j^2-\mu_p^2)^2\}$$

$$-(\mu_j^2+\mu_p^2)/\{\mu_i^4-(\mu_j^2+\mu_p^2)^2\}]\cos\mu_p^2\tilde{t} \;=\; 0 \quad .$$

As the expression should be valid for all $\tilde{t}$,

$$2b_2(\xi)A_{0p}\Psi_p(\xi) = -(1/2)\sum_{i=1}^{\infty}\sum_{j=1}^{\infty}[\beta_{ijp}\Psi_i(\xi)\Psi_j(\xi) \; *$$

$$A_{0j}^2 A_{0p}\mu_j^4(\mu_i^4+\mu_j^4-\mu_p^4)]/[\mu_i^2+\mu_j^2+\mu_p^2)(\mu_i^2+\mu_j^2-\mu_p^2)(\mu_j^2+\mu_p^2-\mu_i^2) \; *$$

$$(\mu_p^2+\mu_i^2-\mu_j^2)] \quad , \quad p = 1, 2, \cdots \infty .$$

Expressing $b_2(\xi)$ as a series in ξ,

$$b_2(\xi) = \sum_{r=1}^{\infty} b_{2r}\xi^{r-1} \quad ,$$

multiplying by $\Psi_p(\xi)$ and integrating

$$2\sum_{r=1}^{\infty} b_{2r}A_{0p}g_{rp} = -(1/2)\sum_{i=1}^{\infty}\sum_{j=1}^{\infty}\beta_{ijp}^2 A_{0j}^2 A_{0p}\mu_j^4(\mu_i^4+\mu_j^4-\mu_p^4)/[(\mu_i^2+\mu_j^2$$

$$+\mu_p^2)(\mu_i^2+\mu_j^2-\mu_p^2)(\mu_j^2+\mu_p^2-\mu_i^2)(\mu_p^2+\mu_i^2-\mu_j^2)], \quad p = 1,2,\cdots \infty, \tag{2.37}$$

where

$$g_{rp} = \int_0^1 \xi^{r-1}\Psi_p^2(\xi)d\xi \quad .$$

This set of equations may be solved for b_{2r}. Hence from Equation (2.27),

$$\tilde{t} = \tau[1+(\sum_{r=1}^{\infty} b_{2r}\xi^{r-1})\alpha^2] \quad . \tag{2.38a}$$

Avoiding secular terms, Equation (2.36) can now be solved for η_2 using zero initial conditions. Hence, the solution can be written as

$$\eta(\xi,\tau) = \xi_0(\xi,\tilde{t})+\alpha\eta_1(\xi,\tilde{t})+\alpha^2\eta_2(\xi,\tilde{t}) \quad , \tag{2.38b}$$

where $\tilde{t}$ is as obtained from(2.38a).

For the positive sign in Equation (2.16a') the solution is similar except that the sign of η_1 is different. The complete solution is obtained by using the two solutions alternately and determining the amplitude at the start of each half cycle.

Now certain particular initial conditions may be considered.

<u>Case 1</u>: Let the initial conditions be

$$\eta(\xi,0) = A\Psi_1(\xi) \quad , \qquad \frac{\partial\eta(\xi,0)}{\partial\tau} = 0 \quad .$$

Here $A_{01} = A$ and $A_{0i} = 0 \quad (i = 2, 3, \cdots \infty)$.

It is apparent that the velocity is negative for the first half cycle. From Equations (2.29) and (2.35),

$$\eta_0(\xi,\tilde{t}) = A\Psi_1(\xi)\cos\mu_1^2\tilde{t} \quad ,$$

$$\eta_1(\xi,\tilde{t}) = -(1/2)\mu_1^4A^2[\beta_{111}\Psi_1(\xi)\{(\cos\mu_1^2\tilde{t}-1)/\mu_1^4$$

$$-(\cos\mu_1^2\tilde{t}-\cos 2\mu_1^2\tilde{t})/(\mu_1^4-4\mu_1^4)\}+\beta_{112}\Psi_2(\xi)\{(\cos\mu_2^2\tilde{t}-1)/$$

$$\mu_2^4-(\cos\mu_2^2\tilde{t}-\cos 2\mu_1^2\tilde{t})/(\mu_2^4-4\mu_1^4)\}+\beta_{113}\Psi_3(\xi)\{(\cos\mu_3^2\tilde{t}$$

$$-1)/\mu_3^4-(\cos\mu_3^2\tilde{t}-\cos 2\mu_1^2\tilde{t})/(\mu_3^4-4\mu_1^4)\}] \quad .$$

Noting that $(\mu_1/\mu_2)^4$, $(\mu_1/\mu_3)^4$ etc. are small compared to 1,

$$\eta_1(\xi,\tilde{t}) = -(1/2)A^2[\beta_{111}\Psi_1(\xi)\{(4/3)\cos\mu_1^2\tilde{t}-(1/3)\cos 2\mu_1^2\tilde{t}-1\}]. \quad (2.39)$$

From Equation (2.37), all the b_{2r}'s can be evaluated. However, for simplicity, neglecting the dependence of b_2 on ξ (i.e. neglecting the variation of the frequency along the array arm),

$$b_2 = -\beta_{111}^2 A^2/6 \quad ;$$

$$\text{hence,} \quad \tilde{t} = \tau[1-\alpha^2\beta_{111}^2 A^2/6] \quad . \qquad (2.40)$$

Using zero initial conditions and avoiding secular terms from Equation (2.36),

$$\eta_2(\xi,\tilde{t}) \simeq (2/3)\beta_{111}^2 A^3\{(4/3)\cos\mu_1^2\tilde{t}-1-(1/3)\cos 2\mu_1^2\tilde{t}\}\Psi_1(\xi)+\cdots \quad .$$

Hence

$$\eta(\xi,\tilde{t}) \simeq A\Psi_1(\xi)[\cos\mu_1^2\tilde{t} + \alpha\beta_{111}A\{(1/2)-(2/3)\cos\mu_1^2\tilde{t}+(1/6)\cos 2\mu_1^2\tilde{t}\}$$

$$-\alpha^2\beta_{111}^2A^2\{(2/3)+(8/9)\cos\mu_1^2\tilde{t}+(2/9)\cos 2\mu_1^2\tilde{t}\}] \quad , \qquad (2.41)$$

where $\tilde{t}$ is as given by (2.40) .

The cylinder comes to rest again when

$$\tau \;=\; \tau_h \;=\; \pi/\mu_1^2(1-\alpha_1^2\beta_{111}^2A^2/6) \quad .$$

Correspondingly, $\eta(\xi,\tau_h) = \bar{A}$(say). The solution can now be obtained for the next half cycle by replacing $-\alpha$ by $+\alpha$ and A by $\bar{A}$.

Case 2: Let the initial displacement correspond to the second mode,

$$\text{i.e.,} \quad \eta(\xi,0) = A\Psi_2(\xi), \quad \frac{\partial\eta(\xi,0)}{\partial\tau} = 0 \quad .$$

Following a procedure similar to that in Case 1, the first order perturbation solution is obtained as

$$\eta(\xi,\tau) \simeq \Psi_2(\xi)[A\cos\mu_2^2\tilde{t} - (\alpha/2)\beta_{222}A^2\{(4/3)\cos\mu_2^2\tilde{t} - 1 - (1/3) *$$

$$\cos 2\mu_2^2\tilde{t}\}] - (\alpha/2)A^2\Psi_1(\xi)\beta_{112}(\mu_2/\mu_1)^4(\cos\mu_1^2\tilde{t}-1) \quad .$$

Note that the coefficient of $\Psi_2(\xi)$ as represented by the square bracket diminishes with time, hence the motion tends to reduce to that given by the first case.

As any set of initial conditions may be written as a linear combination of various mode shapes and since the first few modes are likely to be dominating, the analysis may be confined to the first two modes only.

2.2.2 Forced vibration of an inflated cylindrical cantilever with velocity square damping

Consider an inflated cylindrical cantilever oscillating under the influence of ocean waves. It is assumed that the motion of a water particle due to the waves can be approximated to a sinusoidal function. The steady state response of a viscoelastic system can be studied either using the correspondence principle in conjunction with an elastic solution if it is linear or by including in the equation equivalent dissipative terms representing energy loss due to visco-elasticity. For a three parameter solid the complex modulus can be represented as

$$E^*(\omega) = E_1(E_2+i\nu_2\omega)/[E_1+(E_2+i\nu_2\omega)] = E_1[1-E_1/(E_1+E_2+i\nu_2\omega)] \ .$$

In the present case $(E_1+E_2)/\nu_2$ was found to be of the $O(1/100)$ and hence can be neglected, thus reducing the expression to

$$E^*(\omega) = E_1[1+i\omega(E_1/\nu_2\omega^2)] = E_1[1+i\omega\gamma(\omega)] \quad . \tag{2.42a}$$

Adopting this latter procedure, the nondimensionalized equation can be written as

$$(1+ \gamma \frac{\partial}{\partial\tau}) \frac{\partial^4\eta}{\partial\xi^4} - P \frac{\partial^2\eta}{\partial\xi^2} + \frac{\partial^2}{\partial\tau^2} (\eta + \eta_w) + \alpha\frac{\partial}{\partial\tau} (\eta + \eta_w) *$$

$$|\frac{\partial}{\partial\tau}(\eta + \eta_w)| = 0 \ , \qquad (2.42b)$$

where η is the nondimensionalized displacement of any point on the cantilever with respect to its root and γ represents the energy loss in the viscoelastic structure dependent on frequency. The nondimensionalized wave displacement η_w is given by

$$\eta_w = \eta_0 \cos\omega\tau \quad . \qquad (2.43)$$

Here τ is defined by Equation (2.15) with E replaced by the instantaneous modulus of elasticity E_1.

In general the solution will contain all the harmonics of ω. However, for simplicity, only the fundamental term will be considered, i.e., the solution is assumed to be of the form

$$\eta = \eta_c(\xi)\cos\omega\tau + \eta_s(\xi)\sin\omega\tau \quad . \qquad (2.44)$$

Substitution of (2.43) and (2.44) in (2.42b) leads to

$$(1+ \gamma\frac{\partial}{\partial\tau})[\frac{d^4\eta_c}{d\xi^4} \cos\omega\tau + \frac{d^4\eta_s}{d\xi^4} \sin\omega\tau] - P[\frac{d^2\eta_c}{d\xi^2} \cos\omega\tau + \frac{d^2\eta_s}{d\xi^2} \sin\omega\tau]$$

$$-\omega^2 [(\eta_0+\eta_c)\cos\omega\tau+\eta_s\sin\omega\tau]+\alpha\omega^2[-(\eta_0+\eta_c)\sin\omega\tau+\eta_s\cos\omega\tau] *$$

$$|-(\eta_0+\eta_c)\sin\omega\tau+\eta_s\cos\omega\tau| \quad = \quad 0 \quad .$$

Multiplication by $\cos\omega\tau$ and $\sin\omega\tau$ separately and integration over one period gives

$$\frac{d^4}{d\xi^4}(\eta_c+\gamma\omega\eta_s) - P\frac{d^2\eta_c}{d\xi^2} - \omega^2(\eta_c+\eta_0)+8\alpha\omega^2\eta_s[(\eta_c+\eta_0)^2+\eta_s^2]^{1/2}/3\pi \quad = \quad 0 \quad , \tag{2.45a}$$

and

$$\frac{d^4}{d\xi^4}(-\gamma\omega\eta_c+\eta_s) - P\frac{d^2\eta_s}{d\xi^2} - \omega^2\eta_s-8\alpha\omega^2[\eta_c+\eta_0][(\eta_c+\eta_0)^2+\eta_s^2]^{1/2}/3\pi \quad = \quad 0 \quad . \tag{2.45b}$$

The quantities η_c and η_s can be represented as

$$\eta_c(\xi) \quad = \quad \sum_{k=1}^{\infty} A_k\Phi_k(\xi) \quad , \tag{2.46a}$$

$$\eta_s(\xi) \quad = \quad \sum_{k=1}^{\infty} B_k\Phi_k(\xi) \quad , \tag{2.46b}$$

where $\Phi_k(\xi)$'s are the eigenfunctions of a cantilever (without axial tension) and are given by (2.18b) after putting $K_r = 1$, $P = 0$. Since $\frac{d^2\Phi_k}{d\xi^2}$ can be represented as an infinite sum of $\Phi_i(\xi)$,

$$\frac{d^2\eta_c}{d\xi^2} = \sum_{k=1}^{\infty} A_k \sum_{i=1}^{\infty} C_{ki}\Phi_i(\xi) \quad , \tag{2.47a}$$

where C_{ki} is given by[48]

$$C_{ki} = \int_0^1 \frac{d^2\Phi_k}{d\xi^2}\,\Phi_i d\xi = \begin{cases} 4(\mu_k\sigma_k-\mu_i\sigma_i)/[(-1)^{i+k}-(\mu_i/\mu_k)^2], & i \neq k \\ \mu_k\sigma_k(2-\mu_k\sigma_k), & i = k \,, \end{cases} \tag{2.47b}$$

and σ_i is obtained from (2.19c) after putting P = 0.

Substituting (2.46) and (2.47a) in (2.45), multiplying with $\Phi_m(\xi)$ and integrating with respect to ξ over the length, one obtains

$$\mu_m^4(A_m+\gamma\omega B_m)-P\sum_{k=1}^{\infty} A_k C_{km}-\omega^2(A_m+\delta_m\eta_0)+(8\alpha\omega^2/3\pi)\int_0^1 g_s(\xi)*$$

$$[g_s^2+g_c^2]^{1/2}\Phi_m(\xi)d\xi = 0 \quad , \tag{2.48a}$$

and

$$\mu_m^4(-\gamma\omega A_m+B_m)-P\sum_{k=1}^{\infty} B_k C_{km}-\omega^2 B_m -(8\alpha\omega^2/3\pi)\int_0^1 g_c(\xi)*$$

$$[g_s^2+g_c^2]^{1/2}\Phi_m(\xi)d\xi = 0 \quad , \quad m = 1,2,\cdots\infty, \tag{2.48b}$$

where

$$g_s(\xi) = \sum_{j=1}^{\infty} B_j\Phi_j(\xi) \quad ,$$

$$g_c(\xi) = \eta_0+\sum_{j=1}^{\infty} A_j\Phi_j(\xi) \quad , \qquad \delta_m = 2\sigma_m/\mu_m \quad ,$$

and μ_m are the roots of the equation

$$1 + \cosh\mu \cos\mu = 0 .$$

The set of Equations (2.48) can be solved to yield A_m and B_m. In the actual computation the series were truncated to the first four modes.

2.3 Experimental Set-up

To assess validity of the analytical approach and to generate relevant design information, an experimental programme was undertaken. The tests were performed in a 6' x 3' x 4' rectangular water tank (Figure 2-3) constructed from waterproof plywood with front plexiglas panel to help photographing of the deflected model. The tank was equipped with a moveable head to support the tube centrally. A compressed air bottle pressurized an intermediate water tank which was then used to inflate the tube after the test tank had been filled with water. A pressure gauge in the interconnecting piping indicated the inflation pressure. A system of trolley enabled loading of the tube at any desired station.

For dynamic testing, the mounting block supporting the model was made a part of the scotch yoke mechanism driven by a 3/16 horsepower d.c. motor equipped with a variable speed control unit.

A set of 10 models made from thin films of polyethylene was tested to cover a wide range of L/d_f ratio, an important system parameter. One end of each tube was sealed by inserting a thin plexiglas plug of the same diameter as the tube and bonding it with

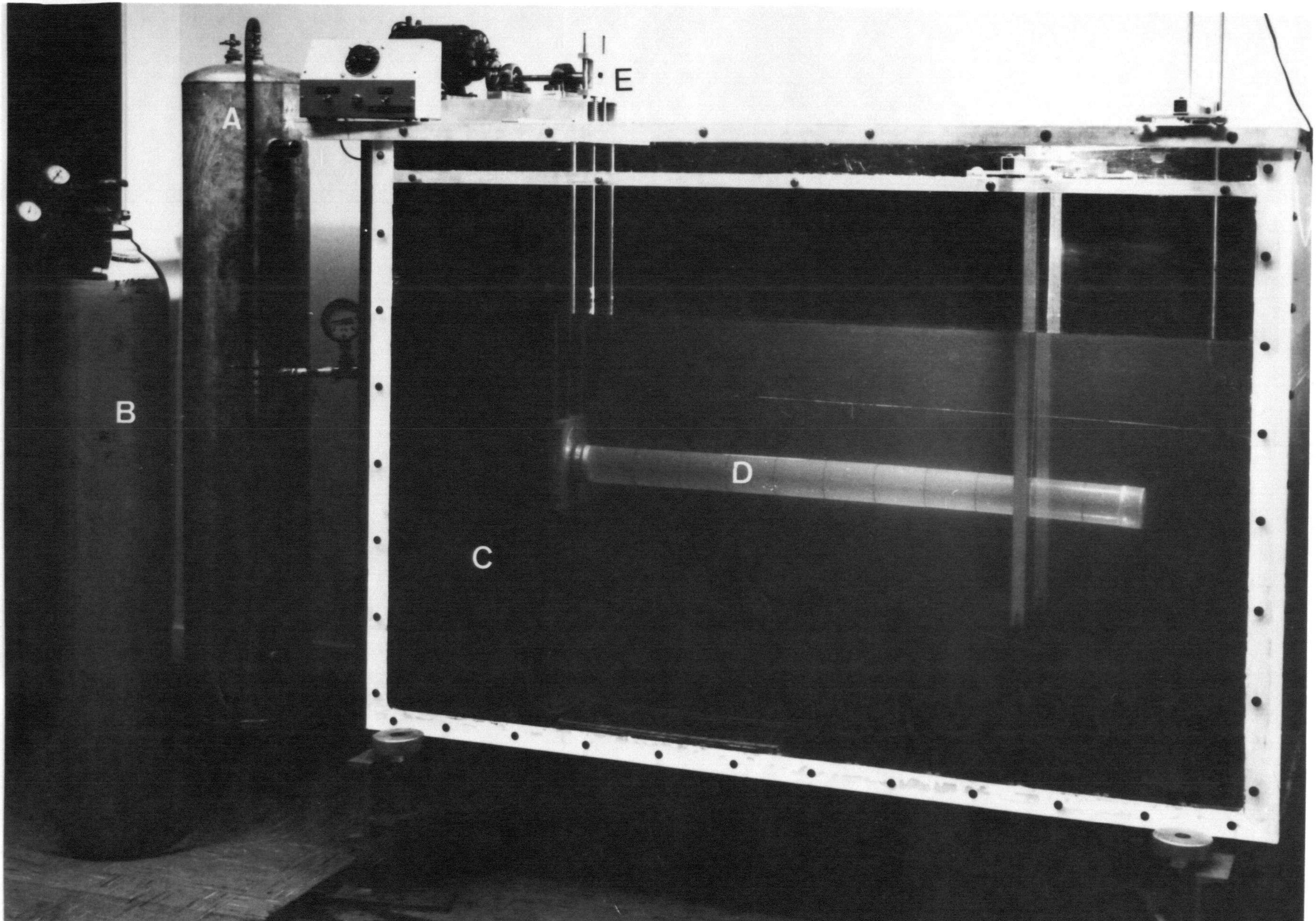

Figure 2-3. Experimental set-up: A. water bottle; B. compressed air bottle; C. water tank; D. test model; E. shaking mechanism.

epoxy. Each tube was divided into 4 in. sections at which the deflections were measured.

Since the static deflections are time varying and the measurements at different stations have to be taken at the same instant, photographic technique was applied to record time history of a beam undergoing creeping deformation. 35 mm pictures were taken, initially 30 sec apart with the interval gradually increasing to 5 minutes as the creep rate diminished. A thin wire strung above the tube served as a reference during these measurements. 16 mm movies were taken for the dynamic tests. The deflection data were analyzed by projecting the pictures on a screen.

2.4 Results and Discussion

Although the amount of experimental information generated is rather extensive,only a few of the typical results helpful in establishing trends and deriving conclusions are presented here. Figure 2-4 shows a typical deflection history during a loading/unloading cycle. It corresponds to a cantilever of 28" length, 2.93" diameter, 0.010" wall thickness and loaded at station 6. The internal pressure is 3 psi. An instantaneous deflection followed by creep is apparent. The creep rate gradually decreases and becomes almost negligible after about 40 minutes. With removal of the load, there is an instantaneous drop in the deflection, of the magnitude equal to the instantaneous initial deflection. The model asymptotically returns to the original position following essentially the same behaviour as that observed during the loading cycle.

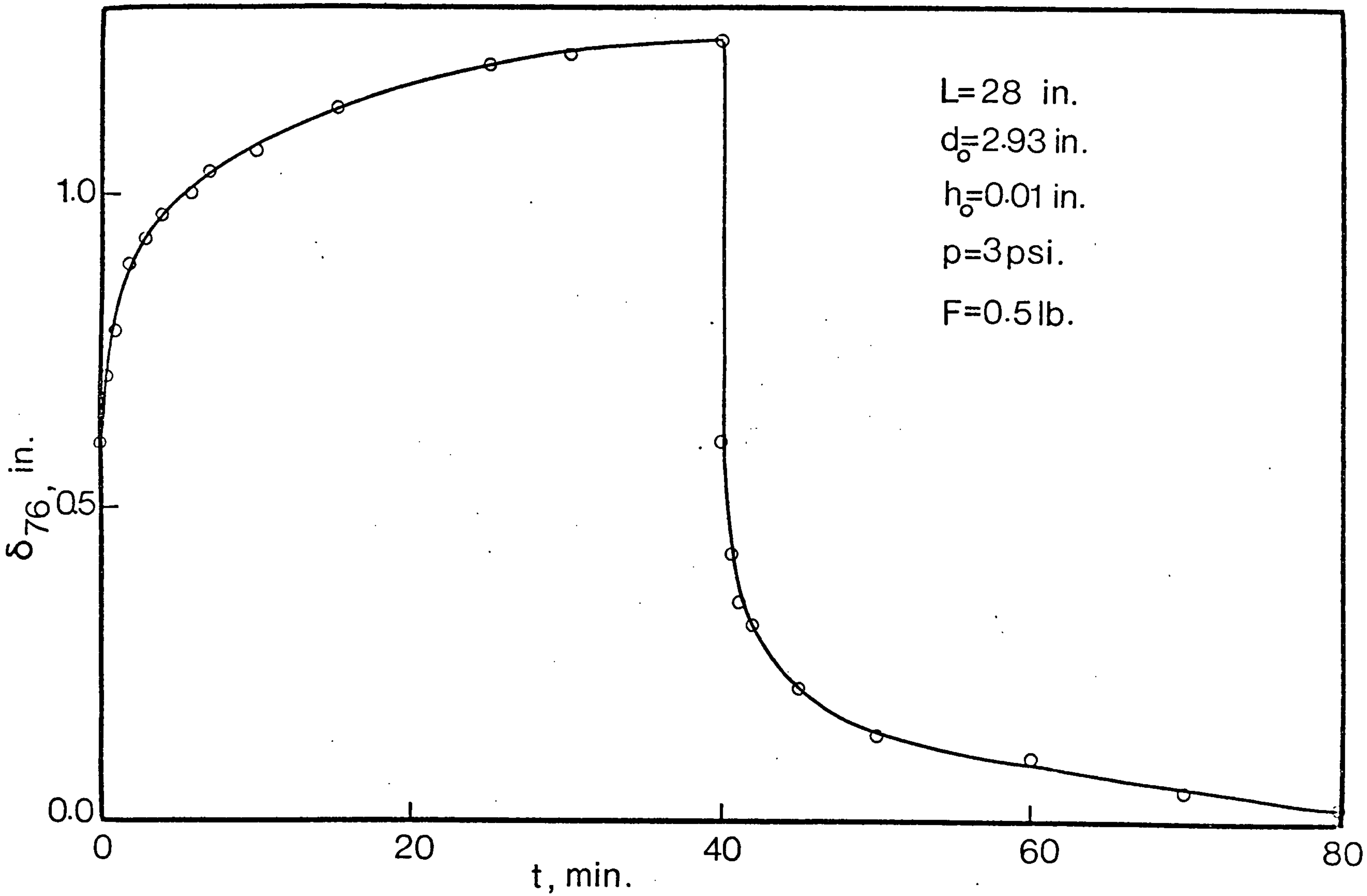

Figure 2-4 A typical deflection history for a point on the beam during a loading-unloading cycle

To evaluate instantaneous stiffness or the influence coefficient matrix, it is essential to obtain instantaneous deflection configuration of the beam. A typical set of such plots is shown in Figure 2-5 which corresponds to a model 40" long, 4.76" in diameter and having a wall thickness of 0.010". Each plot is related to a load station designated as 10, 9, 8,etc. These can be used to construct the flexibility matrix which in conjunction with the matrix iteration method can yield the natural frequencies and the associated mode shapes.

Figure 2-6 compares some of the test results with analytical predictions. In Figure 2-6a both the models are made of polyethylene film of 0.010" thickness and have a diameter of 4.76". The models are 40" and 28" long, respectively. It is interesting to note that the behaviour is more or less that of a three parameter solid. Average values of E_1, E_2, ν_2 have been obtained to give the analytical curves. In the tests ν_2 was found to vary but the instantaneous modulus of elasticity E_1 was fairly constant ($\approx 4.5 \times 10^4$ psi).

In Figure 2-6b, which corresponds to a model 32" long, 4.90" in diameter and having a wall thickness of 0.005", one notices the continuing creep. This is because of the higher stress level due to the reduced thickness of the wall. The three parameter solid does not predict the longtime deformation character very well but a creep compliance of the form

$$J(t) = (0.22 + 0.14t^{0.27}) \times 10^{-4} , \tag{2.49}$$

t in minutes, obtained by fitting a curve to the J(t) given by Lifshitz and Kolsky[49] improves the correlation considerably.

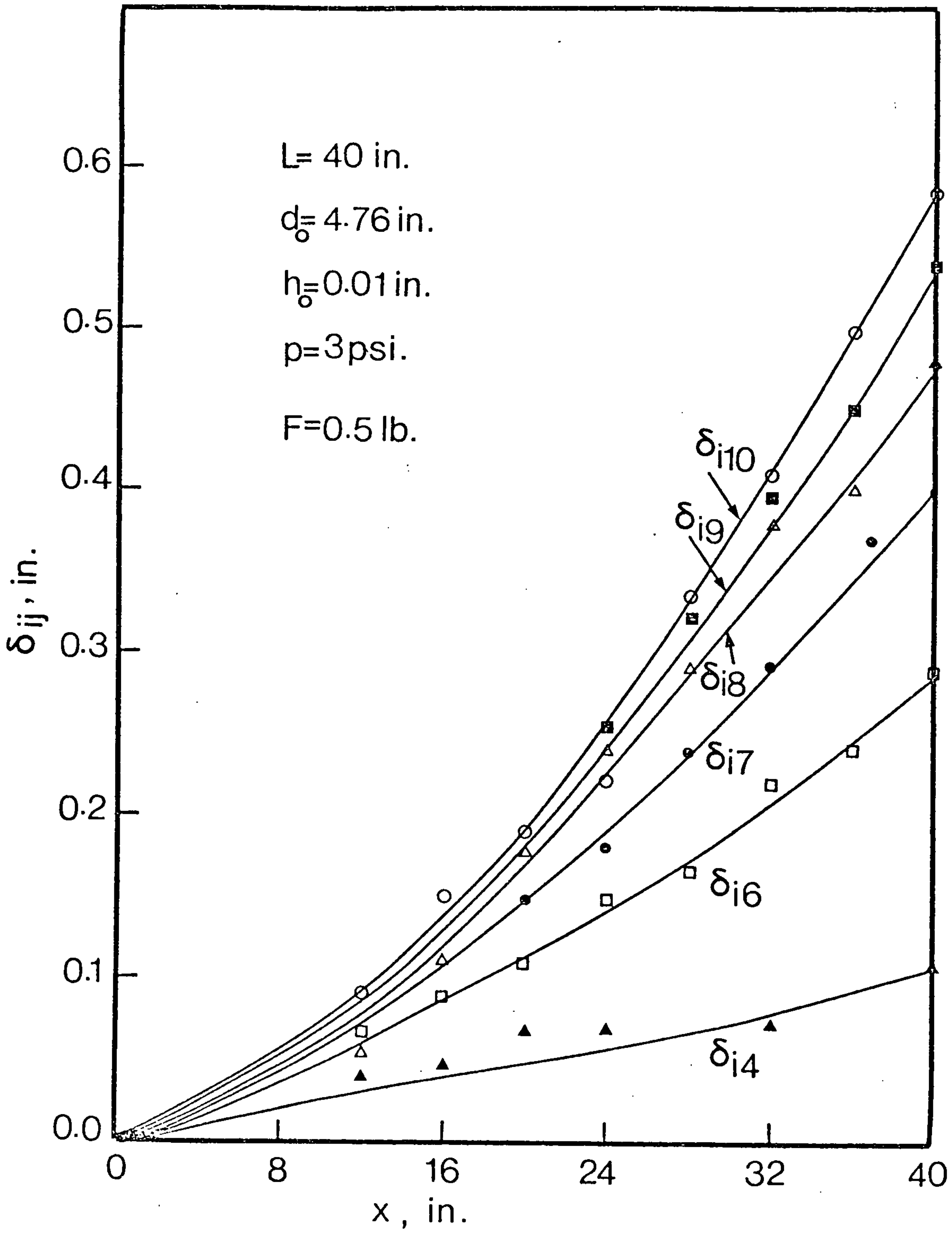

Figure 2-5 Representative instantaneous beam configurations for different loading conditions

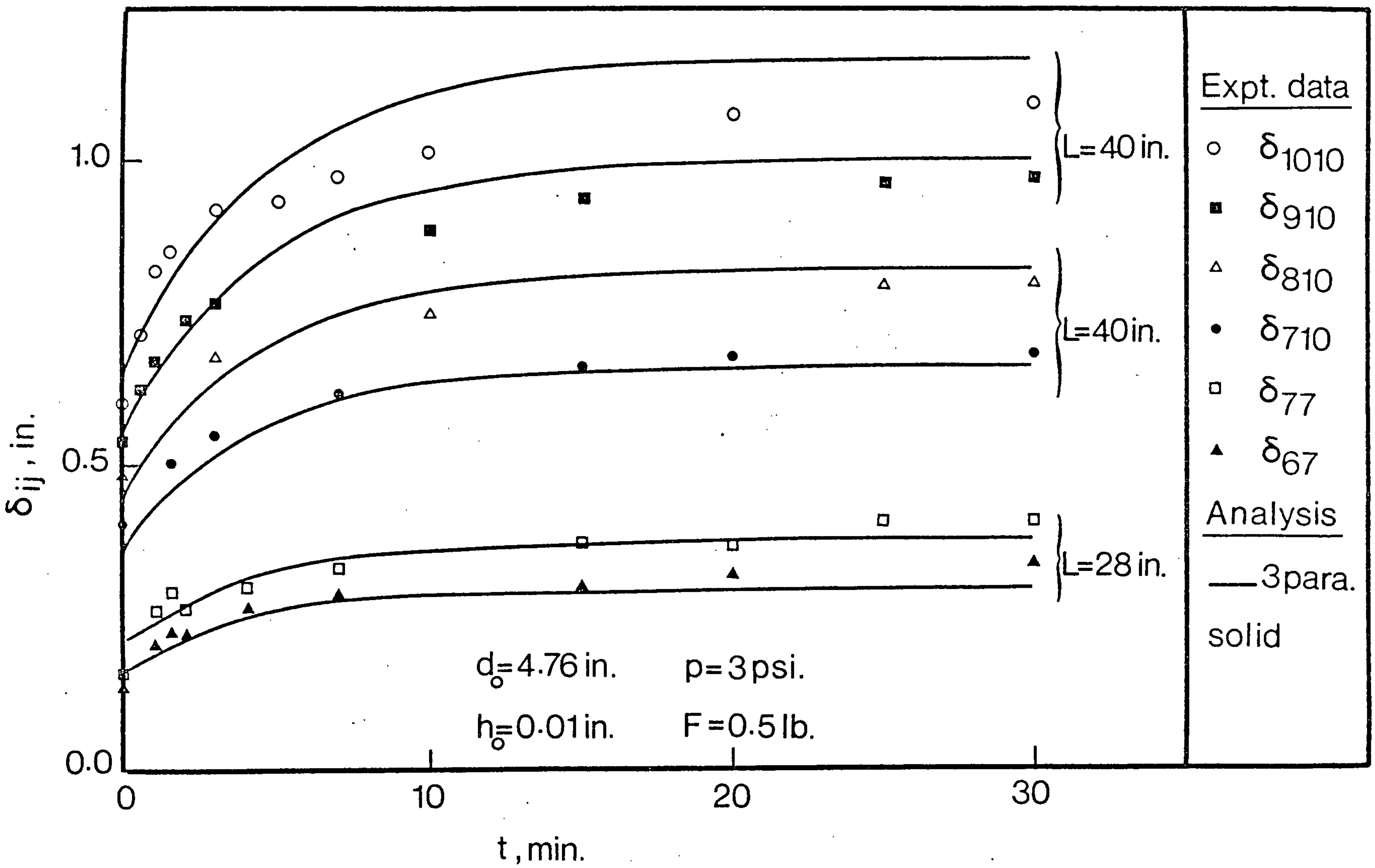

Figure 2-6 Comparison of analytical and experimental results for the static deflection using: (a) three parameter solid model

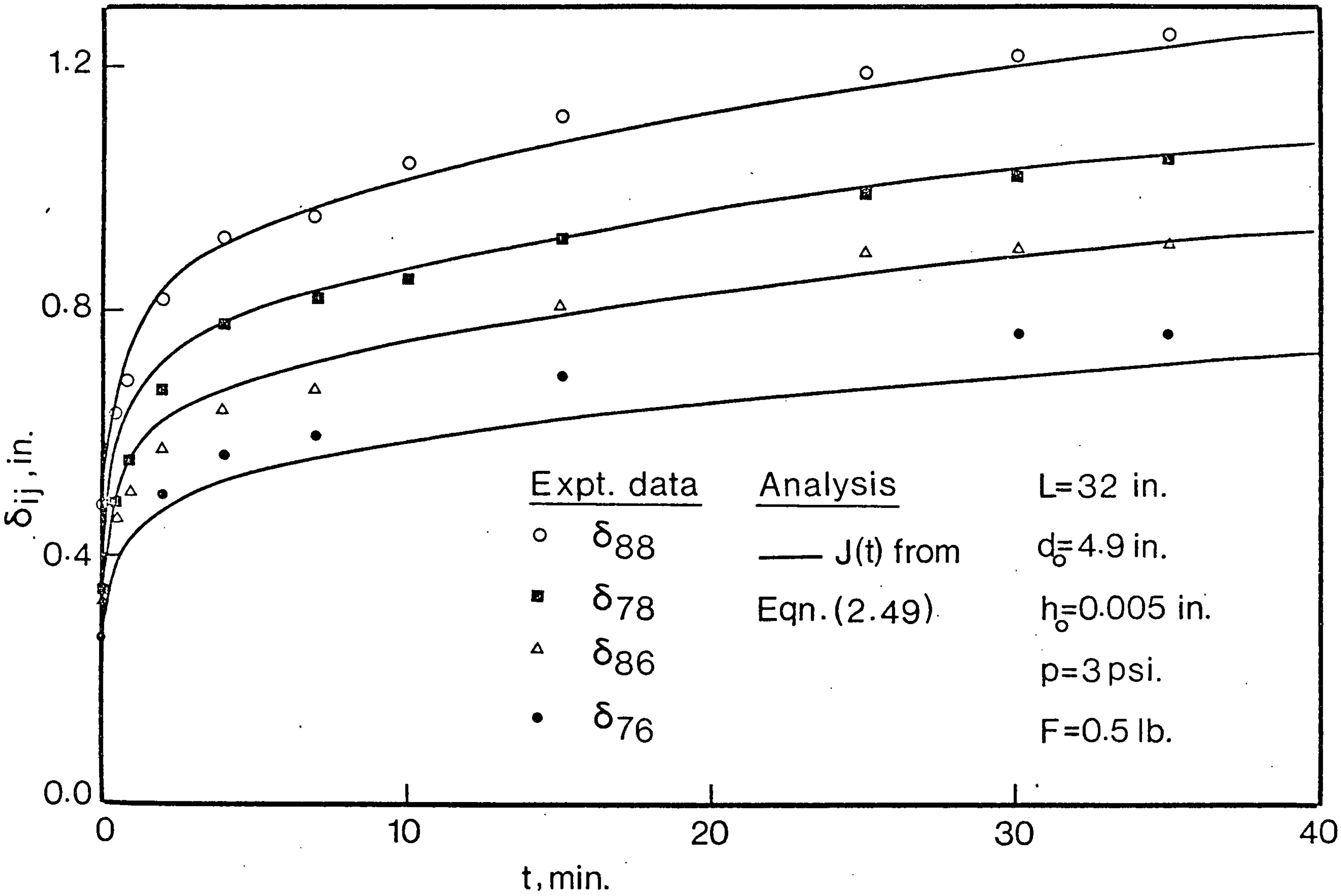

Figure 2-6 Comparison of analytical and experimental results for the static deflection using: (b) J(t) as given by Equation (2.49)

The tip deflections at t = 0 and t = 35 minutes are plotted as functions of L/d_f in Figure 2-7 for the structural models having a wall thickness of 0.010" and tip load of 1/2 lb. The lines represent the analytical results as given by Equation (2.13) while the isolated points indicate the test data. Potential of the analytical approach becomes apparent as it is able to predict with accuracy even large deflections. Physically this would suggest that the curvature can be represented by d^2w/dx^2 without much error even though the deflections are large.

It should be emphasized that long time strain (say after a few hours) for high stress level has a nonlinear relationship with the stress. Findley and Khosla[50] have found the creep of polyethylene to follow the equation

$$\varepsilon_c = \varepsilon'_{c0}\sinh(\sigma/\sigma_e) + m'\sinh(\sigma/\sigma_m)t^n \quad , \tag{2.50}$$

where ε'_{c0}, m', n, σ_e and σ_m are material constants. On the other hand, Kalinnikov[51] observed the creep relation for polyethyleneterephthalate (mylar) to be of the form

$$\varepsilon_c = \varepsilon_{c0} + a\sigma^m t^n \quad ,$$

where a, m, n are constants. A similar equation can also be used for polyethylene. But in the study of dynamics of these structures only the short time creep is of significance, since the period of most of the neutrally buoyant structures is very small (a few seconds).

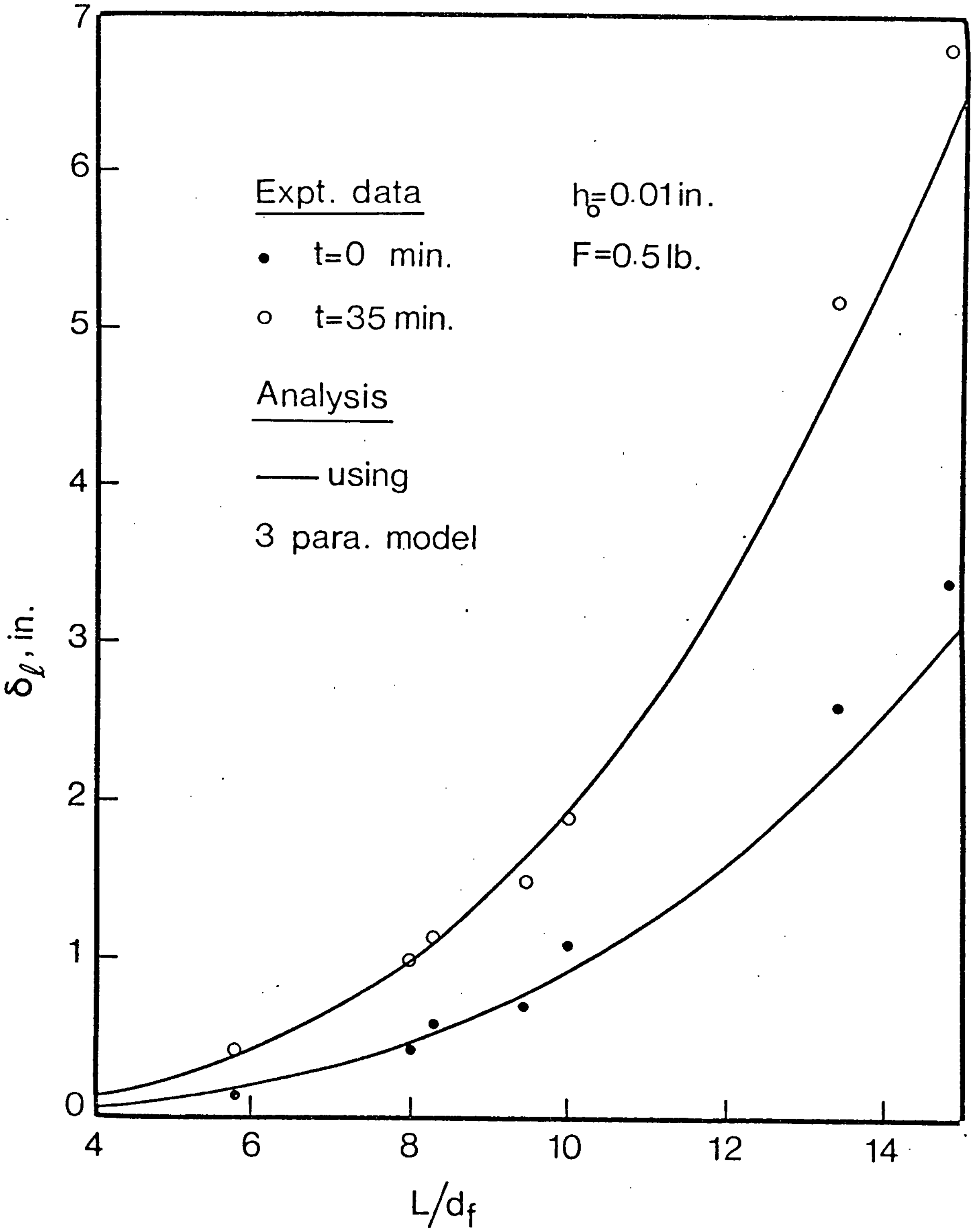

Figure 2-7 Tip deflection as a function of L/d_f

Figure 2-8 shows the variation of the eigenvalues μ_r and the associated quantities μ_r', μ_r'' and K_r as obtained from Equations (2-18) to (2-21) with the axial force parameter P. As observed by Anderson and King,[47] the lowest eigenvalue decreases with an increase in P while the higher eigenvalues increase. K_r decreases with increase in P, but its variation is small for higher modes. It may be noticed that K_1 is very small for large P. Figure 2-9 compares the decay in amplitude due to the hydrodynamic drag as given by the mode approximation, perturbation and numerical solutions. The initial conditions correspond to the first mode shape, i.e. $A(\xi,0) = 0.5\Psi_1(\xi)$. The close agreement between the approximate solution and the numerical method is encouraging.

Figure 2-10 is a typical plot showing the variation of the amplitude at four different points along the length with the forcing frequency and pressure parameter. The peaks correspond to the resonance. As expected, with increase in P, the 1st peak occurs for smaller ω, while the 2nd peak moves to a larger value.

The forcing frequencies at which resonance occurs have been measured for a set of test cylinders.Table 2.1 compares these with the theoretical predictions. Considering a degree of uncertainty introduced by the added inertia coefficient and elastic properties, the agreement may be considered satisfactory.

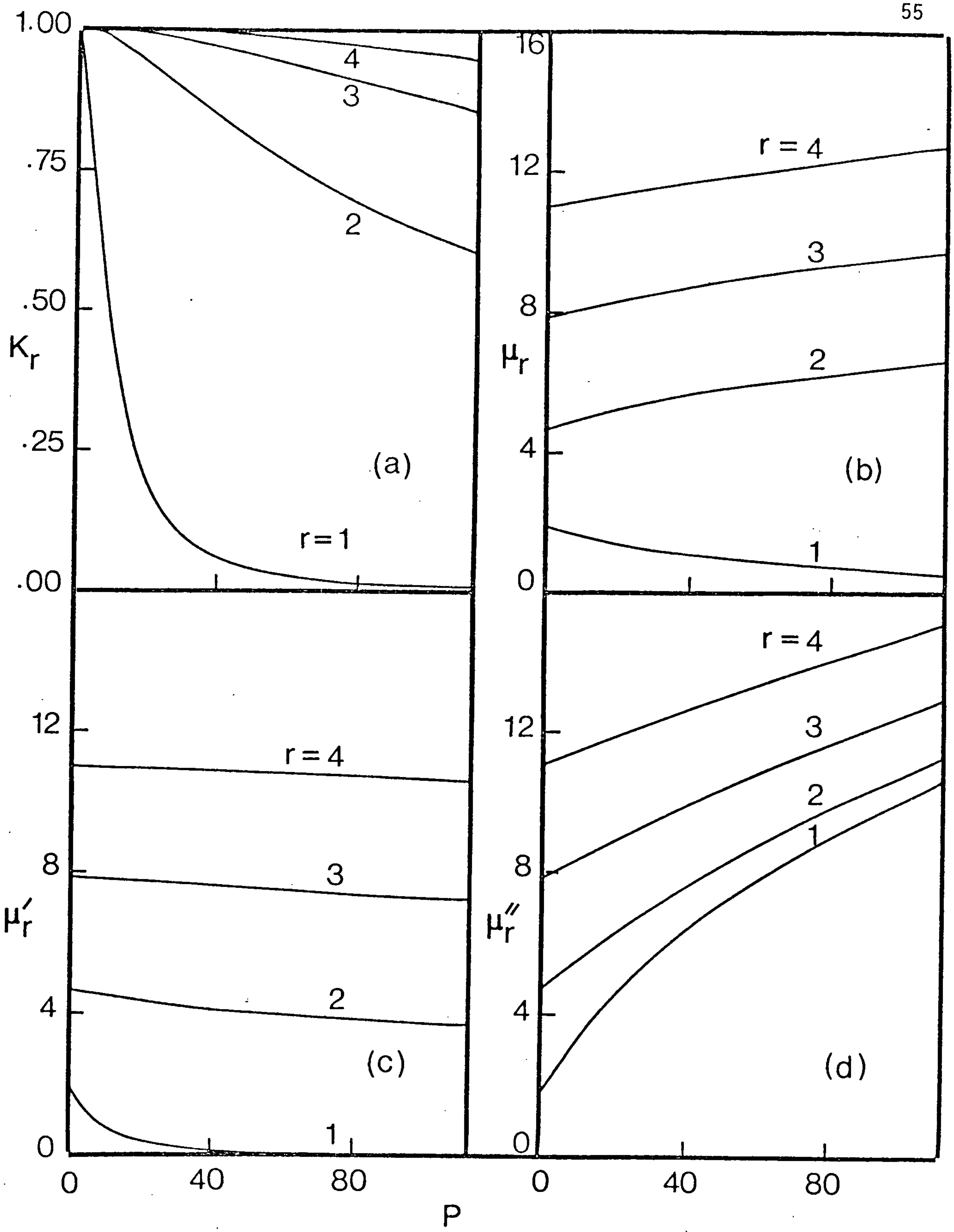

Figure 2-8 Variation of eigenvalues and associated functions with the pressure parameter

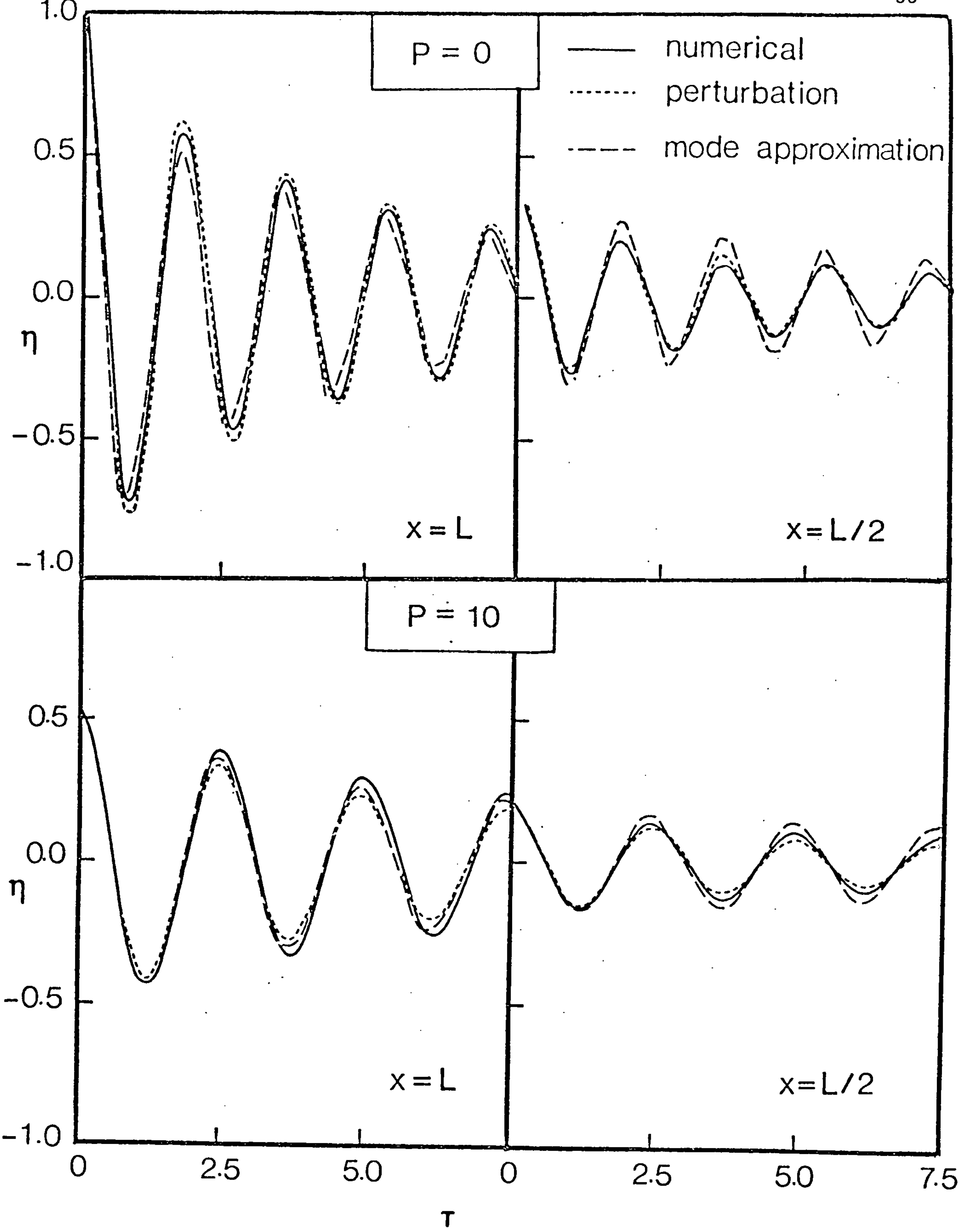

Figure 2-9 Free vibration of an elastic cylindrical cantilever as given by approximate and numerical methods

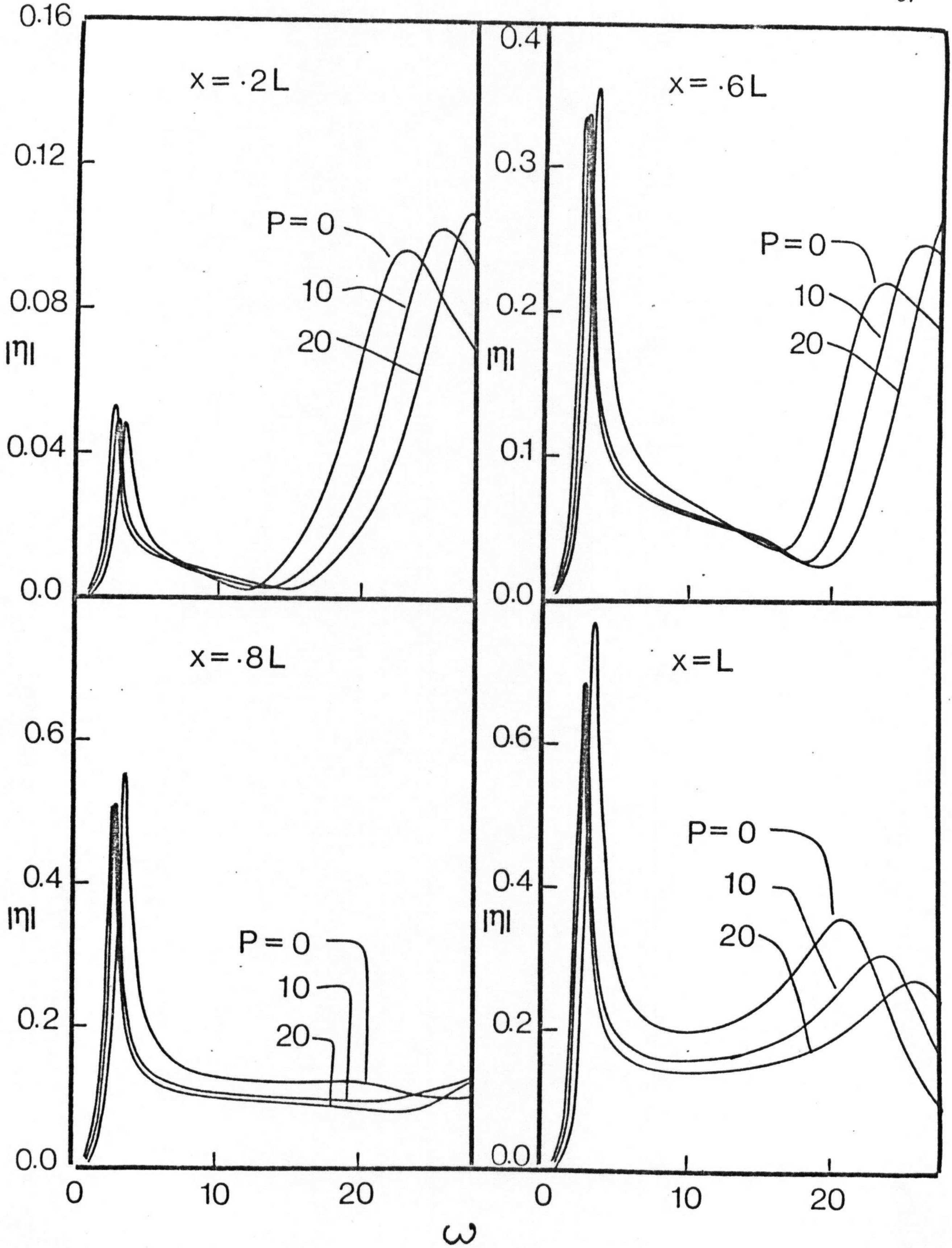

Figure 2-10 Response of an inflated viscoelastic cylindrical cantilever to the surface wave excitation

TABLE 2.1

Comparison Between Analytically and Experimentally Obtained Frequencies

d_0, in.	L_0, in.	h_0, in.	$\omega_{expt.}$, Hz.	$\omega_{anal.}$, Hz.
1.0	12	0.005	16.8	17.8
2.37	19	0.01	15.9	15.5
2.93	44	0.01	4.12	3.20
3.80	40	0.01	4.7	4.44
4.76	40	0.01	5.5	5.20

2.5 Concluding Remarks

The important conclusions based on the analysis can be summarized as follows:

(i) The static analysis suggests that a three parameter solid model can yield results of sufficient accuracy to be useful in any engineering design of a neutrally buoyant inflatable structure. For the long time creep, a modified creep compliance may be used to improve correlation.

(ii) During the free vibration of an inflated elastic cantilever with hydrodynamic drag and a follower force, the governing equation can be suitably nondimensionalized to render the damping parameter independent of geometrical dimensions of the beam. The results of mode approximation and second order perturbation analysis compare well with the numerical and the experimental data.

(iii) Dynamical response of the viscoelastic beam to surface wave excitation accounting for the hydrodynamic drag and internal pressure induced follower force, should prove useful in the design of an underwater submarine detection system.

3. DYNAMICS OF AN ARRAY FORMED BY THREE NEUTRALLY BUOYANT INFLATED CYLINDRICAL CANTILEVERS

The last chapter investigated the flexural behaviour of a single cylinder, in the presence of hydrodynamic forces and a tensile force due to inflation pressure. It was noted that with increasing pressure, the second and subsequent frequencies increase while the fundamental decreases asymptotically to zero. The steady state response of the beam to the surface wave excitation was also studied. The object of this chapter is to extend the previous analysis to the coupled motion of three similar flexible cylindrical cantilevers placed symmetrically around a central head to form an array.

The rigid body rotations of the array and flexural displacements of the legs are superposed on a vertical motion of the central head. Small oscillations are considered and the resulting eigenvalue problem for the coupled motion is investigated. Effects of the inflation pressure and inertia parameters on the natural frequencies of the system and any possibility of dynamic instability are studied.

3.1 Formulation of the Problem

Consider an array of three cylindrical cantilevers connected to a central body symmetrically (Figure 3-1 a). Let L and d be the length and diameter of each leg. The principal body co-ordinate system x, y, z with its origin at the centre O of the array is so located that

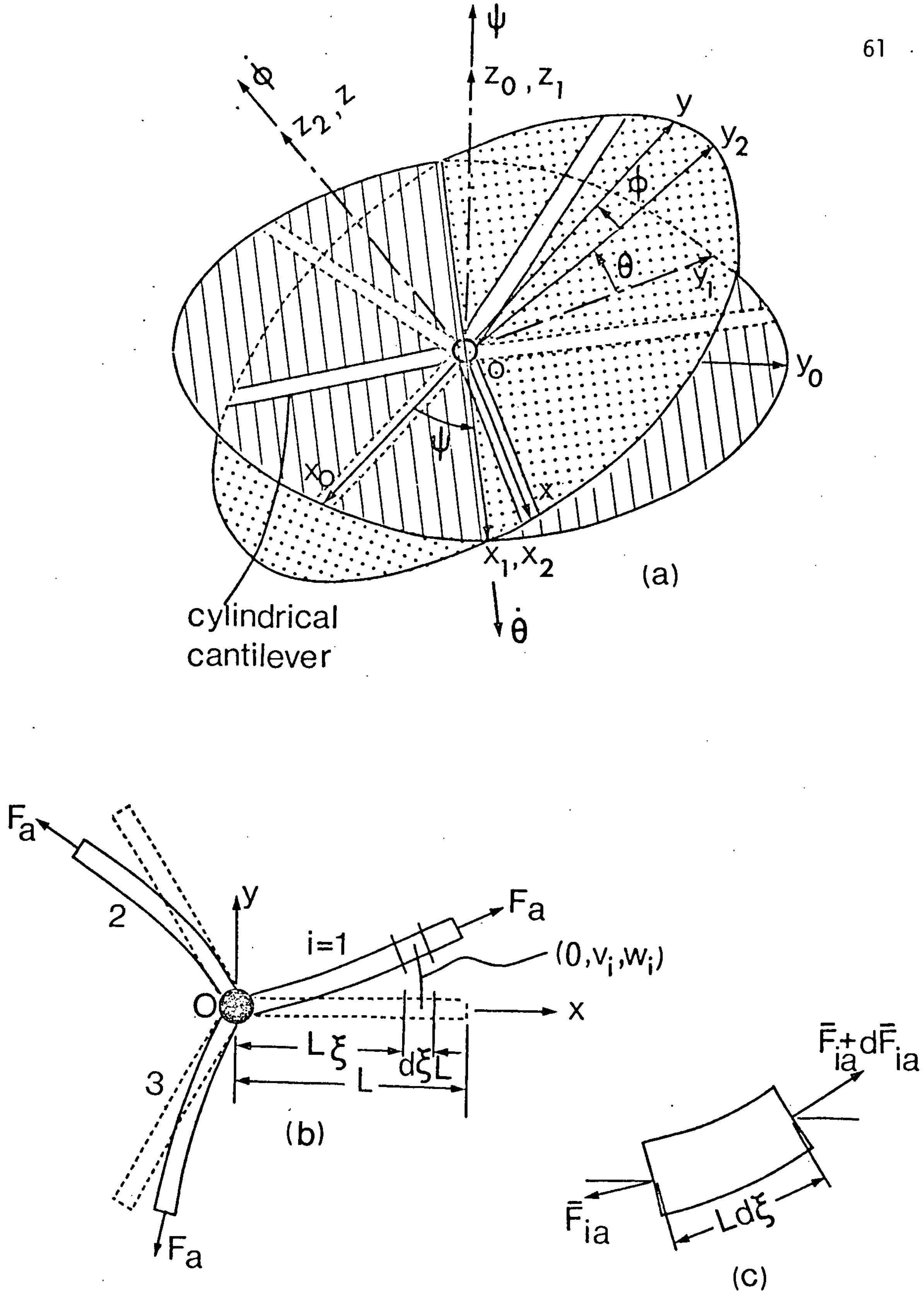

Figure 3-1 Geometry of motion of an array formed by three neutrally buoyant inflated cylindrical cantilevers and a central head

the x-y plane contains the array, while the x-axis coincides with the central line of one of the legs. The orientation of the array can be specified with respect to the inertial co-ordinate system x_0, y_0, z_0 by a vertical displacement z_h of the centre of the head along the z_0 axis and a set of Eulerian rotations: ϕ about the z_0-axis giving x_1, y_1, z_1; θ about the x_1-axis yielding x_2, y_2, z_2; and ψ about the z_2-axis resulting in the final body axes x, y, z. Subsequently, the flexural deflections v_i and w_i $(i = 1,2,3)$, in and out of the plane of the array, respectively, are imposed.

The co-ordinates of a point in the systems x_0, y_0, z_0 and x, y, z are related by

$$(r_0) = [R](r) + (r_h) \quad , \tag{3.1a}$$

where

$$(r_0) \equiv \begin{pmatrix} x_0 \\ y_0 \\ z_0 \end{pmatrix}, \quad (r) \equiv \begin{pmatrix} x \\ y \\ z \end{pmatrix}, \quad (r_h) \equiv \begin{pmatrix} 0 \\ 0 \\ z_h \end{pmatrix}, \tag{3.1b}$$

and

$$[R] = \begin{bmatrix} \cos\phi & -\sin\phi & 0 \\ \sin\phi & \cos\phi & 0 \\ 0 & 0 & 1 \end{bmatrix} \begin{bmatrix} 1 & 0 & 0 \\ 0 & \cos\theta & -\sin\theta \\ 0 & \sin\theta & \cos\theta \end{bmatrix} \begin{bmatrix} \cos\psi & -\sin\psi & 0 \\ \sin\psi & \cos\psi & 0 \\ 0 & 0 & 1 \end{bmatrix} . \tag{3.1c}$$

The kinetic energy (accounting for added inertia) associated with an element of mass dm located at $\bar{r}$ referred to the body co-ordinate system is given by

$$dT_a = (1/2)(1+C_m)\ dm\ \dot{\bar{r}}_0\cdot\dot{\bar{r}}_0$$

$$= (1/2)(1+C_m)\ dm\ [\dot{z}_h^2+2\dot{z}_h\{\dot{x}\ \sin\theta\sin\psi+\dot{y}\ \sin\theta\cos\psi+\dot{z}\ \cos\theta$$

$$+ x(\dot{\theta}\cos\theta\sin\psi+\dot{\psi}\sin\theta\cos\psi)+y(\dot{\theta}\cos\theta\cos\psi-\dot{\psi}\sin\theta\sin\psi)+z(-\dot{\theta}\sin\theta)\}$$

$$+ \dot{x}^2+\dot{y}^2+\dot{z}^2+2(\dot{\phi}\cos\theta+\dot{\psi})(x\dot{y}-y\dot{x})+2(\dot{\phi}\sin\theta\sin\psi+\dot{\theta}\cos\psi)(y\dot{z}-z\dot{y})$$

$$+2(\dot{\phi}\sin\theta\cos\psi-\dot{\theta}\sin\psi)(z\dot{x}-x\dot{z})+x^2\{\dot{\phi}^2(1-\sin^2\theta\sin^2\psi)+\dot{\theta}^2\sin^2\psi+\dot{\psi}^2$$

$$-2\dot{\phi}\dot{\theta}\sin\theta\sin\psi\cos\psi+2\dot{\phi}\dot{\psi}\cos\theta\}+y^2\{\dot{\phi}^2(1-\sin^2\theta\cos^2\psi)+\dot{\theta}^2\cos^2\psi+\dot{\psi}^2$$

$$+2\dot{\phi}\dot{\theta}\sin\theta\sin\psi\cos\psi+2\dot{\phi}\dot{\psi}\cos\theta\}+z^2(\dot{\phi}^2\sin^2\theta+\dot{\theta}^2)+2xy\{-\dot{\phi}^2\sin^2\theta\sin\psi\cos\psi$$

$$+\dot{\theta}^2\sin\psi\cos\psi+\dot{\phi}\dot{\theta}\sin\theta(\sin^2\psi-\cos^2\psi)\}+2yz\{-\dot{\phi}^2\sin\theta\cos\theta\cos\psi+\dot{\phi}\dot{\theta}\cos\theta\sin\psi$$

$$+\dot{\theta}\dot{\psi}\sin\psi-\dot{\phi}\dot{\psi}\sin\theta\cos\psi\}+2zx\{-\dot{\phi}^2\sin\theta\cos\theta\sin\psi-\dot{\phi}\dot{\theta}\cos\theta\cos\psi-\dot{\theta}\dot{\psi}\cos^2\theta\cos\psi$$

$$-\dot{\phi}\dot{\psi}\sin\theta\sin\psi\}]\ , \qquad (3.2)$$

where C_m is the added mass coefficient for a circular cylinder.

The flexural displacements of a point on i^{th} leg at a distance $\xi L(0\leq\xi\leq 1)$ from the root can be resolved into two components v_i and w_i as shown in Figure 3-1b. Hence, the co-ordinates of the above point in the xyz-system are

$$(\xi L\cos I_i - v_i \sin I_i), \quad (\xi L\sin I_i + v_i \cos I_i) \quad , w_i \; , \tag{3.3a}$$

where $I_i = 2\pi(i-1)/3 \; , \quad i = 1,2,3 \; .$ (3.3b)

The displacements v_i and w_i may be expanded in series forms,

$$v_i = \sum_{j=1}^{\infty} \Phi_j(\xi) A_{ij}(t) \quad , \tag{3.4a}$$

and

$$w_i = \sum_{j=1}^{\infty} \Phi_j(\xi) B_{ij}(t) \quad , \tag{3.4b}$$

where $\Phi_j(\xi)$, $j = 1,2,\cdots\infty$, are a set of orthonormal functions. If the two infinite series are truncated to finite number of terms during numerical computations, there will result a residual error which can be minimized by selecting the above functions such that they satisfy the boundary conditions for a cantilever with a follower force, i.e.,

$$\Phi_j(0) = \frac{\partial \Phi_j(0)}{\partial \xi} = \frac{\partial^2 \Phi_j(1)}{\partial \xi^2} = \frac{\partial^3 \Phi_j(1)}{\partial \xi^3} = 0 \quad .$$

It may be noted that if the axial force is not of the follower type but has a fixed direction, the third derivative at the free end is not zero[52]. One may choose Φ_j to be the eigenvalues of a cantilever with no axial force as they satisfy the same boundary conditions, i.e.,

$$\Phi_j(\xi) = (\cosh\mu_j\xi - \cos\mu_j\xi) - \sigma_j(\sinh\mu_j\xi - \sin\mu_j\xi), \qquad (3.5a)$$

where μ_j are the roots of the equation

$$1 + \cosh\mu \cos\mu = 0 \;, \qquad (3.5b)$$

and

$$\sigma_j = (\cosh\mu_j + \cos\mu_j)/(\sinh\mu_j + \sin\mu_j) \;. \qquad (3.5c)$$

Note that Equation (3.5c) represents a particular case of (2.19c) corresponding to zero pressure parameter. Integration of dT_a from Equation (3.2) with the help of Equations (3.3) to (3.5) and summation over the three legs yield

$$T_a = (1/2)m(1+C_m)[3\dot{z}_h^2+(1/2)L^2\{\dot{\phi}^2\sin^2\theta+\dot{\theta}^2+2(\dot{\phi}\cos\theta+\dot{\psi})^2\}$$

$$+\sum_{i=1}^{3}\sum_{j=1}^{3}[\dot{A}_{ij}^2+\dot{B}_{ij}^2+2\dot{z}_h\delta_j\{\sin\theta\cos\psi_i\dot{A}_{ij}+\cos\theta\dot{B}_{ij}+(\dot{\theta}\cos\theta\cos\psi_i$$

$$-\dot{\psi}\sin\theta\sin\psi_i)A_{ij}-\dot{\theta}\sin\theta B_{ij}\}+(4L/\mu_j^2)\{(\dot{\phi}\cos\theta+\dot{\psi})\dot{A}_{ij}-(\dot{\phi}\sin\theta\cos\psi_i$$

$$-\dot{\theta}\sin\psi_i)\dot{B}_{ij}\}+2(\dot{\phi}\sin\theta\sin\psi_i+\dot{\theta}\cos\psi_i)\delta_j(A_{ij}\dot{B}_{ij}-\dot{A}_{ij}B_{ij})$$

$$-(2L/\mu_j^2)\{(\dot{\phi}^2\sin^2\theta-\dot{\theta}^2)\sin 2\psi_i-2\dot{\phi}\dot{\theta}\sin\theta\cos 2\psi_i\}A_{ij}+(2L/\mu_j^2)*$$

$$\{\dot{\phi}^2\sin 2\theta\sin\psi_i+2\dot{\phi}\dot{\theta}\cos\theta\cos\psi_i+2\dot{\theta}\dot{\psi}(\cos^2\theta\cos\psi\cos I_i-\sin\psi\sin I_i)\}B_{ij}$$

$$+\{(\dot\phi^2+\dot\psi^2+2\dot\phi\dot\psi\cos\theta)-(\dot\phi^2\sin^2\theta-\dot\theta^2)\cos^2\psi_i+\dot\phi\dot\theta\sin\theta\sin2\psi_i\}A_{ij}^2$$

$$+(\dot\phi^2\sin^2\theta+\dot\theta^2)B_{ij}^2+\{-\dot\phi^2\sin2\theta\cos\psi_i+2\dot\phi\dot\theta\cos\theta\sin\psi_i+2\dot\theta\dot\psi(\cos^2\theta\cos\psi\sin I_i$$

$$+\sin\psi\cos I_i)-2\dot\phi\dot\psi\sin\theta\cos\psi_i\}A_{ij}B_{ij}]] \quad , \tag{3.6a}$$

$$\text{where} \quad \psi_i = \psi+I_i \quad \text{and} \quad \delta_j = 2\sigma_j/\mu_j \quad . \tag{3.6b}$$

The kinetic energy associated with the central head is

$$T_h = (1/2)[(1+C_{mh})m_h\dot z_h^2+I_{xxa}(\dot\phi\sin\theta\sin\psi+\dot\theta\cos\psi)^2+I_{yya}(\dot\phi\sin\theta\cos\psi$$

$$-\dot\theta\sin\psi)^2+I_{zza}(\dot\phi\cos\psi+\dot\psi)^2] \quad , \tag{3.7}$$

where C_{mh} is the added inertia coefficient, m_h the mass and I_{xxa}, I_{yya} and I_{zza} the apparent moments of inertia of the head about x, y and z axes, respectively. The total kinetic energy T is the sum of T_a and T_h as given by (3.6a) and (3.7), respectively.

The potential energy U due to the flexural displacements can be expressed as

$$U = (1/2)\sum_{i=1}^{3} EI \int_0^L \left[\left\{\frac{\partial^2 v_i}{\partial(L\xi)^2}\right\}^2 + \left\{\frac{\partial^2 w_i}{\partial(L\xi)^2}\right\}^2\right] d(L\xi)$$

$$= (EI/2L^3)\sum_{i=1}^{3}\sum_{j=1}^{\infty}\mu_j^4(A_{ij}^2+B_{ij}^2) \quad . \tag{3.8}$$

The axial tensions arising due to the internal pressure give rise to nonconservative follower forces which do not contribute to the potential energy. However, the resulting generalized forces Q'_{Aij} and Q'_{Bij} must be evaluated. Consider an element of length $d(L\xi)$ on the i^{th} leg at a distance $L\xi$ from the root (Figure 3-1c). The forces acting at the two ends of the element are $\bar{F}_{ia}$ and $\bar{F}_{ia} + \frac{\partial \bar{F}_{ia}}{\partial \xi} d\xi$, where $\bar{F}_{ia}$ is given by

$$\bar{F}_{ia} = F_a[\{\cos I_i-(\frac{\partial v_i}{\partial \xi} \sin I_i)/L\}\bar{u}_x + \{\sin I_i+(\frac{\partial v_i}{\partial \xi} \cos I_i)/L\}\bar{u}_y$$

$$+\{(\frac{\partial w_i}{\partial \xi})/L\}\bar{u}_z] , \tag{3.9}$$

and F_a is the axial tension related to the internal pressure by

$$F_a = p\pi d^2/4 \quad . \tag{3.10}$$

The contribution dQ'_{Aij} to the generalized force Q'_{Aij} from this element is given by

$$dQ'_{Aij} = (d\bar{F}_{ia}) \cdot \left(\frac{\partial \bar{r}_i}{\partial A_{ij}}\right) = \left(\frac{\partial \bar{F}_{ia}}{\partial \xi} d\xi\right) \cdot \left(\frac{\partial \bar{r}_i}{\partial A_{ij}}\right) .$$

Hence, on integration

$$Q'_{Aij} = (F_a/L) \sum_{s=1}^{\infty} C_{sj} A_{is} \quad , \tag{3.11a}$$

where C_{sj} is defined by (2.47b). Similarly Q'_{Bij} can be written as

$$Q'_{Bij} = (F_a/L) \sum_{s=1}^{\infty} C_{sj} B_{is} \quad . \tag{3.11b}$$

It is clear that the contributions of the axial force to Q_ϕ, Q_θ and Q_ψ are zero.

The equation of motion corresponding to the generalized coordinate q_k is

$$\frac{d}{dt}\left(\frac{\partial T}{\partial \dot{q}_k}\right) - \frac{\partial T}{\partial q_k} + \frac{\partial U}{\partial q_k} = Q_k \quad ,$$

where Q_k is the nonconservative generalized force consisting of Q'_k due to the follower force and Q''_k arising because of the hydrodynamic damping. For example, the equation of motion in the A_{ij} degree of freedom is given by,

$$\begin{aligned}
&\ddot{A}_{ij}+\delta_j\ddot{z}_h\sin\theta\cos\psi_i+(2L/\mu_j^2)\{\ddot{\phi}\cos\theta-2\dot{\phi}\dot{\theta}\sin\theta\sin^2\psi_i+\ddot{\psi}+\tfrac{1}{2}(\dot{\phi}^2\sin^2\theta-\dot{\theta}^2)\sin2\psi_i\} \\
&\quad -2\delta_j\dot{B}_{ij}(\dot{\phi}\sin\theta\sin\psi_i+\dot{\theta}\cos\psi_i)-A_{ij}\{(\dot{\phi}^2+\dot{\psi}^2+2\dot{\phi}\dot{\psi}\cos\theta)-(\dot{\phi}^2\sin^2\theta-\dot{\theta}^2)\cos^2\psi_i \\
&\quad +\dot{\phi}\dot{\theta}\sin\theta\sin2\psi_i\}-B_{ij}[\delta_j\{(\ddot{\phi}\sin\theta+\dot{\phi}\dot{\theta}\cos\theta-\dot{\theta}\dot{\psi})\sin\psi_i+(\dot{\phi}\dot{\psi}\sin\theta+\ddot{\theta})\cos\psi_i\} \\
&\quad +\dot{\phi}\dot{\theta}\cos\theta\sin\psi_i-(\dot{\phi}^2\sin\theta\cos\theta-\dot{\theta}\dot{\psi}\cos^2\theta+\dot{\phi}\dot{\psi}\sin\theta)\cos\psi_i]+[EI\mu_j^4/m(1+C_m)L^3]A_{ij} \\
&\quad = [F_a/m(1+C_m)L]\sum_{s=1}^{\infty} C_{sj}A_{is}+Q''_{Aij}/m(1+C_m) \quad .
\end{aligned} \tag{3.12}$$

Similarly, the equations for B_{ij}, z_h, ϕ, θ and ψ degrees of freedom may be obtained. This leads to a set of coupled nonlinear ordinary differential equations, which is not easily tractable. Hence, some simplifications must be made. If the displacements are assumed to be small, the second and third order terms may be ignored. The linearized equations thus obtained are

$$\ddot{A}_{ij}+(2L/\mu_j^2)(\ddot{\phi}+\ddot{\psi})+\{EI/m(1+C_m)L^3\}\mu_j^4 A_{ij}-\{F_a/m(1+C_m)L\}\sum_{s=1}^{\infty} C_{sj}A_{is} = 0, \tag{3.13a}$$

$$\sum_{i=1}^{3}\sum_{j=1}^{\infty}(2L/\mu_j^2)\ddot{A}_{ij}+[L^2+\{I_{zza}/m(1+C_m)\}](\ddot{\phi}+\ddot{\psi}) = 0, \tag{3.13b}$$

$$[3+\{m_h(1+C_{mh})/m(1+C_m)\}]\ddot{z}_h+\sum_{i=1}^{3}\sum_{j=1}^{\infty}\delta_j\ddot{B}_{ij} = 0, \tag{3.13c}$$

$$\delta_j\ddot{z}_h+\ddot{B}_{ij}+(2L/\mu_j^2)\ddot{\theta}\sin I_i+\{EI/m(1+C_m)L^3\}\mu_j^4 B_{ij}$$

$$-\{F_a/m(1+C_m)L\}\sum_{s=1}^{\infty} C_{sj}B_{is} = 0, \tag{3.13d}$$

$$\sum_{i=1}^{3}\sum_{j=1}^{\infty}(2L/\mu_j^2)\ddot{B}_{ij}\sin I_i+[L^2/2+\{I_{xxa}/m(1+C_m)\}]\ddot{\theta} = 0, \tag{3.13e}$$

$$i = 1, 2, 3; \quad j = 1, 2, \cdots \infty .$$

Defining

$$a_{ij} = A_{ij}/L, \quad b_{ij} = B_{ij}/L, \quad \eta_h = z_h/L \quad \text{and}$$

$$\tau = t[EI/m(1+C_m)L^3]^{1/2} ,$$

Equations (3.13) can be nondimensionalized to yield

$$a''_{ij}+(2/\mu_j^2)(\psi''+\phi'')+\mu_j^4 a_{ij}-P\sum_{s=1}^{\infty}C_{sj}a_{is} = 0 \ , \tag{3.14a}$$

$$\sum_{i=1}^{3}\sum_{j=1}^{\infty}(2/\mu_j^2)a''_{ij}+(1+I_z^*)(\psi''+\phi'') = 0 \ , \tag{3.14b}$$

$$(3+r_{h\ell})\eta''_h+\sum_{i=1}^{3}\sum_{j=1}^{\infty}\delta_j b''_{ij} = 0 \ , \tag{3.14c}$$

$$\delta_j\eta''_h+b''_{ij}+(2/\mu_j^2)\theta''\sin I_i+\mu_j^4 b_{ij}-P\sum_{s=1}^{\infty}C_{sj}b_{is} = 0 \ , \tag{3.14d}$$

$$\sum_{i=1}^{3}\sum_{j=1}^{\infty}(2/\mu_j^2)b''_{ij}\sin I_i+(1+2I_x^*)\theta''/2 = 0 \ , \tag{3.14e}$$

$$i = 1,\ 2,\ 3; \quad j = 1,\ 2,\ \cdots \infty$$

where P is given by (2.15) and

$$r_{h\ell} = m_h(1+C_{mh})/m(1+C_m) \ , \tag{3.15a}$$

$$I_x^* = I_{xxa}/m(1+C_m)L^2, \quad I_y^* = I_{yya}/m(1+C_m)L^2,$$

$$I_z^* = I_{zza}/m(1+C_m)L^2, \tag{3.15b}$$

and prime denotes differentiation with respect to τ. It may be noted that for small amplitude motions, the rotations ψ and ϕ always appear as a sum and hence can be replaced by one variable. Elimination of $(\psi+\phi)$, η_h and θ from the above equations gives

$$a''_{ij}-\sum_{r=1}^{3}\sum_{s=1}^{\infty}\{4a''_{rs}/\mu_j^2\mu_s^2(1+I_z^*)\}+\mu_j^4 a_{ij}-P\sum_{s=1}^{\infty}C_{sj}a_{is} = 0, \tag{3.16a}$$

$$b''_{ij}-\sum_{r=1}^{3}\sum_{s=1}^{\infty}[\{\delta_j\delta_s/(3+r_{h\ell})\}+\{8\sin I_i\sin I_r/\mu_j^2\mu_s^2(1+2I_x^*)\}]b''_{rs}$$

$$+\mu_j^4 b_{ij}-P\sum_{s=1}^{\infty}C_{sj}b_{is} = 0 , \tag{3.16b}$$

$$i \text{ and } r = 1, 2, 3; \quad j \text{ and } s = 1, 2, \cdots \infty .$$

These two sets of equations can be analyzed separately. Assuming the solution to be of the form $a_{ij} = |a_{ij}|e^{i\omega\tau}$, Equations (3.16) reduce to

$$(\mu_j^4-\lambda^4)a_{ij}+\sum_{r=1}^{3}\sum_{s=1}^{\infty}[4\lambda^4/\mu_j^2\mu_s^2(1+I_z^*)]a_{rs}-P\sum_{s=1}^{\infty}C_{sj}a_{is} = 0 , \tag{3.17a}$$

and

$$(\mu_j^4-\lambda^4)b_{ij}+\sum_{r=1}^{3}\sum_{s=1}^{\infty}\lambda^4[\{\delta_j\delta_s/(3+r_{h\ell})\}+\{8\sin I_i\sin I_r/\mu_j^2\mu_s^2(1+2I_x^*)\}]b_{rs}$$

$$-P\sum_{s=1}^{\infty}C_{sj}b_{is} = 0, \quad i = 1, 2, 3; \; j = 1, 2, \cdots \infty . \tag{3.17b}$$

where $\omega = \lambda^2$.

This represents two sets each containing an infinite number of frequency equations. In the actual computation for the eigenvalues, however, they were truncated to the first six modes so that each contained 3 x 6 equations.

3.2 Results and Discussion

3.2.1 Inplane motion

The three sets of eigenvalues obtained from Equation (3.17a) correspond to the inplane motion of the array. Two of these are identical while the third set is different. With the help of (3.14b), it can be noticed that there are two types of inplane motion:

(i) oscillation of the cantilevers without any rotation of the central body;

(ii) coupled inplane motion of the array.

The former corresponds to the repeated eigenvalues which are identical to those of a single cantilever having the same axial tension parameter P. For a given P, the eigenvalues for the coupled motion are higher than those in the uncoupled motion, when the lower two modes are considered. But for the higher modes there is little difference between the two sets of frequencies.

When there is no inplane rotation of the array, the corresponding points on two legs move in one direction while that on the third moves in the opposite direction. But in the coupled motion, the corresponding points on all the three legs move in one direction so as

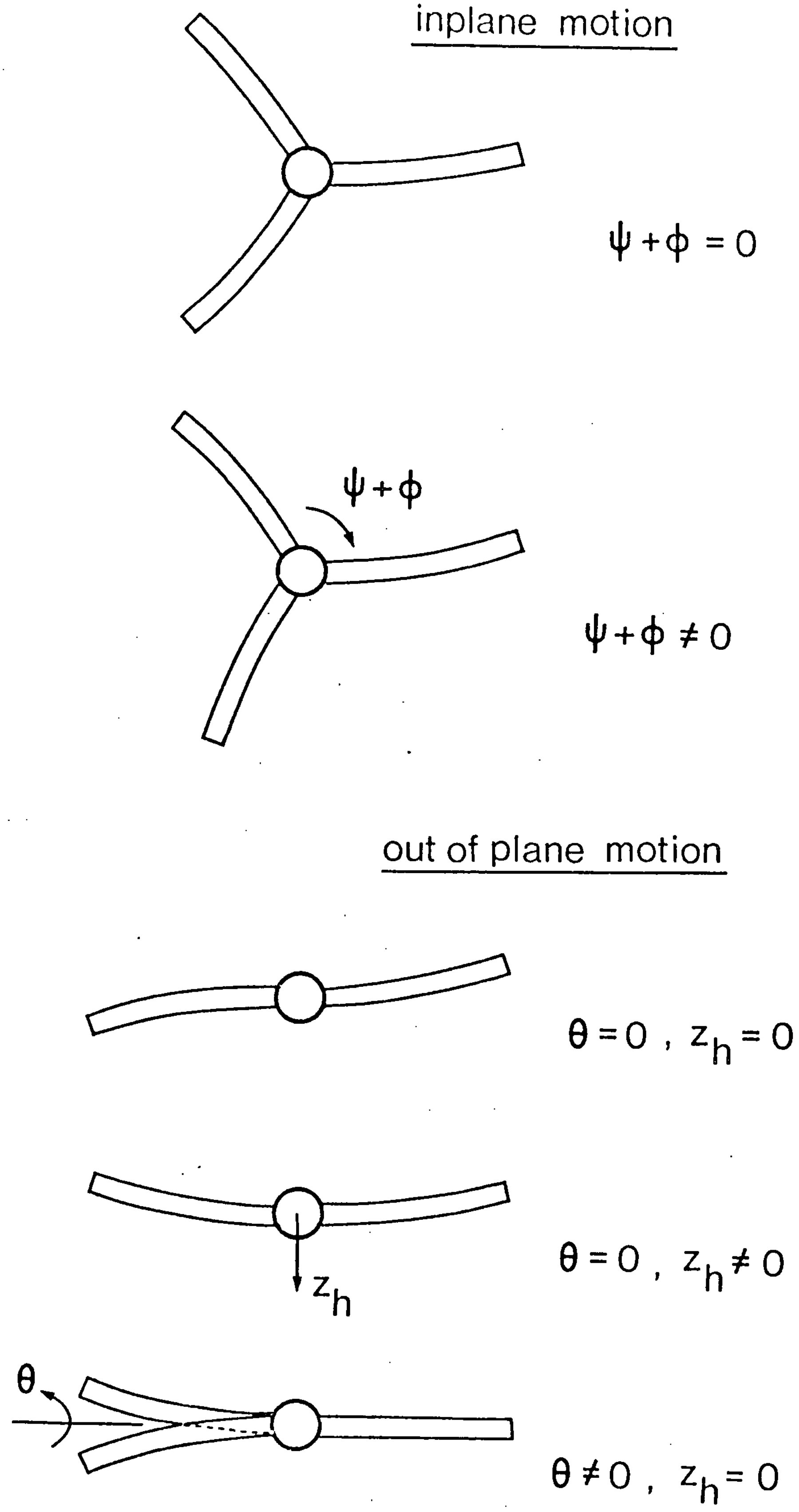

Figure 3-2 Typical inplane and out of plane motion of the array

to balance the moment caused by an opposite rigid body rotation of the array (Figure 3-2).

Since the repeated eigenvalues correspond to a single cylinder with axial tension, their dependence on P is as observed before (Figure 2-8b). Clearly, they are independent of I_z^*. But the coupled eigenvalues are higher for lower I_z^*, gradually approaching the uncoupled values as I_z^* increases (Figure 3-3a). If the inertia parameter is not too small, the variation of the coupled eigenvalues with increasing P is similar to the previous case. But for small I_z^* and above certain P, there is a possibility for the eigenvalues to appear as complex conjugates thus suggesting instability. However, the hydrodynamic damping, which has been neglected because of its second order effect, will oppose this instability to some extent. Since the complex eigenvalues for a real system appear as conjugate pairs, the variation with P before instability is such as to make the real parts of consecutive eigenvalues identical. For example, in Figure 3-3a, the second eigenvalue increases while the third decreases with P, before the instability region shown by the dotted lines is reached.

3.2.2 Out of plane motion

The three sets of eigenvalues obtained from Equation (3.17b) correspond to the out of plane motion of the array. In conjunction with Equations (3.14c) and (3.14e), it is observed that the three sets correspond to the following types of motion:

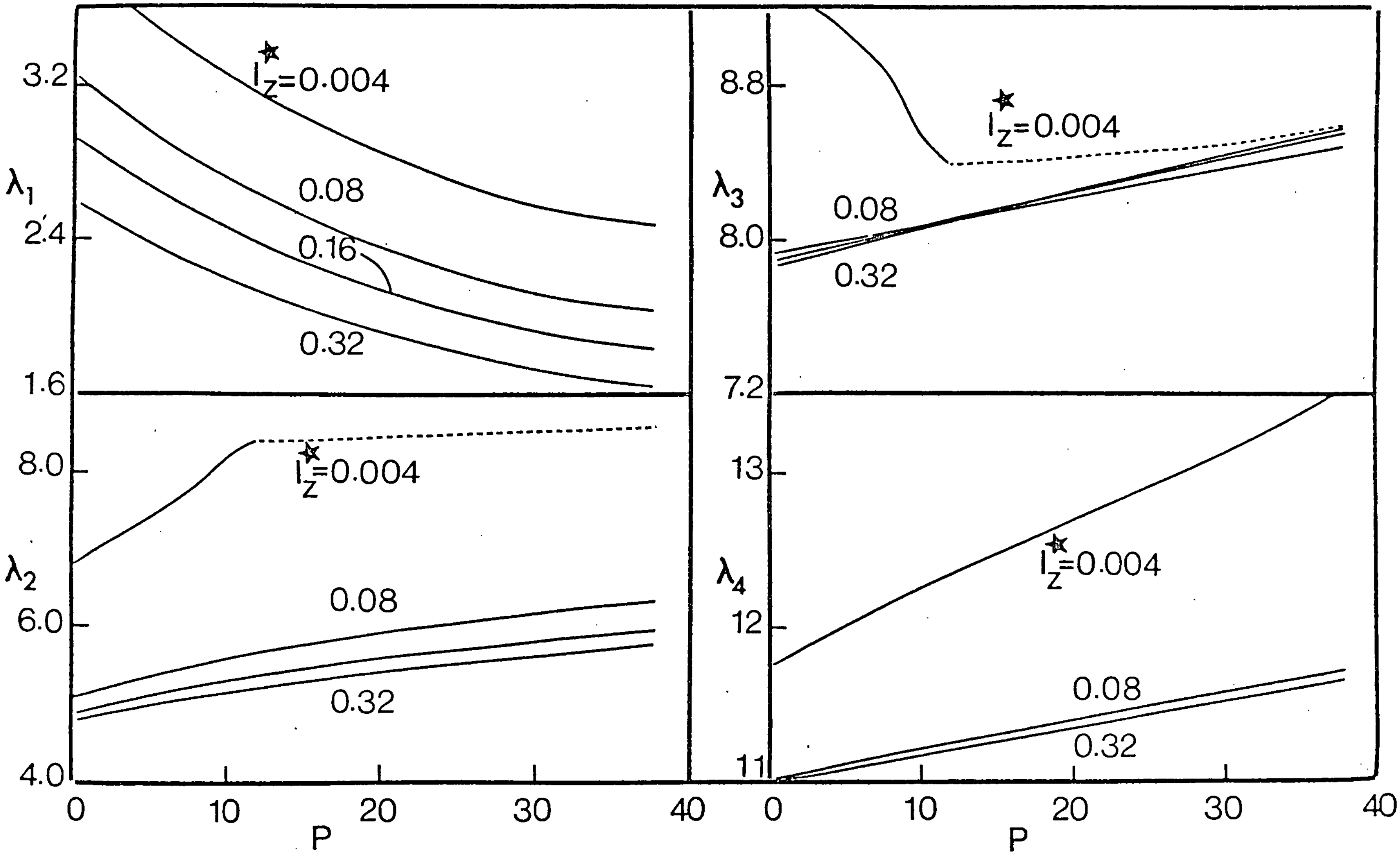

Figure 3-3 Variation of eigenvalues of the coupled motion of the array: (a) inplane motion

(i) The central head remains stationary and there is no rolling motion of the array. Here the eigenvalues are independent of $r_{h\ell}$ and I_x^* and coincide with those of a single cantilever having the same P.

(ii) There is a vertical motion of the central body, but no rolling motion of the array. These eigenvalues are greater than those in the previous set, but the difference becomes smaller for higher modes. The variation of the eigenvalues with P is also similar to that of the first set, but now they depend on $r_{h\ell}$ and I_x^* as well. As $r_{h\ell}$ and I_x^* increase, the eigenvalues decrease, gradually approaching the first set (Figure 3-3b).

(iii) There is no vertical motion of the central head, but the array goes through a rigid body rolling motion. These eigenvalues are greater than those in the second set for the lower modes, but slightly smaller for the higher modes. Their dependence on P is similar to that of the coupled inplane motion. As a matter of fact, for a given I_x^*, there exists an I_z^* such that the eigenvalues for these two types of motion are identical.

3.3 Concluding Remarks

Based on the analysis of inplane and out of plane motions of an array of three cantilevers, joined to a central body, with follower forces, the following remarks can be made:

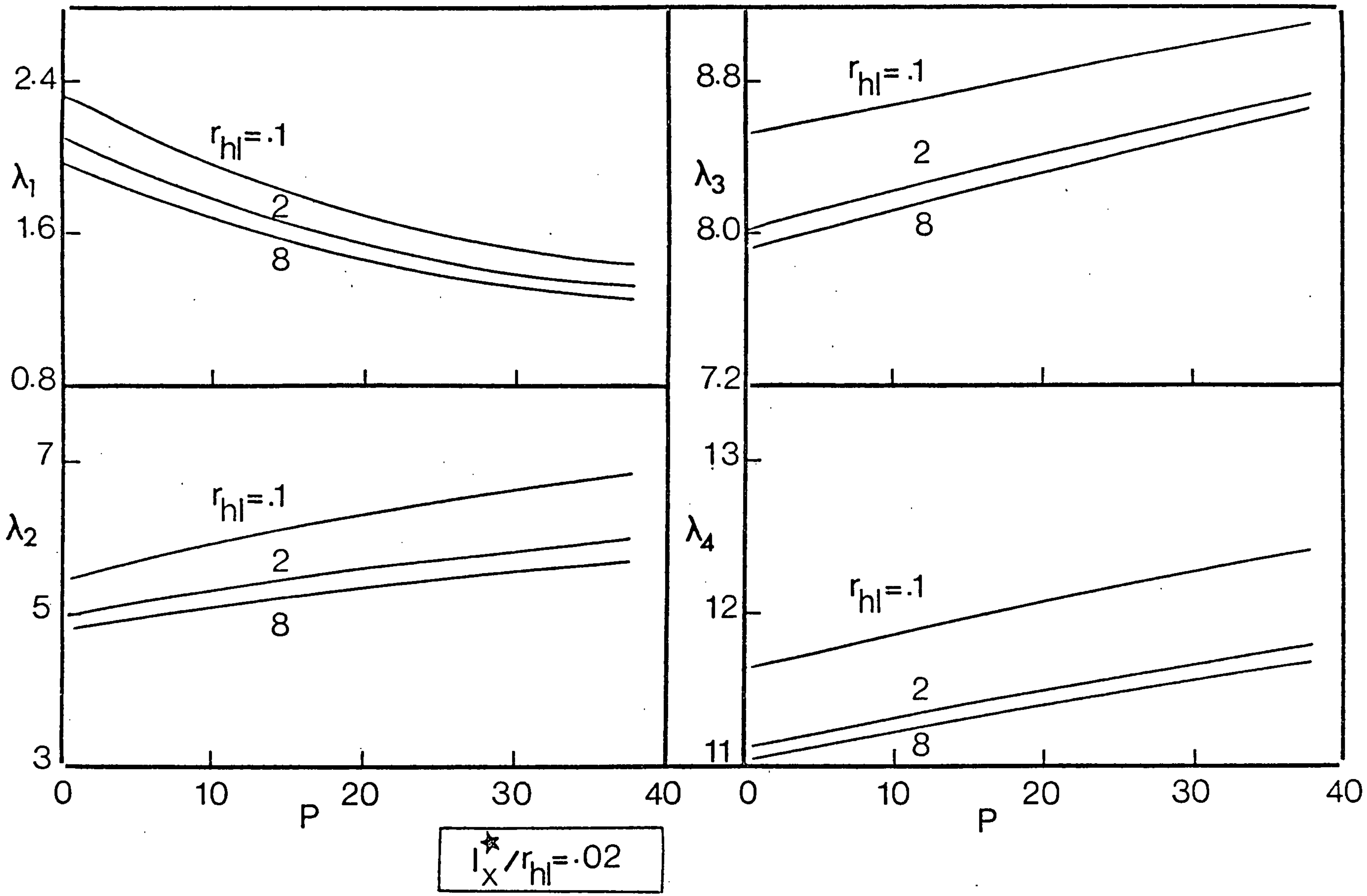

Figure 3-3 Variation of eigenvalues of the coupled motion of the array: (b) out of plane motion

(i) The inplane motion of the array exhibits two different characters -- one involves uncoupled oscillations of the legs at their own natural frequency with the central head remaining stationary, while the other represents the coupled flexural-rotational motion of the whole array. The former corresponds to two sets of repeated eigenvalues.

(ii) The out of plane motion consists of three different forms -- flexural vibrations of the cantilevers at their natural frequency with the central body at rest; bending displacements of the legs superposed on the vertical motion of the array, in the absence of its rolling motion; and flexural-rotational out of plane motion without the vertical motion of the head.

(iii) For pure out of plane motion (without rolling), the eigenvalues approach those of a single cylinder as the inertia parameters are increased. If these parameters are not too small, the eigenvalues of coupled flexural-rotational motion also exhibit a similar behaviour.

(iv) For small values of inertia parameters, there is a possibility of unstable coupled motion above a certain magnitude of P.

4. VERTICAL MOTIONS OF A BUOY-CABLE-ARRAY SYSTEM

The coupled motion of an array having been investigated, the next logical step would be to consider the submarine detection system itself which consists of a similar array joined to a buoy by an elastic cable. It is a rather complex problem due to the large number of degrees of freedom involved. Hence, to start with, only the vertical motion of the assembly is considered.

In this analysis, the cable is replaced by a spring of equivalent stiffness such that the system reduces to a buoy and an array connected by a spring. The central head of the array is allowed to move vertically and the flexural displacements of the legs are superposed on this motion. To start with, a general formulation of the problem is presented using the classical Lagrangian procedure. The free vibration of the system is considered first by equating the forcing terms in the equations of motion to zero. The influence of the important system parameters on the natural frequencies of vertical motion is evaluated. Subsequently, the motion excited by a sinusoidal surface wave is investigated. Attempts are made to determine the effects of various parameters on the tip displacements where the hydrophones are located.

4.1 Formulation of the Problem

Consider a system comprising of a cylindrical surface float connected by an elastic cable to a central head, supporting three

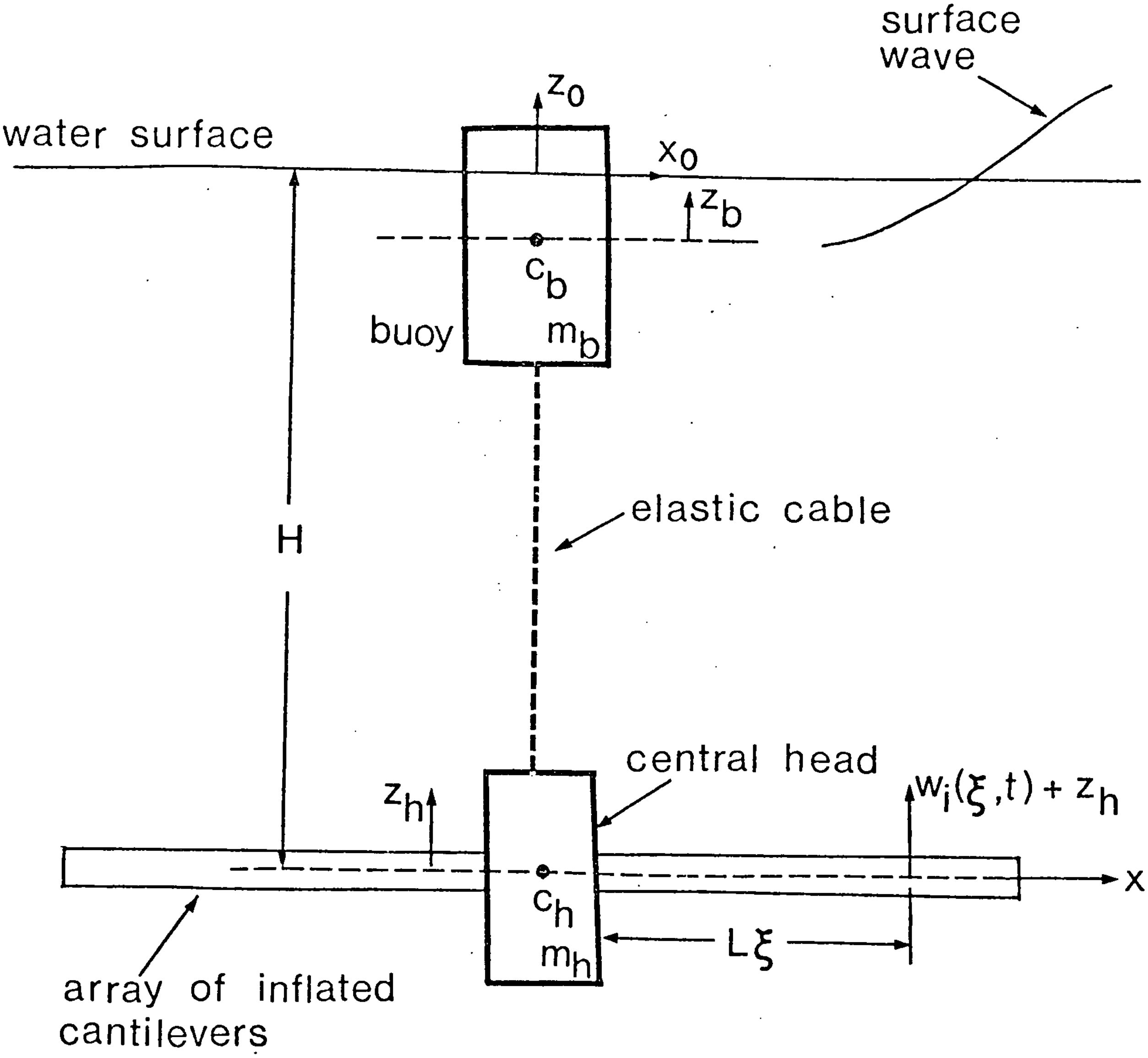

Figure 4-1 Geometry of vertical motion of the buoy-cable-array assembly

neutrally buoyant inflated cylindrical cantilevers (Figure 4-1). Let m_b and m_h be the masses of the buoy and central head, respectively, while L and d the length and diameter of each leg. The cable is replaced by an equivalent spring of stiffness k. An inertial co-ordinate system x_0, y_0, z_0 is located at the free surface as shown in Figure 4-1 such that $(0, 0, z_{b0})$ and $(0, 0, -H)$ are the co-ordinates of the equilibrium positions of the centres of mass of the buoy and central head, respectively. At any instant t, the locations of the centres of mass of the buoy and the head and a point on the i^{th} leg at a distance $\xi L (0 \leq \xi \leq 1)$ from the root, are given by $(0,0,z_{b0}+z_b)$, $(0,0,-H+z_h)$ and $(\xi L\cos I_i,\ \xi L\sin I_i,\ -H+z_h+w_i)$, respectively, where w_i is the flexural displacement and I_i were defined in Equation (3.3b).

As before, w_i can be expanded in a series form,

$$w_i = \sum_{j=1}^{\infty} \Phi_j(\xi) B_{ij}(t) \quad , \tag{4.1}$$

where $\Phi_j(\xi)$ is given by Equation (3.5).

The kinetic energy T of the system is given by

$$T = (m_b/2)\dot{z}_b^2 + (m_h/2)\dot{z}_h^2 + (1/2)\sum_{i=1}^{3} \int_m \{\dot{z}_h + \sum_{j=1}^{\infty} \dot{B}_{ij}\Phi_j\}^2 dm$$

$$= (m_b/2)\dot{z}_b^2 + (m_h/2)\dot{z}_h^2 + (m/2)[3\dot{z}_h^2 + \sum_{i=1}^{3} \sum_{j=1}^{\infty} \dot{B}_{ij}^2 + 2\dot{z}_h \delta_j \dot{B}_{ij}] \ , \tag{4.2}$$

where m is the mass of each cylinder including the water inside it and δ_j as defined in (3.6b). This does not include the kinetic energy associated with the apparent inertia of the assembly as the effect could be accounted in the generalized forces.

The potential energy U of the system consists of three parts: the energy associated with the buoyancy of the buoy, the elastic energy stored in the cable, and that due to the flexural displacements of the legs. The nonconservative follower forces arising because of the internal pressure do not contribute to the potential energy. Hence,

$$U = (c/2)(z_b-z_w)^2+(k/2)(z_b-z_h)^2+(EI/2L^3)\sum_{i=1}^{3}\sum_{j=1}^{\infty}\mu_j^4 B_{ij}^2 , \qquad (4.3)$$

where c is the equivalent stiffness due to buoyancy and can be written as

$$c = (\rho_w g)\ (\text{Area of the cross section of the buoy}),$$

and z_w the displacement of a water particle due to the wave at the free surface. Using Equations (4.2) and (4.3), the classical Lagrangian formulation yields,

$$m_b\ddot{z}_b+c(z_b-z_w)+k(z_b-z_h) = Q_{zb} , \qquad (4.4a)$$

$$(m_h+3m)\ddot{z}_h+k(z_h-z_b)+m\sum_{i=1}^{3}\sum_{j=1}^{\infty}\delta_j\ddot{B}_{ij} = Q_{zh} , \qquad (4.4b)$$

$$m(\ddot{B}_{ij}+\delta_j\ddot{z}_h)+(EI/L^3)\mu_j^4 B_{ij} = Q_{Bij} , \qquad (4.4c)$$

$$i = 1,2,3; \quad j = 1,2,\cdots\infty;$$

where Q_{zb}, Q_{zh} and Q_{Bij} are the generalized forces corresponding to z_b, z_h and B_{ij} degrees of freedom, respectively, arising due to the hydrodynamic forces and internal pressure.

The hydrodynamic forces F_b and F_h acting on the buoy and central head, respectively, are given by

$$F_b = -a_b(\ddot{z}_b-\ddot{z}_w)-(\rho_w/2)C_{db}S_b(\dot{z}_b-\dot{z}_w)|\dot{z}_b-\dot{z}_w| \ , \tag{4.5a}$$

and

$$F_h = -a_h(\ddot{z}_h-\ddot{z}_{wh})-(\rho_w/2)C_{dh}S_h(\dot{z}_h-\dot{z}_{wh})|\dot{z}_h-\dot{z}_{wh}| \ , \tag{4.5b}$$

where a_b, a_h, C_{db}, C_{dh}, S_b and S_h are the corresponding added masses, drag coefficients and areas of cross-section, respectively, and z_{wh} the wave displacement at the head.

The hydrodynamic forces acting on an element $Ld\xi$ located on the i^{th} leg at a distance $L\xi(0\leq\xi\leq1)$ from the root can be written as

$$dF_i = -[a(\ddot{z}_h+\ddot{w}_i-\ddot{z}_{wi})+(\rho_w/2)C_d d(\dot{z}_h+\dot{w}_i-\dot{z}_{wi})\,|\dot{z}_h+\dot{w}_i-\dot{z}_{wi}|L]d\xi \ , \tag{4.6a}$$

where z_{wi} is the wave displacement at the element and

$$a = \rho_w C_m SL \ . \tag{4.6b}$$

Realizing that the generalized force Q_j arising due to a set of forces $\bar{F}_k (k = 1,2,\cdots n)$ acting at the points $\bar{r}_k$ $(k = 1,2,\cdots n)$ is given by[53]

$$Q_j = \sum_{k=1}^{n} \bar{F}_k \cdot \frac{\partial \bar{r}_k}{\partial q_j} \quad ,$$

one obtains from Equations (4.5) and (4.6)

$$Q''_{zb} = -a_b(\ddot{z}_b-\ddot{z}_w)-(\rho_w/2)C_{db}S_b(\dot{z}_b-\dot{z}_w)|\dot{z}_b-\dot{z}_w| \quad , \tag{4.7a}$$

$$Q''_{zh} = -a_h(\ddot{z}_h-\ddot{z}_{wh})-(\rho_w/2)C_{dh}S_h(\dot{z}_h-\dot{z}_{wh})|\dot{z}_h-\dot{z}_{wh}| \quad ,$$

$$-a[3\ddot{z}_h-\sum_{i=1}^{3}\int_0^1 \ddot{z}_{wi}d\xi+\sum_{i=1}^{3}\sum_{s=1}^{\infty}\delta_s\ddot{B}_{is}]-(\rho_w/2)C_dLd\sum_{i=1}^{3}\int_0^1\{\dot{z}_h$$

$$-\dot{z}_{wi}+\sum_{s=1}^{\infty}\Phi_s(\xi)\dot{B}_{is}\}|\dot{z}_h-\dot{z}_{wi}+\sum_{s=1}^{\infty}\Phi_s(\xi)\dot{B}_{is}|d\xi \quad , \tag{4.7b}$$

and

$$Q''_{Bij} = -a[\delta_j\ddot{z}_h+\ddot{B}_{ij}-\int_0^1\ddot{z}_{wi}\Phi_j(\xi)d\xi]-(\rho_w/2)C_dLd\int_0^1|\dot{z}_h-\dot{z}_{wi}+\sum_{s=1}^{\infty}\Phi_s(\xi)*$$

$$B_{is}|[\dot{z}_h-\dot{z}_{wi}+\sum_{s=1}^{\infty}\Phi_s(\xi)B_{is}]\Phi_j(\xi)d\xi \quad , \tag{4.7c}$$

where Q''_{zb}, Q''_{zh} and Q''_{Bij} are the generalized forces due to the hydrodynamic forces only.

The contribution of the follower forces to the total generalized force Q_{Bij} is obtained from (3.11b), i.e.,

$$Q'_{Bij} = (F_a/L) \sum_{s=1}^{\infty} C_{sj} B_{is} \quad . \tag{4.8a}$$

Clearly,

$$Q'_{zb} = Q'_{zh} = 0 \quad . \tag{4.8b}$$

Defining

$$\eta_b = z_b/d, \quad \eta_h = z_h/d, \quad b_{ij} = B_{ij}/d, \quad \eta_w = z_w/d,$$

$$\eta_{wh} = z_{wh}/d, \quad \eta_{wi} = z_{wi}/d \quad \text{and} \quad \tau = t[c/(m_b+a_b)]^{1/2},$$

the equations of motion as given by (4.4) in conjunction with (4.7) and (4.8), can be nondimensionalized to yield

$$\eta_b''+(1+\bar{\Omega}^2)\eta_b-\bar{\Omega}^2\eta_h+\alpha_b(\eta_b'-\eta_w')|\eta_b'-\eta_w'| = (\eta_w+f_b\eta_w''), \tag{4.9a}$$

$$(3+r_{h\ell})\eta_h''+\sum_{i=1}^{3}\sum_{s=1}^{\infty}\delta_s b_{is}''+\bar{\Omega}^2 r_{b\ell}(\eta_h-\eta_b)+\alpha_h(\eta_h'-\eta_{wh}')|\eta_h'-\eta_{wh}'|$$

$$+\alpha\sum_{i=1}^{3}\int_0^1\{\eta_h'-\eta_{wi}'+\sum_{s=1}^{\infty}\Phi_s(\xi)b_{is}'\}|\eta_h'-\eta_{wi}'+\sum_{s=1}^{\infty}\Phi_s(\xi)b_{is}'|d\xi$$

$$= f_h\eta_{wh}''+f\sum_{i=1}^{3}\int_0^1\eta_{wi}''\,d\xi \quad , \tag{4.9b}$$

and

$$b_{ij}''+\delta_j\eta_h''+\Omega_j^2 b_{ij}-\bar{P}\sum_{s=1}^{\infty}C_{sj}b_{is}+\alpha\int_0^1\{\eta_h'-\eta_{wi}'+\sum_{s=1}^{\infty}\Phi_s(\xi)b_{is}'\} *$$

$$|\eta_h' - \eta_{wi}' + \sum_{s=1}^{\infty} \Phi_s(\xi) b_{is}' | \Phi_j(\xi) d\xi = f\int_0^1 \eta_{wi}'' \Phi_j(\xi) d\xi \quad , \tag{4.9c}$$

$$i = 1, 2, 3; \quad j = 1, 2, \cdots \infty ;$$

where

$$\bar{\Omega}^2 = k/c, \quad r_{b\ell} = (m_b + a_b)/(m+a), \quad \bar{P} = (F_a/cL)(m_b+a_b)/(m+a)$$

$$\Omega_j^2 = \mu_j^4 [EI/(m+a)L^3][(m_b+a_b)/c], \quad \alpha_b = (\rho_w/2) C_{db} S_b d/(m_b+a_b),$$

$$\alpha_h = (\rho_w/2) C_{dh} S_h d/(m+a), \quad f_b = a_b/(m_b+a_b), \quad f_h = a_h/(m+a),$$

$$f = 1/(1+C_m), \tag{4.10}$$

with $r_{h\ell}$ and α obtained from Equations (3.15a) and (2.16b), respectively. To incorporate viscoelastic effects of the legs, E in the expression for Ω_j^2 in Equation (4.10), should be replaced by the complex modulus $E^*(\omega)$ as given by (2.42a).

4.2 Vertical Free Vibrations of the System

For the free vibrations of the system, the forcing terms in the equations of motion are equated to zero, i.e.,

$$\eta_w = \eta_{wh} = \eta_{wi} = 0 \quad .$$

Since the effect of the damping terms on the natural frequencies and the modes of the system is of the second order, they may be ignored. If the motion is assumed to be sinusoidal with ω as its dimensionless frequency, Equations (4.9) transform to

$$(1+\bar{\Omega}^2-\omega^2)\eta_b - \bar{\Omega}^2\eta_h = 0 \quad , \tag{4.11a}$$

$$-\bar{\Omega}^2 r_{b\ell}\eta_b+[\bar{\Omega}^2 r_{b\ell}-(3+r_{h\ell})\omega^2]\eta_h-\omega^2\sum_{i=1}^{3}\sum_{s=1}^{\infty}\delta_s b_{is} = 0, \tag{4.11b}$$

and

$$-\omega^2\delta_j\eta_h+(\Omega_j^2-\omega^2)b_{ij}-\bar{P}\sum_{s=1}^{\infty}C_{sj}b_{is} = 0 \quad , \tag{4.11c}$$

$$i = 1,\ 2,\ 3; \quad j = 1,\ 2,\ \cdots \infty \ .$$

The above set contains infinite number of equations. In the numerical computations, however, only the first six modes were retained so that Equation (4.11) reduced to an eigenvalue problem of the type

$$[A](x) = \omega^2[B](x) \quad , \tag{4.12a}$$

of order 20. Premultiplying (4.12a) with $[B]^{-1}$ one obtains

$$[B]^{-1}[A](x) = \omega^2(x)$$

or

$$[C](x) = \omega^2(x) \quad , \tag{4.12b}$$

where $$[C] = [B]^{-1}[A] \quad .$$

The system of Equations (4.12b) can now be solved by an iteration procedure (for example UBC DREIGN) to obtain the frequencies and mode shapes.

4.3 Response of the System to Surface Wave Excitations

The system under normal operating condition will be subjected to the ocean waves which, in general, would lead to both horizontal and vertical motions of the buoy. Obviously, the resulting dynamical analysis of the system will indeed be quite complicated. Fortunately, considerable simplification in the analysis can be achieved without substantially affecting the physics of the problem by examining the system response with the buoy at the crest of a standing wave. Moreover, a complex wave can always be expanded in a Fourier series and the general forced motion can be obtained by following a similar procedure.

It can be shown that for a standing wave[54]

$$\eta_w = \eta_0 \cos 2\pi(t/\bar{T}) \quad ,$$

$$\eta_{wh} = \eta_0 e^{-2\pi H/L_\lambda} \cos 2\pi(t/\bar{T}) \quad ,$$

$$\eta_{wi} = \eta_0 e^{-2\pi H/L_\lambda} \cos 2\pi(x/L_\lambda) \cos 2\pi(t/\bar{T}) \quad ,$$

provided the crest lies along the vertical axis of the system. Here η_0, $\bar{T}$ and L_λ are the amplitude, period and length of the wave, respectively. It may be noticed that the particle motion decreases rapidly with depth. For $H = L_\lambda/2$, the amplitude of particle motion is $\eta_0/23.1$, while at a depth equal to the wavelength, the motion reduces to $\eta_0/535$. With the average wavelength of around 100 ft (sea state 3) and cable length of 100-400 ft, it may be assumed that

$$\eta_{wh} = \eta_{wi} \simeq 0 \quad , \tag{4.13a}$$

and

$$\eta_w = \eta_0 \cos 2\pi(t/\bar{T}) \equiv \eta_0 \cos\omega\tau \quad , \tag{4.13b}$$

where ω is the dimensionless frequency.

The forced motion, in general, will involve all the harmonics of ω; but for simplicity only the fundamental term, which is usually the most important one, is considered. To account for the system damping, both sine and cosine terms should be included in the solution. Hence

$$\eta_b = \eta_{bc}\cos\omega\tau + \eta_{bs}\sin\omega\tau \quad , \tag{4.14a}$$

$$\eta_h = \eta_{hc}\cos\omega\tau + \eta_{hs}\sin\omega\tau \quad , \tag{4.14b}$$

$$b_{ij} = b_{ijc}\cos\omega\tau + b_{ijs}\sin\omega\tau \quad . \tag{4.14c}$$

Substitution of (4.14) in (4.9) will not, in general, satisfy the equations for all τ. But one can use Ritz's averaging technique which involves multiplying both the sides of each equation by $\cos\omega\tau$ and $\sin\omega\tau$ in turn and integrating over a period. The resulting algebraic equations are

$$(1+\bar{\Omega}^2-\omega^2)\eta_{bc}-\bar{\Omega}^2\eta_{hc}+\alpha_b(8\omega^2/3\pi)\eta_{bs}[(\eta_{bc}-\eta_0)^2+\eta_{bs}^2]^{1/2}=(1-f_b\omega^2)\eta_0, \quad (4.15a)$$

$$(1+\bar{\Omega}^2-\omega^2)\eta_{bs}-\bar{\Omega}^2\eta_{hs}-\alpha_b(8\omega^2/3\pi)(\eta_{bc}-\eta_0)[(\eta_{bc}-\eta_0)^2+\eta_{bs}^2]^{1/2}=0, \quad (4.15b)$$

$$-r_{b\ell}\bar{\Omega}^2\eta_{bc}+[r_{b\ell}\bar{\Omega}^2-(3+r_{h\ell})\omega^2]\eta_{hc}-\omega^2\sum_{i=1}^{3}\sum_{k=1}^{\infty}\delta_k b_{ikc}+\alpha_h(8\omega^2/3\pi)\eta_{hs} *$$

$$(\eta_{hc}^2+\eta_{hs}^2)^{1/2}+\alpha(8\omega^2/3\pi)\sum_{i=1}^{3}\int_0^1 D_s(D_c^2+D_s^2)^{1/2}d\xi = 0, \quad (4.15c)$$

$$-r_{b\ell}\bar{\Omega}^2\eta_{bs}+[r_{b\ell}\bar{\Omega}^2-(3+r_{h\ell})\omega^2]\eta_{hs}-\omega^2\sum_{i=1}^{3}\sum_{k=1}^{\infty}\delta_k b_{iks}-\alpha_h(8\omega^2/3\pi) *$$

$$\eta_{hc}(\eta_{hc}^2+\eta_{hs}^2)^{1/2}-\alpha(8\omega^2/3\pi)\sum_{i=1}^{3}\int_0^1 D_c(D_c^2+D_s^2)^{1/2}d\xi = 0, \quad (4.15d)$$

$$(\Omega_j^2-\omega^2)b_{ijc}+\gamma\omega\Omega_j^2 b_{ijs}-\omega^2\delta_j\eta_{hc}-\bar{P}\sum_{k=1}^{\infty}C_{kj}b_{ikc}+\alpha(8\omega^2/3\pi) *$$

$$\int_0^1\Phi_j(\xi)D_s(D_c^2+D_s^2)^{1/2}d\xi = 0, \quad (4.15e)$$

$$-\gamma\omega\Omega_j^2 b_{ijc}+(\Omega_j^2-\omega^2)b_{ijs}-\omega^2\delta_j\eta_{hs}-\bar{P}\sum_{k=1}^{\infty}C_{kj}b_{iks}-\alpha(8\omega^2/3\pi) *$$

$$\int_0^1\Phi_j(\xi)D_c(D_c^2+D_s^2)^{1/2}d\xi = 0, \quad (4.15f)$$

$$i = 1,2,3; \quad k = 1,2,\cdots;$$

where

$$D_c = \eta_{hc}+\sum_{k=1}^{\infty}\Phi_k(\xi)b_{ikc},$$

$$D_s = \eta_{hs}+\sum_{k=1}^{\infty}\Phi_k(\xi)b_{iks},$$

and γ the equivalent viscoelastic damping.

The solution of these simultaneous equations gives the sine and cosine components of each generalized co-ordinate. Since the first few modes are likely to be the most important ones, only the first two are considered in the numerical computations.

4.4 Results and Discussion

4.4.1 Free vibration

By truncating the infinite order system to the first m modes, (3m+2) eigenvalues are obtained from (4.11). Two identical sets of m eigenvalues result along with a third set containing (m+2) frequencies. The repeated eigenvalues correspond to the independent motion of the cantilevers at their natural frequencies while the buoy and the central body are at rest. On the other hand, the nonrepeated eigenvalues describe the coupled motion in which all the legs move identically and hence only (m+2) eigenvalues can correspond to this type of motion. In the present case m is taken to be 6.

The typical amplitudes of motion of the buoy, central head and the cylindrical legs during coupled motion at fundamental and higher natural frequencies are shown in Figure 4-2. It may be pointed out that to emphasize the relative motion, only the displacements are presented to the scale (unit central head displacement), geometrical dimensions being left arbitrary for clarity. One may notice that for the lowest three frequencies, the shape of the cylinder resembles its fundamental mode since it is the most dominating one. However, the

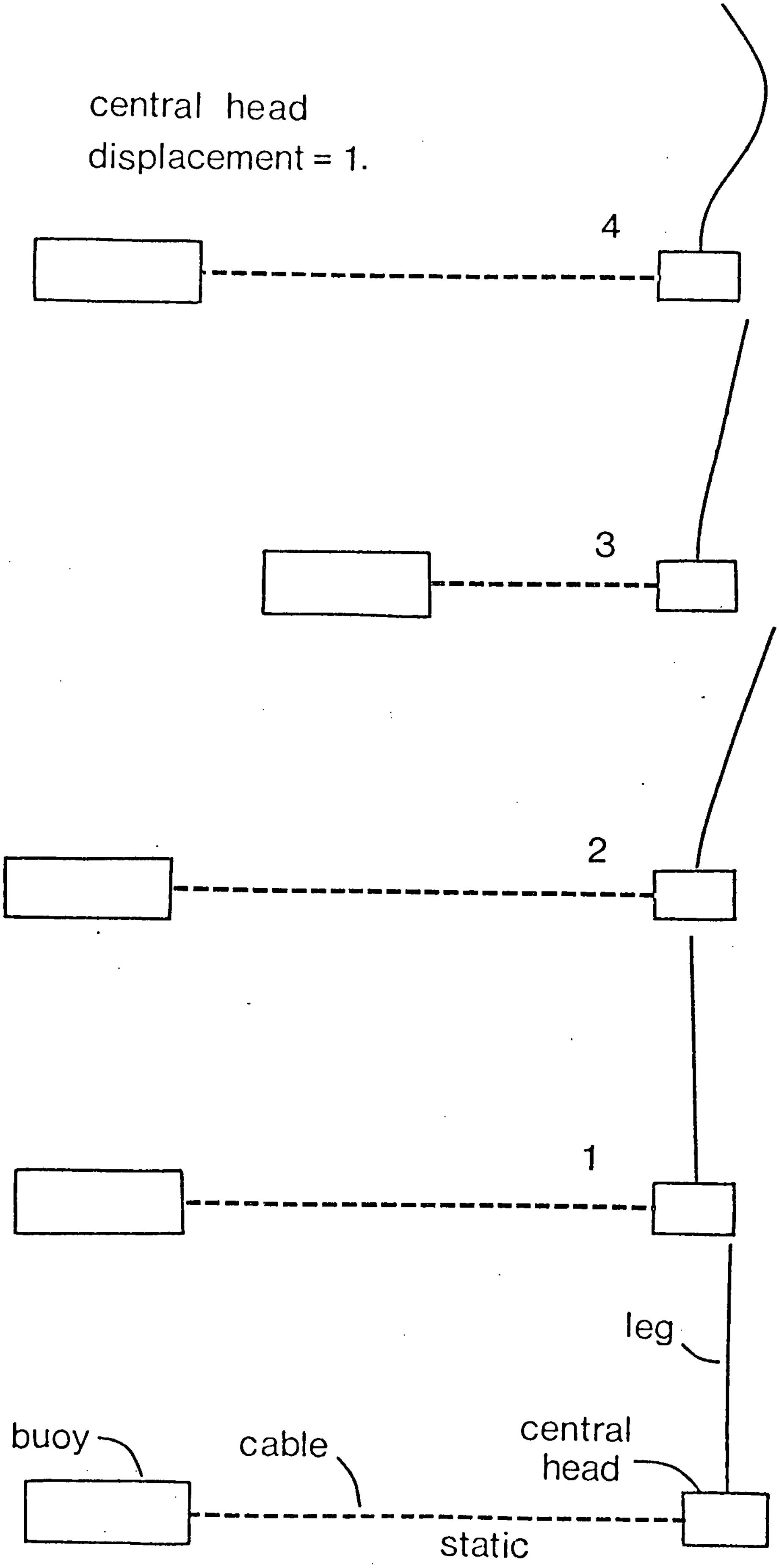

Figure 4-2 Modes of coupled vertical motion: (a) i = 1 to 4

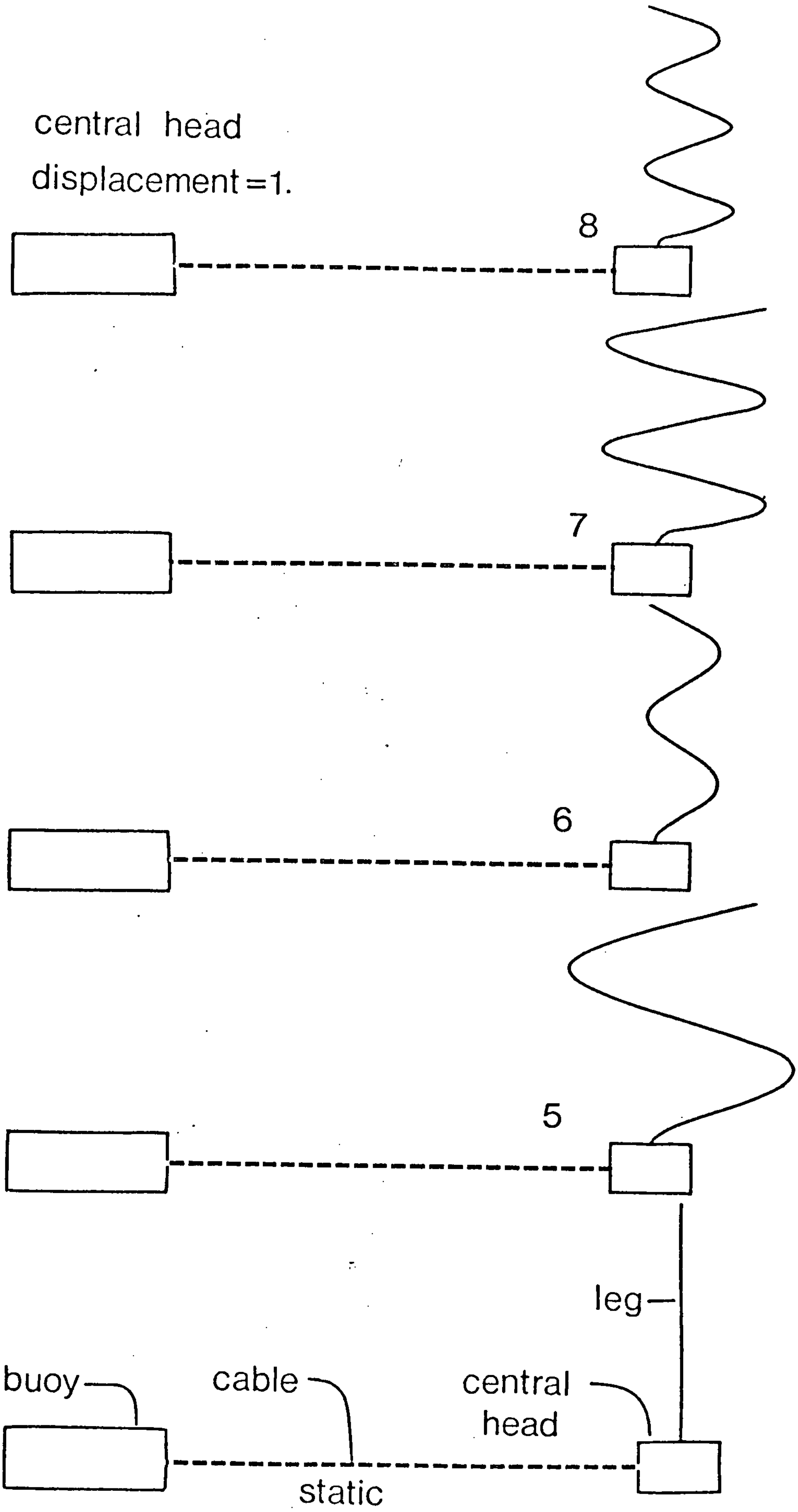

Figure 4-2 Modes of coupled vertical motion: (b) i = 5 to 8

subsequent frequencies correspond to the second and higher modes of the leg. Since the third natural frequency of the coupled motion is quite close to the natural frequency of the buoy due to its buoyancy, the buoy has a large displacement.

The variation of the coupled natural frequencies with $\bar{P}$ and Ω_1 for given $\bar{\Omega}$, $r_{h\ell}$ and $r_{b\ell}$ is shown in Figure 4-3. Here $\bar{P}$ characterizes the effect of internal pressure while Ω_1 the fundamental frequency of each leg. The first three of these frequencies, for a given $\bar{P}$, first decrease and then increase with increasing Ω_1 (Figure 4-3a). For large values of Ω_1, these frequencies decrease with increasing $\bar{P}$, while for small values of the fundamental frequency, the behaviour is exactly the opposite. This is so, because for large Ω_1 the structure behaves like a cantilever while for small Ω_1 it acts as a string. As is well known, increasing the axial tension has opposite effects on these two structures. The behaviour of the fourth (Figure 4-3a) and higher frequencies (Figure 4-3b) is the same as that of the second and higher frequencies of a single cylinder, i.e., they increase with Ω_1 and $\bar{P}$. If Ω_1 is not too small, they vary linearly.

The variation of the coupled frequencies with $\bar{\Omega}^2$ and $r_{b\ell}$ for given $\bar{P}$, Ω_1 and $r_{h\ell}/r_{b\ell}$ is plotted in Figure 4-4. The first three increase with $\bar{\Omega}$, i.e. the stiffness of the spring, while the subsequent ones are almost independent of it. The parameter $r_{b\ell}$, representing the ratio of the apparent masses of the buoy and the leg, has opposite effects on the lower and higher frequencies. The higher frequencies (Figure 4.4b), which are characterized by the stiffness of the legs,

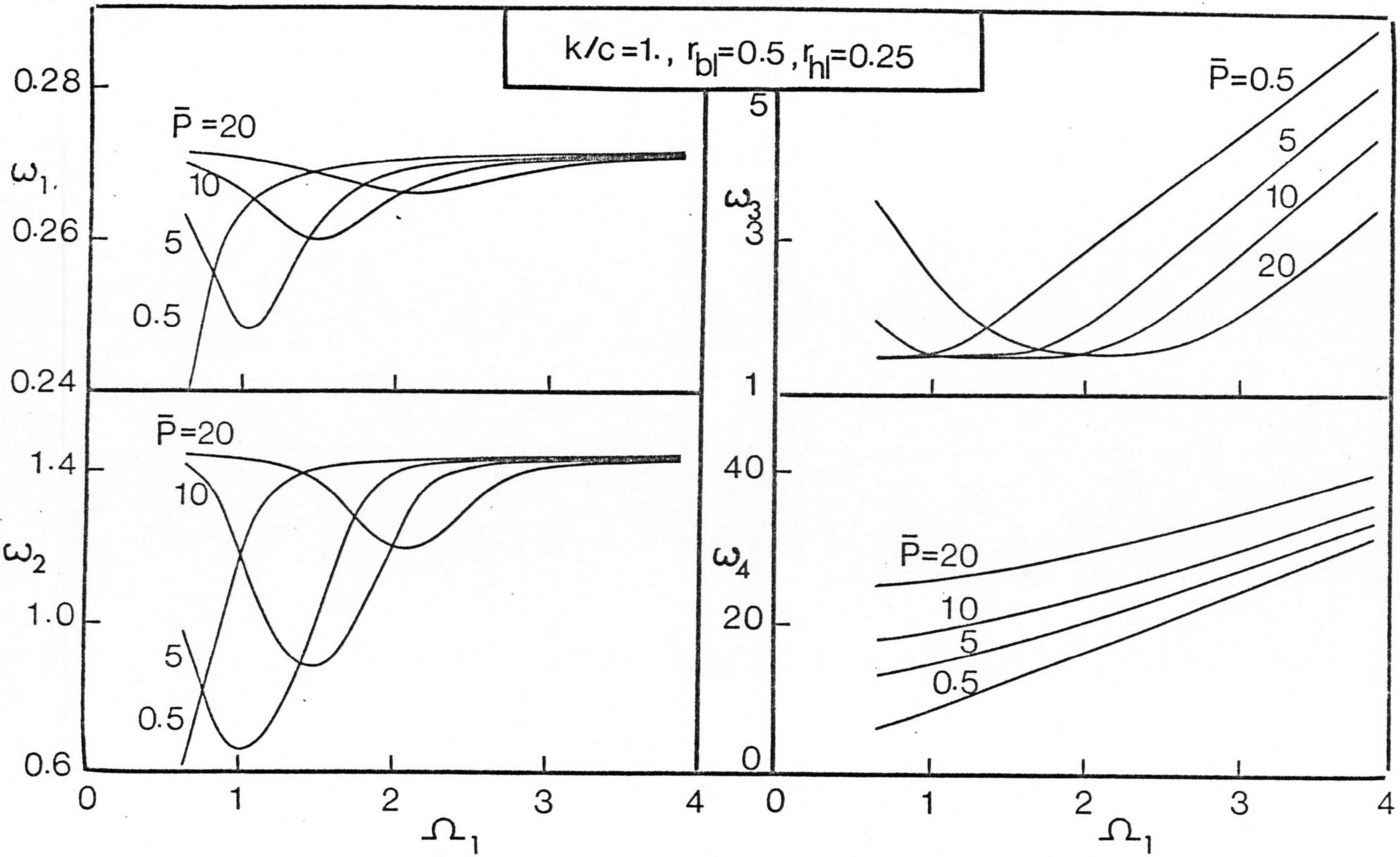

Figure 4-3 Variation of natural frequencies of coupled vertical motion with the pressure parameter and dimensionless fundamental leg frequency: (a) i = 1 to 4

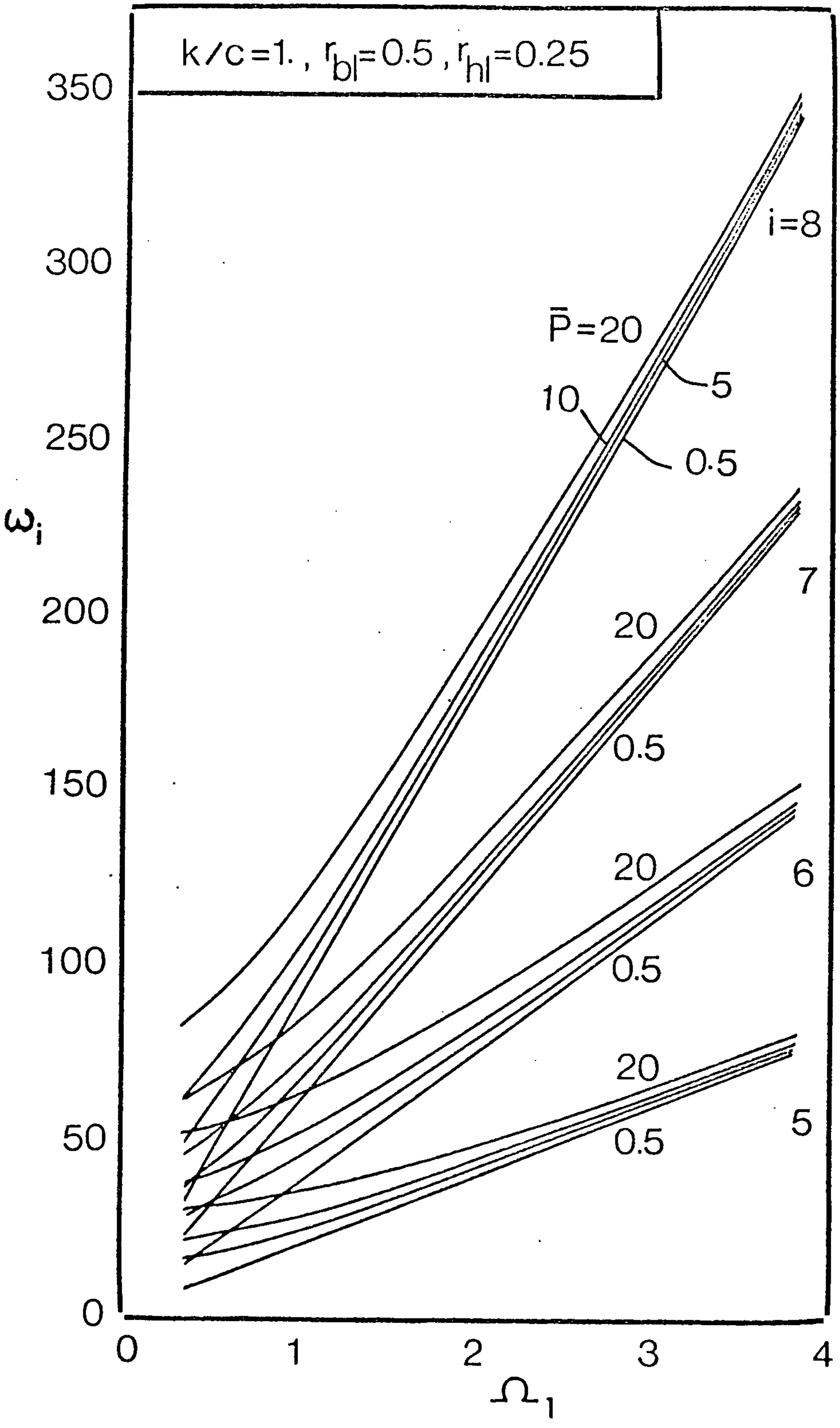

Figure 4-3 Variation of natural frequencies of coupled vertical motion with the pressure parameter and dimensionless fundamental leg frequency: (b) i = 5 to 8

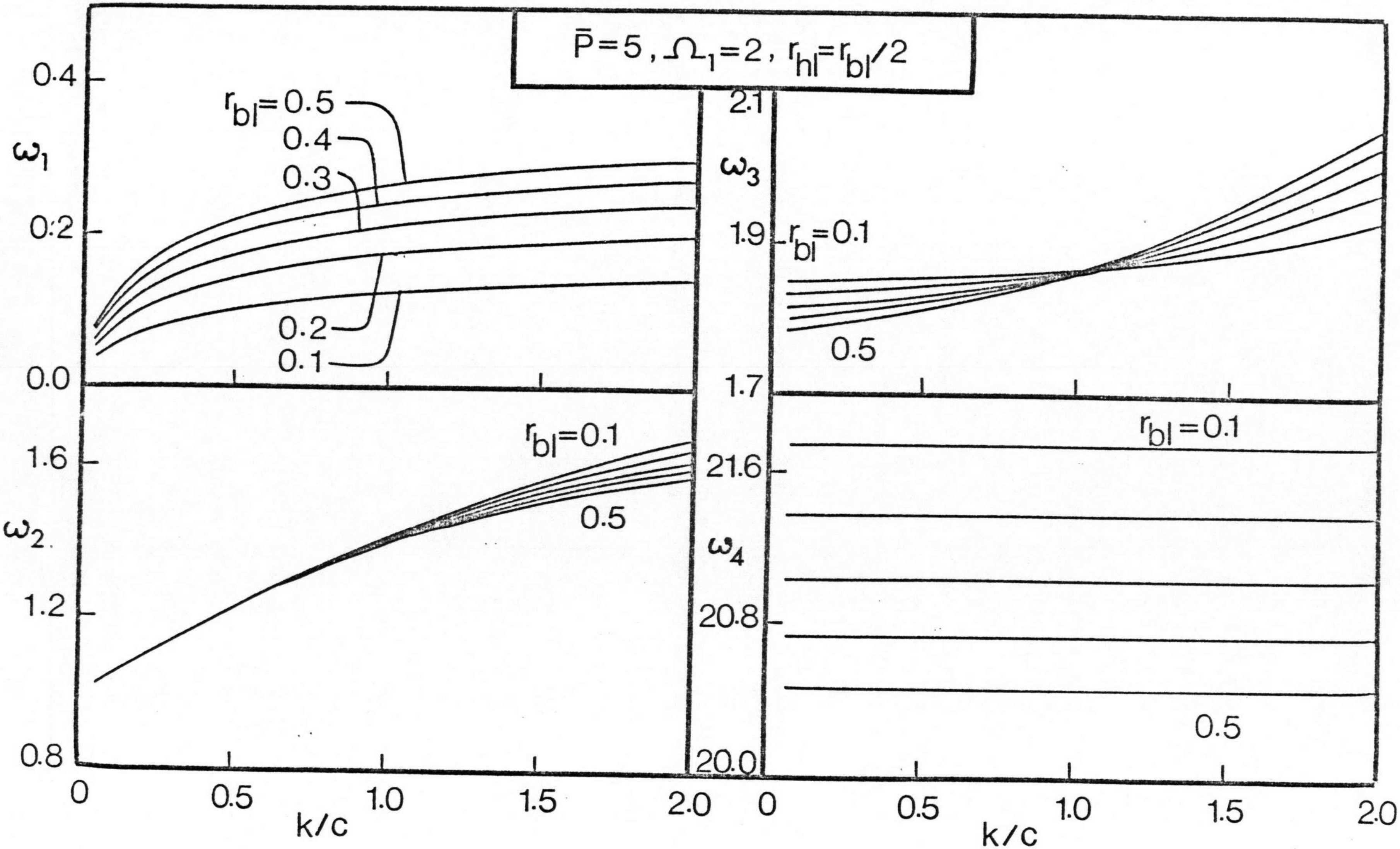

Figure 4-4 Variation of natural frequencies of coupled vertical motion with the spring stiffness and weight of the head: (a) i = 1 to 4

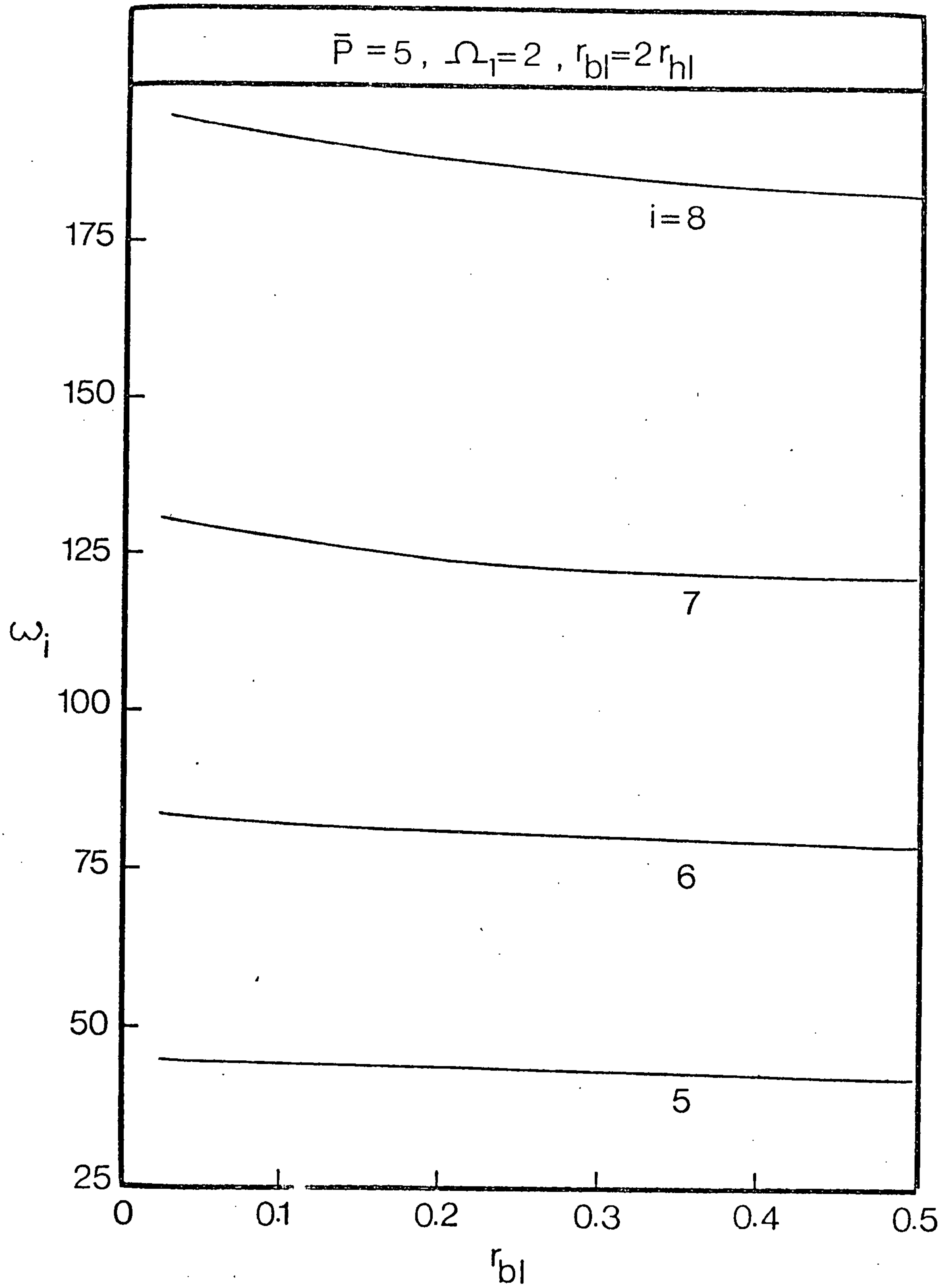

Figure 4-4 Variation of natural frequencies of coupled vertical motion with the spring stiffness and weight of the head: (b) i = 5 to 8

decrease slightly with $r_{b\ell}$ while the lowest one which involves large coupling between the buoy and the array increases with the same parameter.

Given the operating sea conditions, the parameters must be so chosen as to yield the natural frequencies of the system (at least the lower ones) far removed from the forcing frequencies.

4.4.2 Forced vibration

The frequency response of the buoy, central head and the tip of a leg, for different $\bar{\Omega}^2$ (=k/c), are plotted in Figure 4-5a. One may notice that the buoy displacement peaks at smaller frequencies with reduction in k/c. For k/c = 1, there is a less conspicuous peak since around this value of k/c the array acts somewhat like a dynamic absorber. For the motions of the central head and leg tips, resonance is observed first at a very small frequency (fundamental) and subsequently at higher frequencies. It may be observed that these resonant displacements diminish with k/c, i.e., if the elastic cable is a soft spring, the motion at the water surface is not transmitted to the array.

Figure 4-5b shows the frequency response when Ω_1 is varied. It is evident that the displacements of the tips of the legs could be reduced by increasing Ω_1, i.e., by making the legs more stiff. This implies reduction in length of the legs and increase in their diameter, thickness and elastic modulus. Moreover, it may be noted from Figure 4-5c (in logarithmic scales) that for a given Ω_1, $\bar{P}$ and $\bar{\Omega}$, the tip displacement for higher forcing frequencies diminishes with increasing $r_{h\ell}$, while that at lower frequencies remains unaffected.

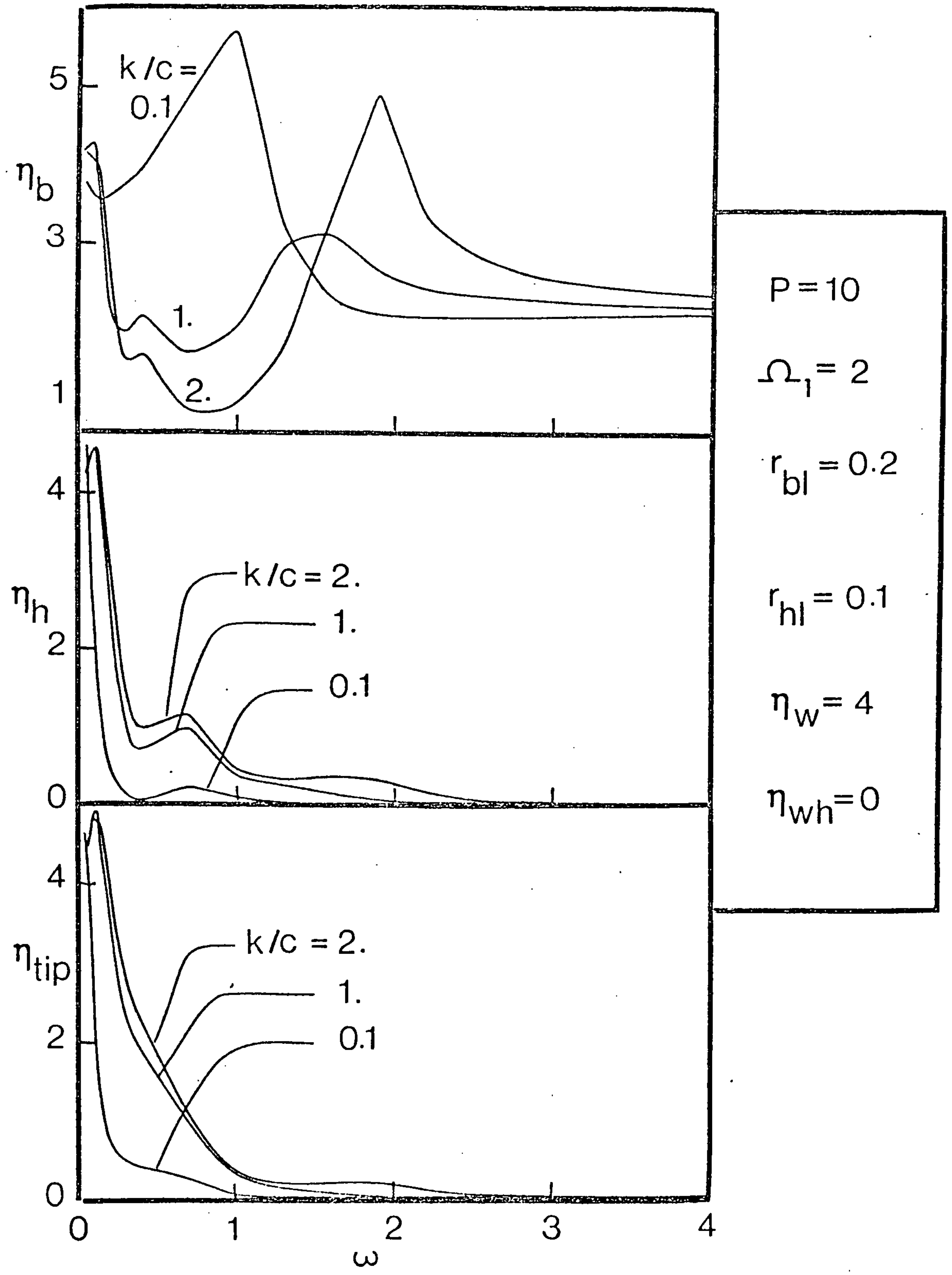

Figure 4-5 Frequency response of the buoy, central head and the tip of a leg as affected by: (a) equivalent spring stiffness

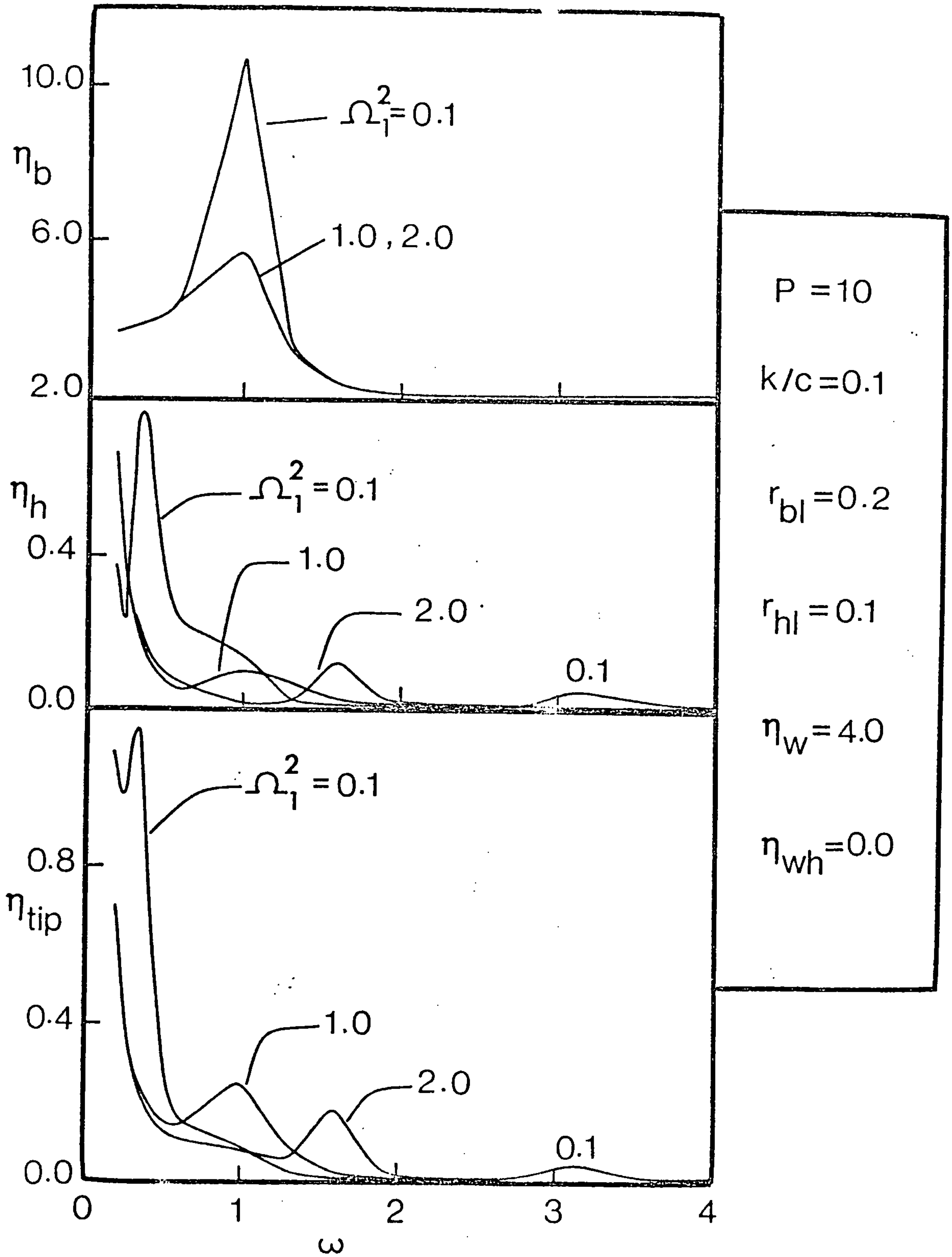

Figure 4-5 Frequency response of the buoy, central head and the tip of a leg as affected by: (b) fundamental frequency of a leg

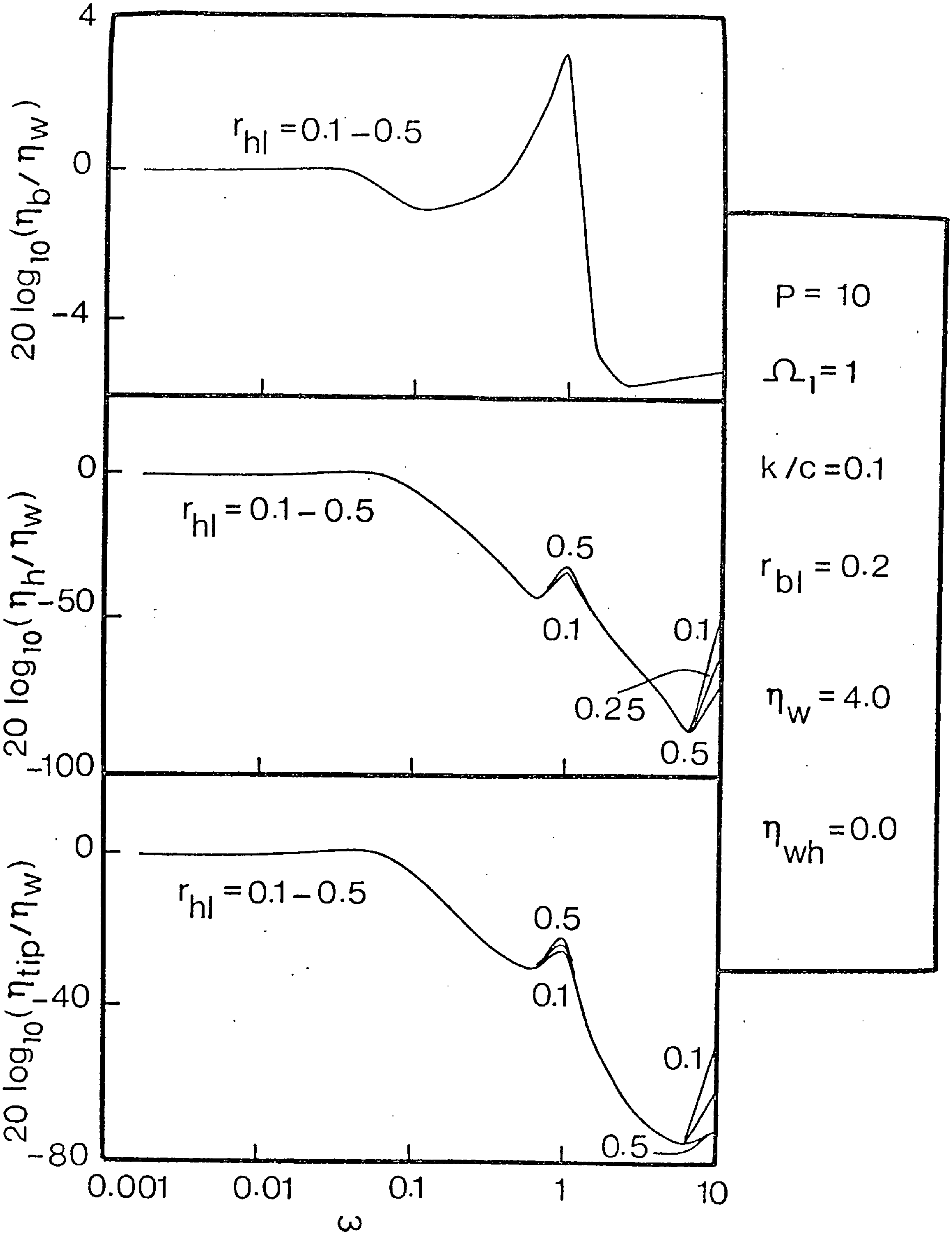

Figure 4-5 Frequency response of the buoy, central head and the tip of a leg as affected by: (c) weight of the central head

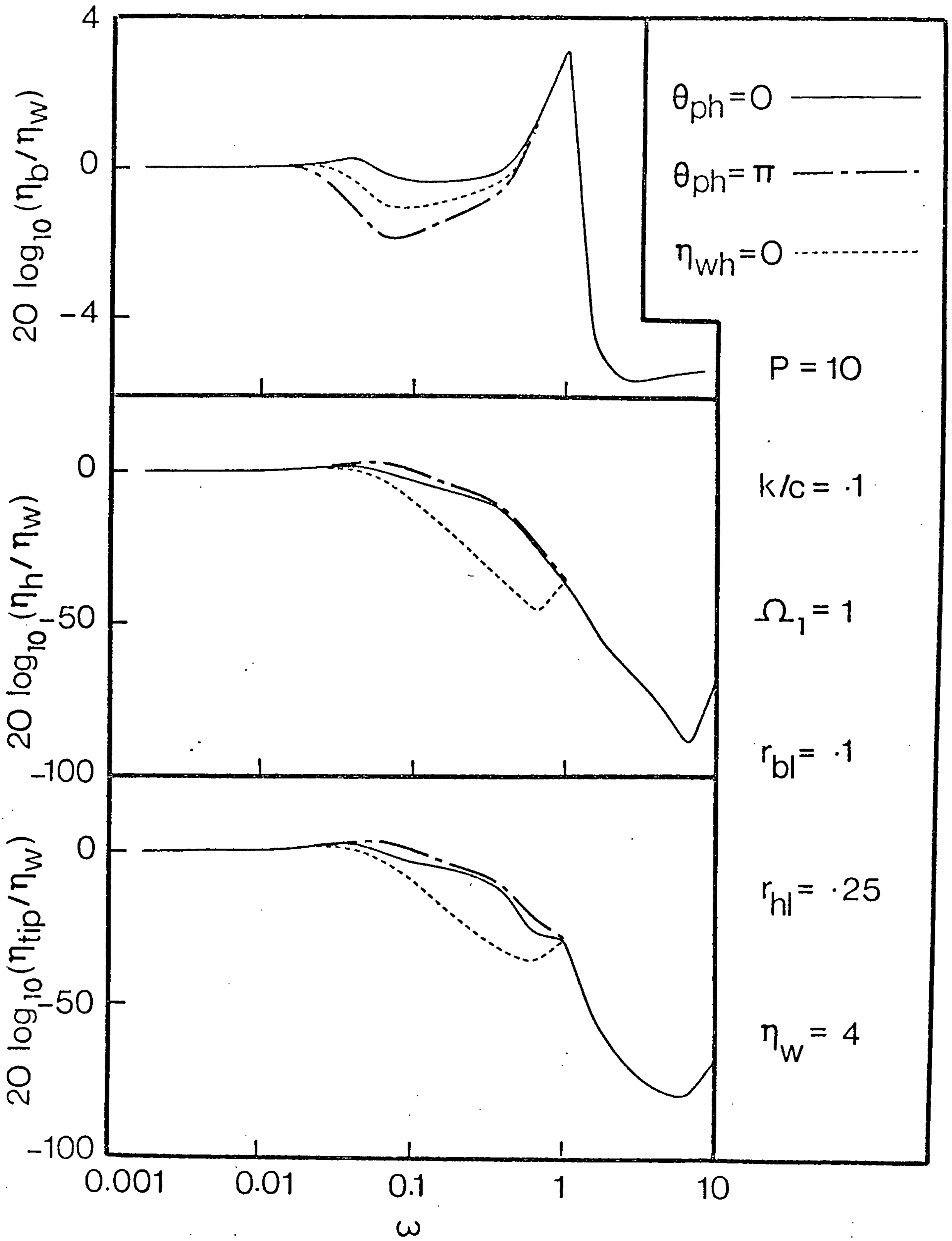

Figure 4-5 Frequency response of the buoy, central head and the tip of a leg as affected by: (d) wave amplitude at the central head

The effect of taking the wave displacements η_{wh} and η_{wi} into account is indicated in Figure 4-5d. Here η_{wh} and η_{wi} are assumed to be equal and have a constant phase difference θ_{ph} with respect to the surface wave displacement η_w. Clearly, consideration of η_{wh} and η_{wi} increases the displacements of the central head and tip of each leg for moderate forcing frequencies. $\theta_{ph} = \pi$ represents a more adverse situation than $\theta_{ph} = 0$.

4.5 Concluding Remarks

The important conclusions based on the analysis can be summarized as follows:

(i) The solution of the eigenvalue problem for free vertical oscillation of the buoy-cable-array system yields two sets of repeated natural frequencies corresponding to the independent motion of the legs and a third set describing the coupled motion. All the three legs move identically during the coupled pure vertical oscillations.

(ii) The variation of the natural frequencies with different system parameters as obtained in this study, should prove useful in a design procedure aimed at avoiding resonance.

(iii) Analysis of the response of the system to surface wave excitations suggests that the displacements of the leg tips can be reduced by using an elastic cable with small stiffness and legs having a large fundamental frequency. The typical value of this frequency as observed in the prototype structures is below 2 cycles/sec. The analysis suggests that any increase in this value is likely to have beneficial influence on the structural response. On the other hand, as emphasized by Figure 4-5b, very small values of leg frequency may lead the buoy to leave the water surface and hence must be avoided.

(iv) Although an increase in the inertia of the central head is likely to reduce tip deflections, it would be difficult to realize this from design considerations.

5. DYNAMICS OF A DRIFTING BUOY-CABLE-ARRAY ASSEMBLY USING DOUBLE PENDULUM APPROXIMATION

The previous chapter considered the vertical motions of the submarine detection system when it was stationed at one location. Although the response of the system to surface waves was considered, it was assumed that the waves are not associated with any drifting velocity. The objective of this chapter is to investigate its behaviour when drifting in an ocean current.

The drifting motion of the system is rather complex because of the large number of degrees of freedom involved: the spatial oscillations of the buoy superimposed on its drifting, three dimensional motion of the flexible cable, the motion of the array in its own plane and that of the plane of the array itself. Hence it was thought appropriate to study, at least in the beginning, a relatively simple model to obtain some appreciation regarding the physical character of the problem.

It is assumed that the system is drifting with a constant velocity and oscillations take place around the corresponding steady state configuration. Furthermore, the effect of these vibrations of the cable and array on the drifting velocity is neglected. In actual practice, occassionally a small velocity gradient across the current is observed; however, for simplicity it is ignored. Of course, this does not affect the mathematical procedure and if required, its influence can be included quite readily. The up and down and rocking motion of the buoy are assumed to be absent. Thus the buoy is considered to have a uniform drifting velocity and hence the origin of the inertial co-ordinate system can be located at the centre of the buoy. The mass of the cable is considered to be continuously and uniformly distributed along its length, but its shape is approximated by two straight lines, i.e., the system behaves like a double pendulum. For the time being, the flexibility effects of the legs are ignored.

With these assumptions, the steady state configurations are determined and their dependence on the system parameters examined. The double pendulum type motion of the system along with the rotational oscillations of the array, around these equilibrium positions, are studied. The analysis provides useful information concerning the stability of the motion and influence of various system parameters on damping rates.

5.1 Formulation of the Problem

5.1.1 Equations of motion

Consider a buoy-cable-array assembly drifting with a uniform velocity V (Figure 5-1). Let x_0, y_0, z_0 be an inertial coordinate system fixed to the centre of the buoy. The cable of length L_c, connecting the centres of mass of the array and buoy, is approximated by two straight lines inclined at angles $\beta_1(t)$ and $\beta_2(t)$ to the vertical, respectively. Let $\theta(t)$ be the inclination of the plane of the array to the flow and let angles $\psi_i (i=1,2,3)$ measured from the projected direction of the flow in the plane of the array, define the orientation of the legs. Clearly

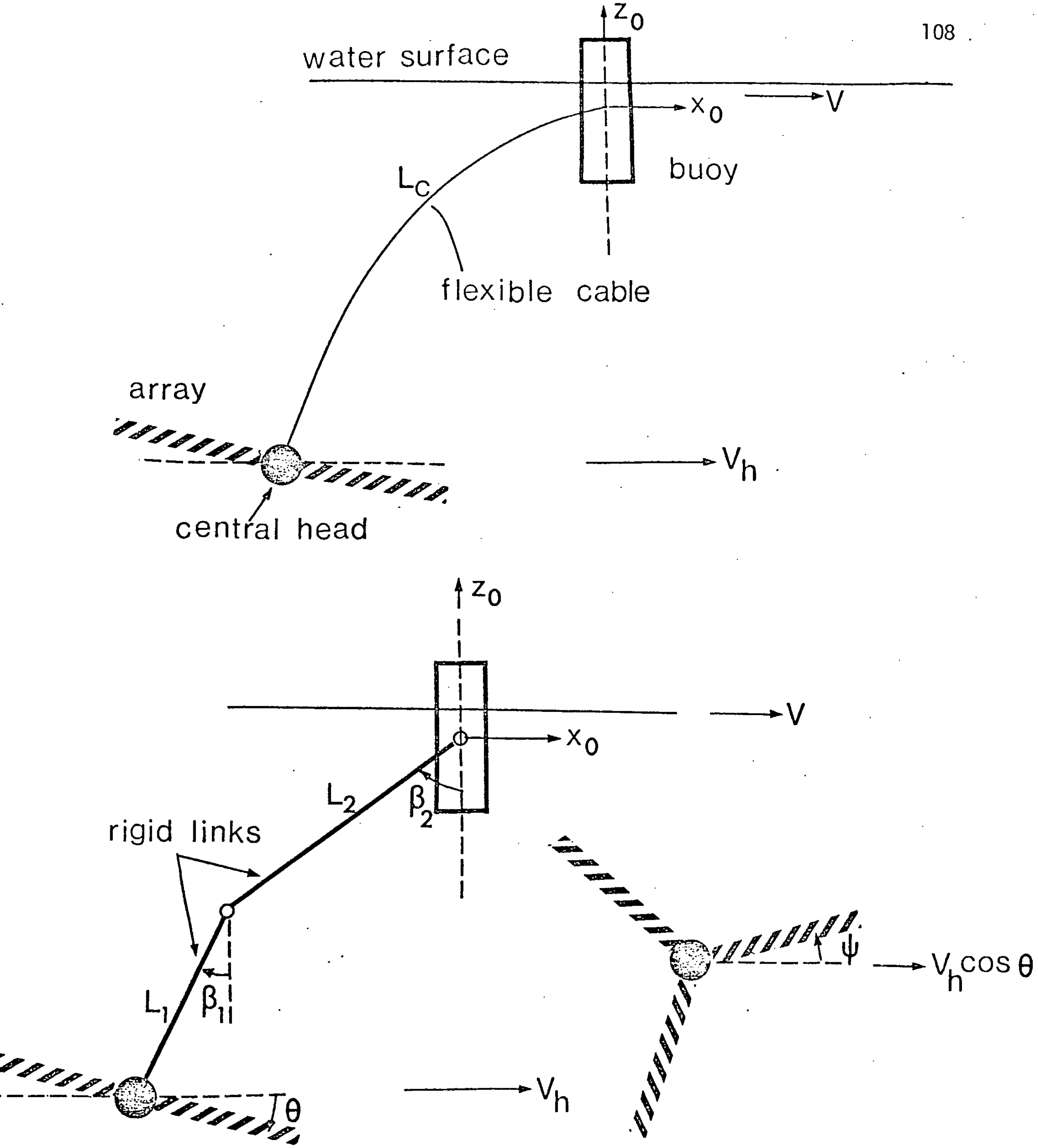

Figure 5-1 Geometry of motion of a drifting buoy-cable-array assembly using double pendulum approximation

$$\psi_i = \psi_1 + 2\pi(i-1)/3 \quad . \tag{5.1}$$

The position vector $\bar{r}_h$ of the centre of mass of the head is given by

$$\bar{r}_h = -(L_1\sin\beta_1+L_2\sin\beta_2)\bar{i}-(L_1\cos\beta_1+L_2\cos\beta_2)\bar{k} \quad , \tag{5.2a}$$

where L_1 and L_2 are lengths of the two linear parts of the cable and $\bar{i}$, $\bar{j}$ and $\bar{k}$ the unit vectors in x_0, y_0 and z_0 directions, respectively. The location of a point P on the i^{th} leg, at a distance $\xi L(0\leq\xi\leq 1)$ from the centre of the head, can be written as

$$\bar{r}_i = \bar{r}_h + \xi L\bar{e}_{ti} \quad , \tag{5.2b}$$

where $\bar{e}_{ti}$ is the unit vector along the i^{th} leg and can be expressed in terms of the array rotations as follows:

$$\bar{e}_{ti} = \cos\theta\cos\psi_i\bar{i}+\sin\psi_i\bar{j}-\sin\theta\cos\psi_i\bar{k} \quad . \tag{5.2c}$$

The expressions for the kinetic and potential energy must be obtained for the Lagrangian formulation. The kinetic energy of the system consists of three parts: T_a of the legs, T_h of the central head and T_c of the cable. Considering the kinetic energy of an element $Ld\xi$ and summing over the three legs, one obtains

$$T_a = (1/2)\sum_{i=1}^{3}\int_0^1(\dot{\bar{r}}_i\cdot\dot{\bar{r}}_i)(1+C_m)(\pi d^2/4)\rho_w L d\xi \quad .$$

Substituting from (5.2), the above expression yields

$$T_a = (1+C_m)(\rho_w/2)(\pi d^2 L/4)\sum_{i=1}^{3}\int_0^1[V_h^2+2\xi L\dot{\psi}(-V_{hx_0}\sin\psi_i\cos\theta+V_{hy_0}\cos\psi_i$$

$$+V_{hz_0}\sin\psi_i\sin\theta)-2\xi L\dot{\theta}(V_{hx_0}\cos\psi_i\sin\theta+V_{hz_0}\cos\psi_i\cos\theta)+\xi^2L^2(\dot{\psi}^2$$

$$+\dot{\theta}^2\cos\psi_i)]d\xi$$

$$= (m/2)(1+C_m)[3V_h^2+L^2\dot{\psi}^2+L^2\dot{\theta}^2/2] \quad , \tag{5.3a}$$

where $\bar{V}_h$ is the velocity of the head given by

$$\bar{V}_h = -(L_1\dot{\beta}_1\cos\beta_1+L_2\dot{\beta}_2\cos\beta_2)\bar{i}+(L_1\dot{\beta}_1\sin\beta_1+L_2\dot{\beta}_2\sin\beta_2)\bar{k}$$

$$\equiv V_{hx_0}\bar{i}+V_{hy_0}\bar{j}+V_{hz_0}\bar{k} \quad \text{(say)}, \quad V_h = |\bar{V}_h| \; , \tag{5.3b}$$

and

$$\dot{\psi} = \dot{\psi}_i \quad (i = 1, 2, 3) \quad . \tag{5.3c}$$

The kinetic energy of the central head is given by

$$T_h = (1/2)[(1+C_{mh})m_h V_h^2+\dot{\theta}^2(I_{xxa}\sin^2\psi+I_{yya}\cos^2\psi)+I_{zza}\dot{\psi}^2] \;, \tag{5.4}$$

while that of the cable can be obtained from

$$T_c = (1+C_{mc})[\int_{m_{c1}} |\bar{V}_{c1}(s_1)|^2 dm_{c1}+\int_{m_{c2}} |\bar{V}_{c2}(s_2)|^2 dm_{c2}]/2 \;, \tag{5.5a}$$

where m_{c1}, m_{c2} and C_{mc} are the masses of the two sections of the cable and its added inertia coefficient, respectively and $\bar{V}_{c1}(s_1)$ and $\bar{V}_{c2}(s_2)$ the velocities of elements on the two portions of the cable. It can be shown that

$$\bar{V}_{c1}(s_1) = -(s_1\dot{\beta}_1\cos\beta_1+L_2\dot{\beta}_2\cos\beta_2)\bar{i}+(s_1\dot{\beta}_1\sin\beta_1+L_2\dot{\beta}_2\sin\beta_2)\bar{k}, \tag{5.5b}$$

and

$$\bar{V}_{c2}(s_2) = -s_2\dot{\beta}_2\cos\beta_2\bar{i}+s_2\dot{\beta}_2\sin\beta_2\bar{k} \;, \tag{5.5c}$$

where s_1 and s_2 are distances of the elements from the hinges of the first and second pendulum, respectively. Hence

$$T_c = (1+C_{mc})[(m_{c1}/2)\{(L_1^2/3)\dot{\beta}_1^2+L_2^2\dot{\beta}_2^2+L_1L_2\dot{\beta}_1\dot{\beta}_2\cos(\beta_1-\beta_2)\}$$

$$+(m_{c2}/2)L_2^2\dot{\beta}_2^2/3] \;. \tag{5.5d}$$

The potential energy of the system can be obtained as

$$U = -m_h g(L_1\cos\beta_1+L_2\cos\beta_2)-(m_{c1}/2)g(L_1\cos\beta_1+2L_2\cos\beta_2)$$

$$-(m_{c2}/2)L_2\cos\beta_2 \quad . \tag{5.6}$$

Using Equations (5.3)-(5.6), Lagrange's equations of motion are

$$(1+C_m)mL^2\ddot{\psi} = Q_\psi , \tag{5.7a}$$

$$(1+C_m)(m/2)L^2\ddot{\theta} = Q_\theta , \tag{5.7b}$$

$$[(1+C_m)m(3+r_{h\ell})+(1+C_{mc})(m_{c1}/3)]L_1^2\ddot{\beta}_1+[(1+C_m)m(3+r_{h\ell})+(1+C_{mc})(m_{c1}/2)] *$$

$$L_1L_2[\ddot{\beta}_2\cos(\beta_1-\beta_2)+\dot{\beta}_2^2\sin(\beta_1-\beta_2)]+[m_h+(m_{c1}/2)]gL_1\sin\beta_1 = Q_{\beta 1}, \tag{5.7c}$$

$$[(1+C_m)m(3+r_{h\ell})+(1+C_{mc})(1+3L_1/L_2)(m_{c2}/3)]L_2^2\ddot{\beta}_2+[(1+C_m)m(3+r_{h\ell})$$

$$+(1+C_{mc})(m_{c1}/2)]L_1L_2[\ddot{\beta}_1\cos(\beta_1-\beta_2)-\dot{\beta}_1^2\sin(\beta_1-\beta_2)]+[m_h+m_{c1}+(m_{c2}/2)] *$$

$$gL_2\sin\beta_2 = Q_{\beta 2}, \tag{5.7d}$$

where Q_ψ, Q_θ, $Q_{\beta 1}$ and $Q_{\beta 2}$ are the generalized forces corresponding to co-ordinates ψ, θ, β_1 and β_2, respectively, arising due to the hydrodynamic forces.

5.1.2 Evaluation of the generalized forces

In order to determine $Q_i (i = \theta, \psi, \beta_1, \beta_2)$, an accurate knowledge of the hydrodynamic loading on an inclined circular cylinder is required. The drag forces on an element, proportional to the square of the velocity, can be resolved into two components F_N and F_T, normal and tangential to the element, respectively. As discussed earlier, F_N exhibits a sine square dependence on the angle of attack of the cylindrical element. However, no single form for F_T has been agreed upon. In this analysis, the functions used to describe F_N and F_T, are the ones proposed by Schneider and Nickels[24]. From the experimental data, they observed that F_N and F_T for unit length are given by

$$F_N = (\rho_w/2) C_N V^2 d \sin^2(\text{angle of attack})$$

and

$$F_T = (\rho_w/2) C_T V^2 d \cos^2(\text{angle of attack})$$

where V is the relative velocity of the element with respect to the fluid.

The coefficient C_N is obtained by noting that the normal drag is primarily a pressure drag. A detailed plot of C_N versus the Reynolds number Re(based on diameter) is given by Hoerner[21]. It is seen that C_N is approximately constant ($\approx$1.18) over the range $Re = 10^3 - 5 \times 10^5$ which covers the region of interest in the present situation.

The tangential drag is mainly the contribution of skin friction and the corresponding coefficient C_T is inversely proportional to the square root of the Reynolds number[21],

$$C_T = (\text{constant})\ R_e^{-1/2} .$$

Cannon[43] obtained a value of 7.69 for the proportionality constant by fitting the data of Relf and Powell[20] for a 0.388 inch diameter cable.

The hydrodynamic forces acting on an element $Ld\xi$ of the i^{th} leg can now be written as

$$d\bar{F}_{iT} = (\rho_w/2)C_T L d(\bar{W}_{\ell i}\cdot \bar{e}_{ti})|\bar{W}_{\ell i}\cdot \bar{e}_{ti}|\bar{e}_{ti}d\xi , \tag{5.8a}$$

and

$$d\bar{F}_{iN} = -(\rho_w/2)C_N L d\{\bar{W}_{\ell i}-(\bar{W}_{\ell i}\cdot \bar{e}_{ti})\bar{e}_{ti}\}|\bar{W}_{\ell i}-(\bar{W}_{\ell i}\cdot\bar{e}_{ti})\bar{e}_{ti}|d\xi, \tag{5.8b}$$

where $\bar{W}_{\ell i}$ is the relative velocity of the element with respect to the fluid and can be obtained by differentiating (5.2b) with the help of (5.2c) and (5.3b) and adding V to it. (The signs of the above expressions are exactly opposite to those in Reference 43, because of the difference in the definition of the relative velocity used).

Similarly, the hydrodynamic forces acting on an element ds_j on the j^{th} portion of the cable are given by

$$d\bar{F}_{Tcj} = (\rho_w/2)C_{Tc}d_c(\bar{W}_{cj}\cdot\bar{e}_{tcj})|\bar{W}_{cj}\cdot\bar{e}_{tcj}|\bar{e}_{tcj}ds_j \quad , \tag{5.8c}$$

and

$$d\bar{F}_{Ncj} = -(\rho_w/2)C_{Nc}d_c\{\bar{W}_{cj}-(\bar{W}_{cj}\cdot\bar{e}_{tcj})\bar{e}_{tcj}\}|\bar{W}_{cj}$$

$$-(\bar{W}_{cj}\cdot\bar{e}_{tcj})\bar{e}_{tcj}|ds_j \ , \qquad j = 1,\ 2\ , \tag{5.8d}$$

where d_c, C_{Tc} and C_{Nc} are the diameter, tangential and normal drag coefficients of the cable, respectively. The unit tangential vectors $\bar{e}_{tcj}$ are given by

$$\bar{e}_{tcj} = -(\sin\beta_j\bar{i} + \cos\beta_j\bar{k}) \quad , \tag{5.9a}$$

and $\bar{W}_{cj}$ can be obtained from

$$\bar{W}_{cj} = V\bar{i} + \bar{V}_{cj}(s_j) \quad , \tag{5.9b}$$

where $\bar{V}_{cj}(s_j)$ are as defined in Equation (5.5).

Consider a typical case of an array made of 6 inch diameter cylinders drifting with a velocity of 1 ft/sec. The corresponding Re is approximately 5×10^4. Hence

$$C_T{}' = 7.69\ Re^{-1/2} \simeq 0.034\ ,$$

which is substantially smaller than C_N. Although the value of C_{Tc} is slightly higher due to the smaller diameter of the cable, it is still small compared to C_{Nc}. Hence, in this simplified analysis, the tangential drag components will be ignored.

The generalized forces Q_k corresponding to the co-ordinates q_k are given by

$$Q_k = \sum_s \bar{F}_s \cdot \frac{\partial \bar{r}_s}{\partial q_k} ,$$

where $\bar{r}_s$ is the position vector, with respect to the inertial co-ordinate system, of the point of application of $\bar{F}_s$. Hence

$$Q_\psi = (\rho_w/2)C_N L^2 d \sum_{i=1}^{3} \int_0^1 \xi|\bar{A}_i|[\{(V+V_{hx_0})\cos\theta - V_{hz_0}\sin\theta\}\sin\psi_i - \xi L\dot{\psi}]d\xi , \tag{5.10a}$$

$$Q_\theta = (\rho_w/2)C_N L^2 d \sum_{i=1}^{3} \int_0^1 \xi|\bar{A}_i|[(V+V_{hx_0})\sin\theta + V_{hz_0}\cos\theta - \xi L\dot{\theta}\cos\psi_i]\cos\psi_i d\xi , \tag{5.10b}$$

$$Q_{\beta 1} = (\rho_w/2)C_N L L_1 d[\sum_{i=1}^{3} \int_0^1 |\bar{A}_i|\{(V+V_{hx_0})\cos\beta_1 - V_{hz_0}\sin\beta_1 - \cos(\beta_1-\theta)\cos^2\psi_i \,*$$

$$((V+V_{hx_0})\cos\theta - V_{hz_0}\sin\theta) - \xi L\dot{\psi}\sin\psi_i\cos(\beta_1-\theta) + \xi L\dot{\theta}\cos\psi_i\sin(\beta_1-\theta)\}d\xi]$$

$$+(\rho_w/2)C_{Nc}d_c[\int_0^1 |V\cos\beta_1 - s_1\dot{\beta}_1 - L_2\dot{\beta}_2\cos(\beta_1-\beta_2)|\{V\cos\beta_1 - s_1\dot{\beta}_1$$

$$-L_2\dot{\beta}_2\cos(\beta_1-\beta_2)\}s_1 ds_1] , \tag{5.10c}$$

and

$$Q_{\beta 2} = (\rho_w/2)C_N L L_2 d[\sum_{i=1}^{3}\int_0^1 |\bar{A}_i|\{(V+V_{hx_0})\cos\beta_2 - V_{hz_0}\sin\beta_2 - \cos(\beta_2-\theta)\cos^2\psi_i *$$

$$((V+V_{hx_0})\cos\theta - V_{hz_0}\sin\theta) - \xi L\dot{\psi}\sin\psi_i\cos(\beta_2-\theta) + \xi L\dot{\theta}\cos\psi_i\sin(\beta_2-\theta)\}d\xi]$$

$$+(\rho_w/2)C_{Nc}d_c[L_2\int_0^1 |V\cos\beta_1 - s_1\dot{\beta}_1 - L_2\dot{\beta}_2\cos(\beta_1-\beta_2)|\{V\cos\beta_1 - s_1\dot{\beta}_1$$

$$-L_2\dot{\beta}_2\cos(\beta_1-\beta_2)\}\cos(\beta_1-\beta_2)ds_1 + \int_0^{L_2}|V\cos\beta_2 - s_2\dot{\beta}_2|(V\cos\beta_2$$

$$-s_2\dot{\beta}_2)s_2 ds_2 \quad , \tag{5.10d}$$

where

$$\bar{A}_i = \bar{W}_{\ell i} - (\bar{W}_{\ell i}\cdot \bar{e}_{ti})\bar{e}_{ti} \quad .$$

Defining a dimensionless time τ by

$$\tau = 10Vt/(L_1+L_2) = 10Vt/L_c \quad , \tag{5.11}$$

the equations of motion (5.7) in conjunction with (5.10) may now be written as

$$\psi'' = \alpha R\{(R_1+R_2)/10\}^2 \sum_{i=1}^{3}\int_0^1 |\bar{a}_i|[\{(1+u_{hx_0})\cos\theta - u_{hz_0}\sin\theta\}\sin\psi_i - 10\xi\psi'$$

$$/(R_1+R_2)]\xi d\xi \quad , \tag{5.12a}$$

$$\theta'' = 2\alpha R\{(R_1+R_2)/10\}^2 \sum_{i=1}^{3}\int_0^1 |\bar{a}_i|\{(1+u_{hx_0})\sin\theta+u_{hz_0}\cos\theta-10\xi\theta'\cos\psi_i$$

$$/(R_1+R_2)\}\cos\psi_i\xi d\xi \quad , \tag{5.12b}$$

$$\{(3+r_{h\ell})+R_1r_{c\ell}/3(R_1+R_2)\}\beta_1''+\{(3+r_{h\ell})+R_1r_{c\ell}/2(R_1+R_2)\}(R_2/R_1) *$$

$$\{\beta_2''\cos(\beta_1-\beta_2)+\beta_2'^2\sin(\beta_1-\beta_2)\}+\{1+(R_1r_{ch}/2)/(R_1+R_2)\}r_1(R/R_1)*$$

$$r_{hd}\sin\beta_1 \quad = \quad \bar{Q}_{\beta 1} \quad , \tag{5.12c}$$

and

$$\{(3+r_{h\ell})+(1/3)(3R_1+R_2)r_{c\ell}/(R_1+R_2)\}\beta_2''+\{(3+r_{h\ell})+(R_1r_{c\ell}/2)/(R_1+R_2)\}*$$

$$(R_1/R_2)\{\beta_1''\cos(\beta_1-\beta_2)-\beta_1'^2\sin(\beta_1-\beta_2)\}+\{1+(1/2)(2R_1+R_2)r_{ch}/(R_1+R_2)\}*$$

$$r_1(R/R_2)r_{hd}\sin\beta_2 \quad = \quad \bar{Q}_{\beta 2}, \tag{5.12d}$$

where $r_{c\ell} = m_c(1+C_{mc})/m(1+C_m)$, $r_{ch} = m_c/m_h$, $(m_c = m_{c1}+m_{c2})$,

$r_1 = 2\{(R_1+R_2)/10\}^2/\pi(1+C_m)$, $R = L/d$, $R_1 = L_1/L$, $R_2 = L_2/L$,

$$R_d = d_c/d, \quad R_\rho = \rho_c/\rho_w, \quad r_{hd} = 2m_h g/\rho_w V^2 L d,$$

$$u_{hj} = V_{hj}/V, (j = x_0, y_0, z_0) \quad ,$$

$$\bar{Q}_{\beta 1} = (Rr_1)[(C_N/R_1)\sum_{i=1}^{3}\int_0^1 |\bar{a}_i|\{((1+u_{hx_0})\cos\beta_1 - u_{hz_0}\sin\beta_1$$

$$-\cos(\beta_1-\theta)\cos^2\psi_i((1+u_{hx_0})\cos\theta - u_{hz_0}\sin\theta) - 10\xi\psi'\sin\psi_i\cos(\beta_1$$

$$-\theta)/(R_1+R_2)+10\xi\theta'\cos\psi_i\sin(\beta_1-\theta)/(R_1+R_2)\}d\xi + C_{Nc}R_d\int_0^1 |\cos\beta_1$$

$$-10R_2\beta_2'\cos(\beta_1-\beta_2)/(R_1+R_2) - 10R_1\beta_1'(s_1/L_1)/(R_1+R_2)|\{\cos\beta_1$$

$$-10R_2\beta_2'\cos(\beta_1-\beta_2)/(R_1+R_2) - 10R_1\beta_1'(s_1/L_1)/(R_1+R_2)\}(s_1/L_1)d(s_1/L_1)],$$

$$\bar{Q}_{\beta 2} = (Rr_1)[(C_N/R_2)\sum_{i=1}^{3}\int_0^1 |\bar{a}_i|\{((1+u_{hx_0})\cos\beta_2 - u_{hz_0}\sin\beta_2 - \cos(\beta_2-\theta)\cos^2\psi_i *$$

$$((1+u_{hx_0})\cos\theta - u_{hz_0}\sin\theta) - 10\xi\psi'\sin\psi_i\cos(\beta_2-\theta)/(R_1+R_2) + 10\xi\theta'\cos\psi_i \; *$$

$$\sin(\beta_2-\theta)/(R_1+R_2)\}d\xi + C_{Nc}R_d(R_1/R_2)\int_0^1 |\cos\beta_1 - 10R_2\beta_2'\cos(\beta_1-\beta_2)/(R_1+R_2)$$

$$-10R_1\beta_1'(s_1/L_1)/(R_1+R_2)|\{\cos\beta_1-10R_2\beta_2'\cos(\beta_1-\beta_2)/(R_1+R_2)$$

$$-10R_1\beta_1'(s_1/L_1)/(R_1+R_2)\}\cos(\beta_1-\beta_2)d(s_1/L_1)+C_{Nc}R_d\int_0^1|\cos\beta_2$$

$$-10R_2\beta_2'(s_2/L_2)/(R_1+R_2)|\{\cos\beta_2-10R_2\beta_2'(s_2/L_2)(R_1+R_2)\}(s_2/L_2)\ *$$

$$d(s_2/L_2)]$$

and

$$|\bar{a}_i|^2 = (1+u_{hx_0})^2(1-\cos^2\psi_i\cos^2\theta)+u_{hz_0}^2(1-\cos^2\psi_i\sin^2\theta)+2(1+u_{hx_0})u_{hz_0}$$

$$\cos^2\psi_i\sin\theta\cos\theta-\{20\xi/(R_1+R_2)\}[\psi'\{(1+u_{hx_0})\cos\theta-u_{hz_0}\sin\theta\}\sin\psi_i$$

$$+\theta'\{(1+u_{hx_0})\sin\theta+u_{hz_0}\cos\theta\}\cos\psi_i]+\{10/(R_1+R_2)\}^2\xi^2(\psi'^2+\theta'^2\cos^2\psi_i). \tag{5.12e}$$

Here prime denotes differentiation with respect to the dimensionless time. The objective is to analyze this set of highly nonlinear and coupled equations of motion to assess the influence of system parameters on its equilibrium configurations and free vibration.

5.2 Steady State Configurations and System Response

For equilibrium configurations, time derivatives in the equations of motion must vanish. Hence

$$\sum_{i=1}^{3} |\bar{a}_{i0}| \cos\theta_0 \sin\psi_{i0} = 0 \;, \tag{5.14a}$$

$$\sum_{i=1}^{3} |a_{i0}| \sin\theta_0 \cos\psi_{i0} = 0 \;, \tag{5.14b}$$

$$[1+(r_{ch}R_1/2)/(R_1+R_2)](r_{hd}/R_1)\sin\beta_{10}-[(C_N/R_1)\sum_{i=1}^{3}|\bar{a}_{i0}|\{\cos\beta_{10}$$

$$-\cos(\beta_{10}-\theta_0)\cos^2\psi_{i0}\cos\theta_0\}+(C_{Nc}R_d/2)\cos^2\beta_{10}] = 0 \;, \tag{5.14c}$$

and

$$[1+(r_{ch}/2)(2R_1+R_2)/(R_1+R_2)](r_{hd}/R_2)\sin\beta_{20}-[(C_N/R_2)\sum_{i=1}^{3}|\bar{a}_{i0}|\{\cos\beta_{20}$$

$$-\cos(\beta_{20}-\theta_0)\cos^2\psi_{i0}\cos\theta_0\}+C_{Nc}R_d\{(R_1/R_2)\cos^2\beta_{10}\cos(\beta_{10}-\beta_{20})$$

$$+(1/2)\cos^2\beta_{20}\}] = 0 \;, \tag{5.14d}$$

where

$|\bar{a}_{i0}|^2 = 1-\cos^2\psi_{i0}\cos^2\theta_0$ and subscript '0' refers to equilibrium configurations. Examination of (5.14a) and (5.14b) yields the following combinations of θ_0 and $\psi_0(= \psi_{i0}-I_i)$:

$$
\begin{aligned}
&\text{(i)} \quad \theta_0 = 0, \quad \psi_0 = 0; \\
&\text{(ii)} \quad \theta_0 = 0, \quad \psi_0 = \pi/3; \\
&\text{(iii)} \quad \theta_0 = \pi/2, \quad \psi_0 = 0; \\
&\text{(iv)} \quad \theta_0 = \pi/2, \quad \psi_0 = \pi/3.
\end{aligned}
\tag{5.15}
$$

Equations (5.14c) and (5.14d) in conjunction with (5.15) can now be solved to determine β_{10} and β_{20} for a given set of system parameters.

Efforts were made to isolate the effects of different parameters on the dynamical behaviour around the steady state configuration of the system. Since the length of the cable is decided by considerations other than just the stability of the system, it was used to define a dimensionless time τ in Equation (5.11). The real damping time can now easily be determined from τ once the drifting velocity and the cable length are given. As the equations of motion were highly nonlinear, the response of the system was studied by numerical method. An Adams-Bashforth predictor-corrector quadrature with a Runge-Kutta starter was used. Initial disturbances of 20° from the equilibrium configurations were given to all the degrees of freedom. As the displacements were rather large, a small step size of 0.002 was required to give sufficient accuracy. (For a system drifting with a velocity of 1 ft/sec and having a cable 100 ft long, this amounts to 0.02 sec). For larger cable lengths, the step size had to be reduced further.

5.3 Results and Discussion

Of the four possible steady state configurations cited in Equation (5.15), only the first one was found to be stable. This corresponds to the array remaining horizontal and the leading leg

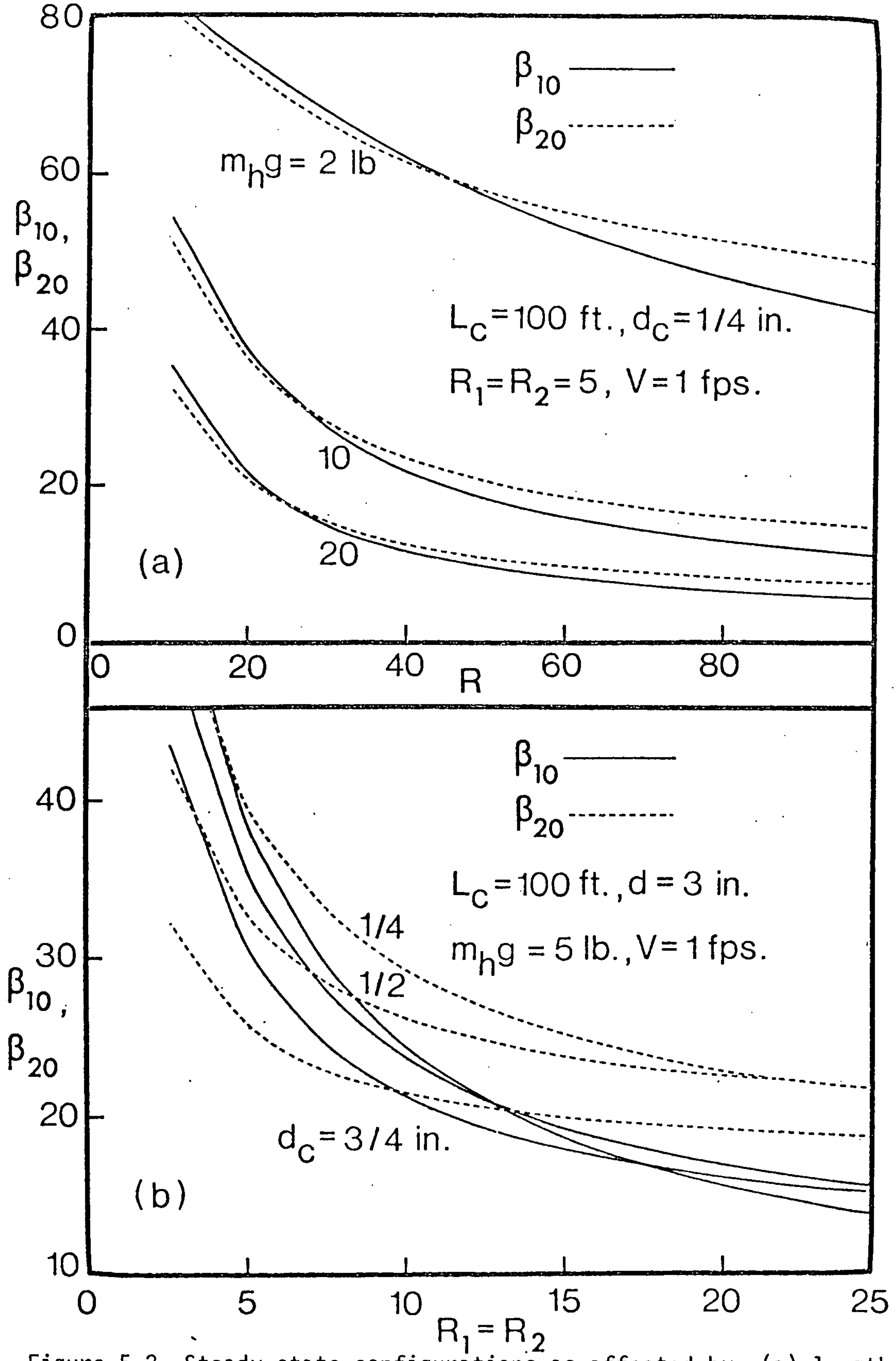

Figure 5-2 Steady state configurations as affected by: (a) length to diameter ratio (R) of a leg and the weight ($m_h g$) of the central head; (b) length ratios R_1 and R_2, and the diameter of the cable

aligned in the direction of drifting. It may be pointed out that the equilibrium orientation corresponds to $\theta_0 = 0$, because the cable was assumed to be connected to the centre of mass of the array. In practice, this may not be strictly true and θ_0 may acquire a small non-zero value.

The variation of angles β_{10} and β_{20} which characterize the steady state shape of a given cable is shown in Figure 5-2. The effects of a given parameter on β_{10} and β_{20} are essentially similar. The shape of a given cable when viewed from the buoy changes from convex to concave as the diameter or length of each leg is reduced. It may be observed from Figure 5-2a that both β_{10} and β_{20} decrease with an increase in R as well as r_{hd}. Hence a smaller diameter of the legs or a heavier central head keeps the system closer to the vertical. The effect of increasing the length ratios R_1 and R_2 or the diameter of the cable is to make β_{10} and β_{20} smaller (Figure 5-2b).

Figure 5-3 shows some typical plots of the system response. It may be noticed that when a disturbance is given to the $\psi_0 = 60°$ equilibrium configuration (ii, in Equation 5.15) ψ increases, finally reaching a value of 120° (Figure 5-3a). This corresponds to the other steady state orientation in which the leading leg is aligned with the direction of drifting. But if an initial displacement is given to $\psi_0 = 0$ configuration, the system returns to the starting equilibrium position (Figure 5-3b). Hence the former is an unstable equilibrium while the latter a stable one. Of course, for the second case, a disturbance exceeding 60° would result in the system attaining an alternate stable orientation.

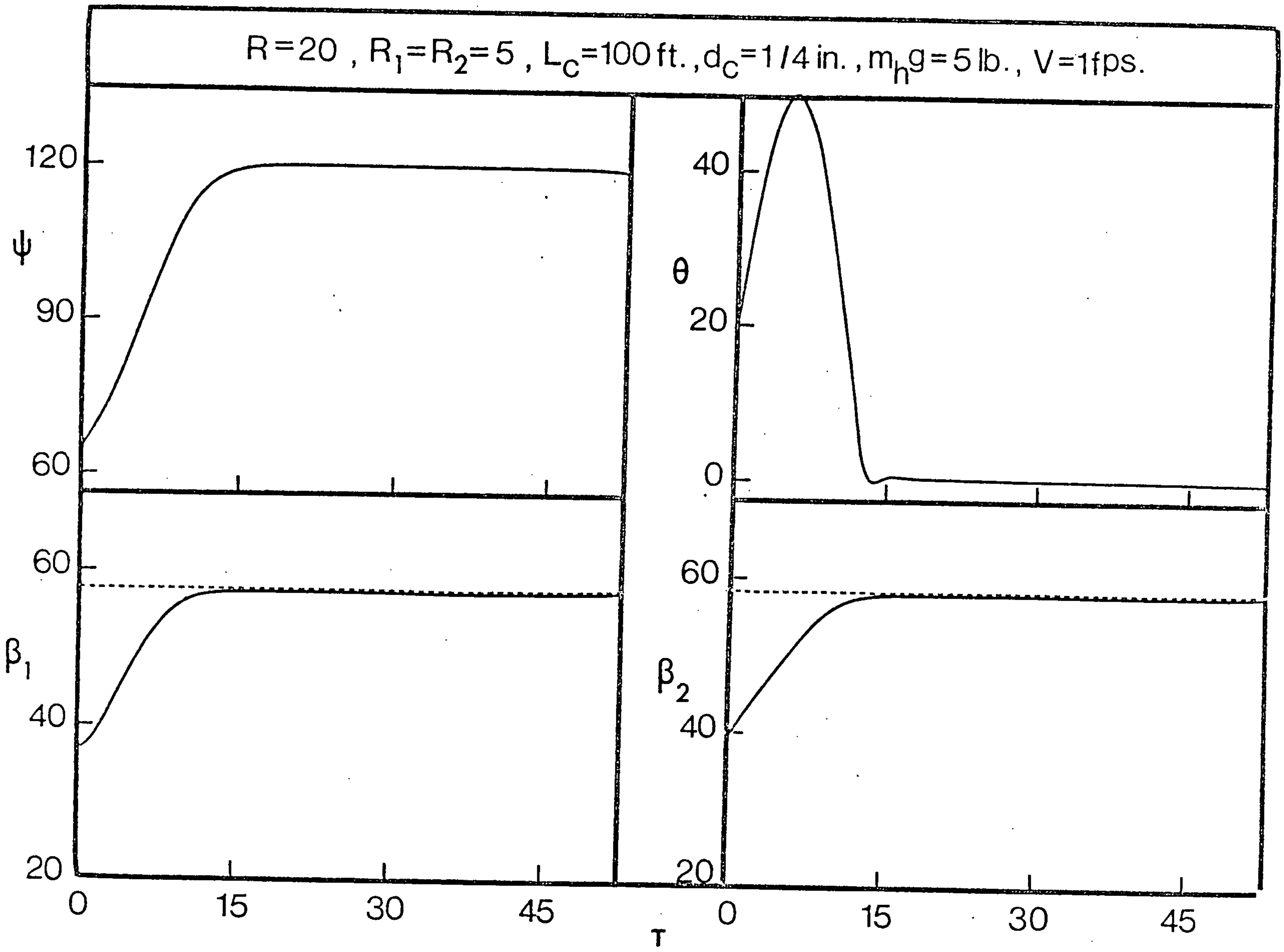

Figure 5-3 Typical response plots of the simplified drifting model: (a) unstable orientation

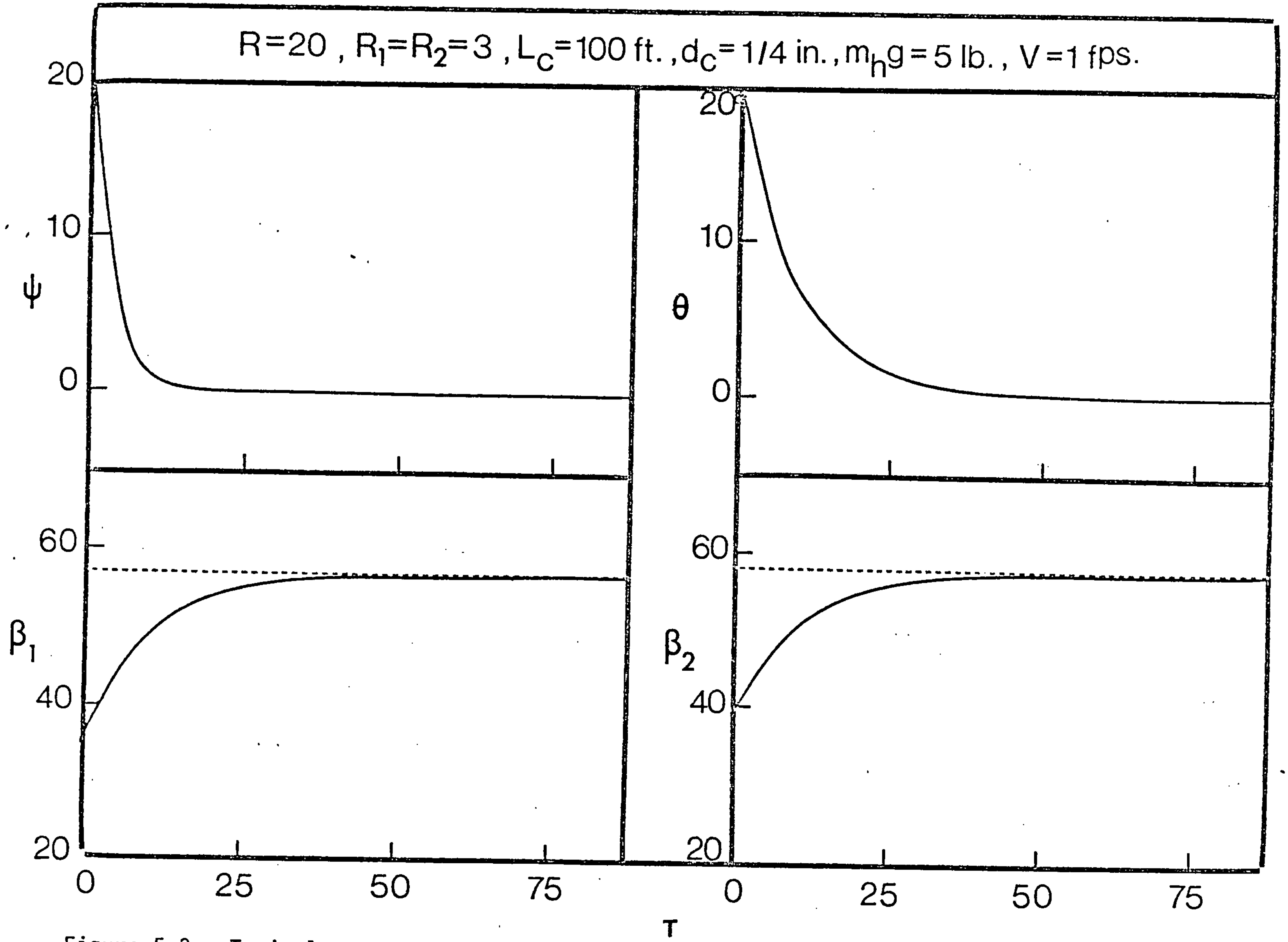

Figure 5-3 Typical response plots of the simplified drifting model: (b) stable orientation

It was noticed that initial disturbances given to the steady state configuration characterized by $\psi_0 = 0$, damp out asymptotically in the range of parameter values considered. No oscillatory motion was encountered. However, decaying rates are dependent on the system parameters. In order to compare the damping ratio, arbitrary displacements of 20° were given to each degree of freedom and the time taken to come within 1° of the equilibrium angles was noted. It was observed that the decay of the yawing motion of the array is the fastest followed by that of its pitching motion and the pendulum type oscillations of the cable.

Figure 5-4 shows the variation of damping rates with R_1 and R_2 (i.e. ratios of the lengths of two linear portions of the cable to that of the leg) and R (length to diameter ratio of the leg). It is of interest to recognize that increase in R_1 and R_2 improves the decaying characteristics (Figure 5-4a). Hence for a given cable length, shorter arm lengths are desirable. But this would create an apparent problem in signal processing due to a reduction in phase difference of the detected signals. Thus, as is often the case in a practical design, one is faced with a situation demanding a compromise between conflicting requirements. For specified L_c, R_1 and R_2, a larger R reduces the damping times for θ, β_1 and β_2 increasing that for ψ slightly (Figure 5-4b). This indicates that a smaller diameter of the legs is preferrable. Table 5-1 indicates the influence of the central head, cable and drifting velocity associated parameters on the damping rate. Changing the weight of the central head does not have significant effect

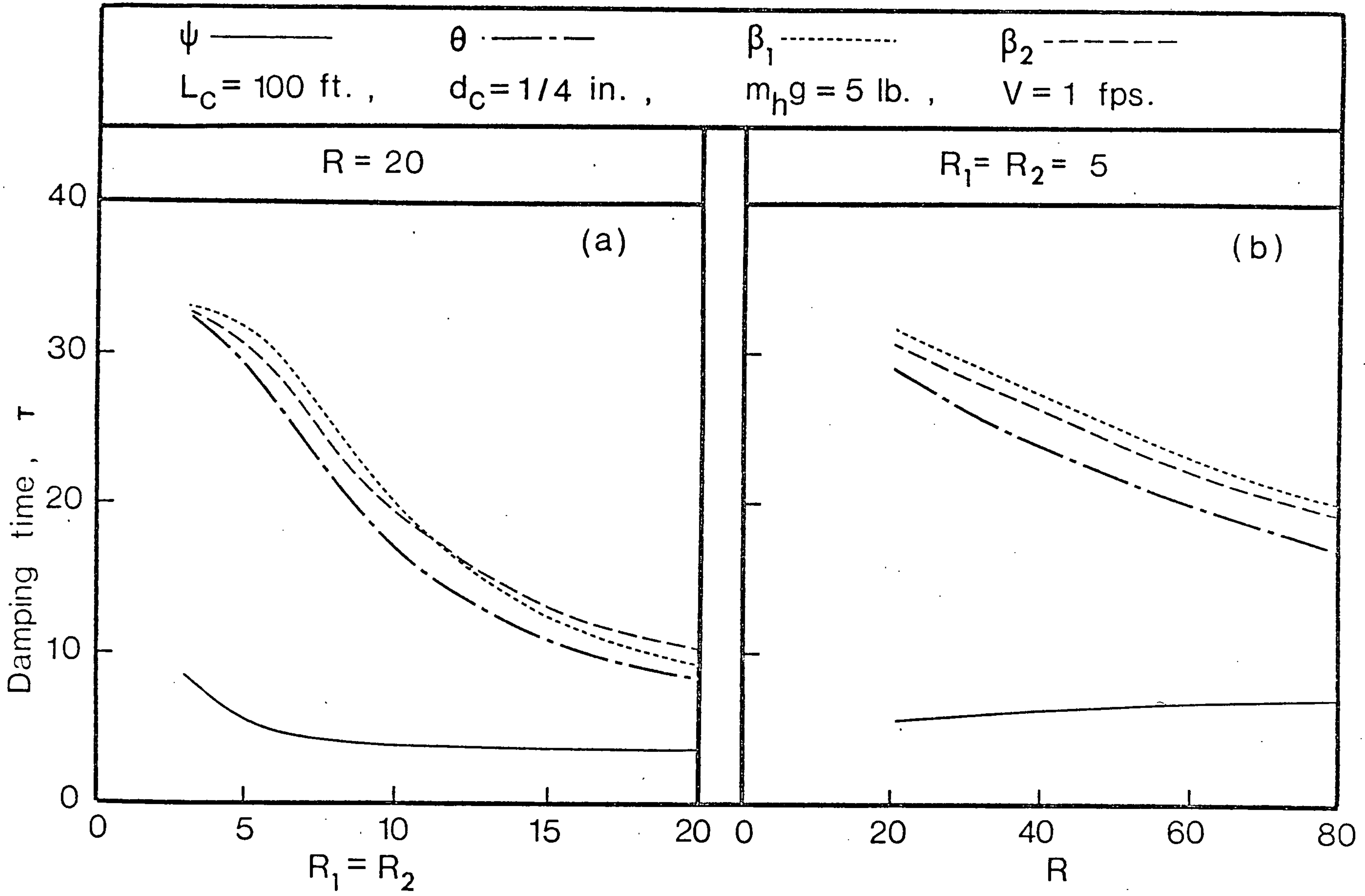

Figure 5-4 Variation of damping rates of the disturbances with: (a) length ratios R_1 and R_2; (b) length to diameter ratio (R) of a leg

TABLE 5.1

Influence of the Central Head, Cable Dimensions and Drifting Velocity on Damping Time

Parameters Varied	Damping Time t, sec $t = L_c\tau/10\ V$				Comment
	ψ	θ	β_1	β_2	
$m_h g = 5$ lb $m_h g = 7.5$ lb	55.5 58	292 270	316 301	306 293	$R = 20$, $R_1 = R_2 = 5$, $L_c = 100$ ft, $d_c = (1/4)$in, $V = 1$ ft/sec
$d_c = (1/4)$in $d_c = (1/2)$in	55.5 58	292 263	316 294	306 269	$R = 20$, $R_1 = R_2 = 5$, $L_c = 100$ ft, $V = 1$ ft/sec, $m_h g = 5$ lb
$L_c = 100$ ft $L_c = 200$ ft	38.5 58	169 large	198 520	195 520	$R = 20$, $R_1 = R_2 = 10$, $d_c = (1/4)$in, $V = 1$ ft/sec, $m_h g = 5$ lb
$V = 1$ ft/sec $V = 0.5$ ft/sec	55.5 145	292 273	316 340	306 327	$R = 20$, $R_1 = R_2 = 5$, $L_c = 100$ ft, $d_c = (1/4)$in, $m_h g = 5$ lb

on the decay of the disturbances. It affects only the steady state shape of the cable (Figure 5-2). For a given array, an increase in the diameter of the cable with its length fixed improves the stability slightly while an increase in the length with its diameter fixed slows down the decay. Finally, for a higher drifting velocity, the decay of the disturbances (except θ) is faster, because the drag forces involved are larger.

5.4 Concluding Remarks

The significant conclusions based on the above analysis of drifting assembly can be summarized as follows:

(i) Of the four possible steady state orientations, only the one in which the array lies in a horizontal plane with its leading leg aligned in the direction of drifting, is stable. Other orientations, when disturbed, tend to reach this stable configuration.

(ii) Smaller length and diameter of the legs or a heavier central head keeps the cable closer to the vertical.

(iii) The system is asymptotically stable in the range of parameters of practical interest.

(iv) Reduction in the length or diameter of the arms generally improves the decaying characteristics of the system. However, as the minimum acceptable length is governed by the signal processing considerations, the final design will reflect a degree of compromise.

(v) Although a smaller diameter has favourable influence on the stability according to this rigid array analysis, consideration of flexibility (accentuated by smaller diameter) may alter this conclusion.

6. GENERAL DYNAMICS OF THE DRIFTING ASSEMBLY

Having gained a preliminary understanding of the system dynamics, the next logical step would be to remove some of the restrictions inherent in the simplified model analyzed. The flexibility of the legs, which was ignored before, must be taken into account since it may affect the stability of the system to a great extent. The bilinear approximation of the cable should be removed to bring the model closer to the reality. Moreover, the effect of the tangential drag, which was neglected before, must be considered. The purpose of this chapter is to bring over these improvements in the analysis of a drifting buoy-cable-array system.

At first, a general Lagrangian formulation of the problem is presented. The steady state configurations of the flexible legs subjected to hydrodynamic loading are determined, and an approximate equilibrium shape of the three dimensional cable developed in terms of the slope and curvature at the central head. As the system with all its nonlinearities is not easily tractable, a linearized perturbation analysis around the steady state is undertaken. Frequencies for both lateral and longitudinal motions of the system are determined by analyzing the resulting eigenvalue problem, and the effects of different system parameters on the decay of the disturbances evaluated.

6.1 Formulation of the Problem

Consider a buoy-cable-array assembly drifting with a uniform velocity V (Figure 6-1). Let x_0, y_0, z_0 be an inertial co-ordinate system with its origin B fixed to the centre of the buoy. A parallel frame of reference x_1, y_1, z_1 has its origin at the centre H of the array. Clearly,

$$(x_1,y_1,z_1) = (x_0,y_0,z_0) + (x_{1b},y_{1b},z_{1b}) \quad , \tag{6.1}$$

where x_{1b}, y_{1b} and z_{1b} are the co-ordinates of B referred to the co-ordinate axes x_1, y_1 and z_1, respectively. Consider an element ds at a distance s from H, measured along the cable. The unit vectors $\bar{e}_{tc}$, $\bar{e}_{nc}$ and $\bar{e}_{pc}$ define the orientation of the element such that $\bar{e}_{tc}$ is tangential to it and positive in the direction of travel upstream along the cable, and $\bar{e}_{nc}$ is normal to the element and lies in the plane formed by $\bar{e}_{tc}$ and $\bar{W}_c$, the relative velocity with respect to the fluid. The sense of $\bar{e}_{nc}$ is such as to make $\bar{e}_{nc} \cdot \bar{W}_c \leq 0$. The third unit vector $\bar{e}_{pc}$ completes the right hand orthonormal system. Let β be the inclination of the element to the vertical and ε the angle made by its projection in the horizontal plane with the x_0 axis. The above mentioned unit vectors can be expressed in terms of β, ε, $\bar{i}$, $\bar{j}$ and $\bar{k}$ as follows:

$$\bar{e}_{tc} = \sin\beta\cos\varepsilon\bar{i}+\sin\beta\sin\varepsilon\bar{j}+\cos\beta\bar{k} \quad , \tag{6.2a}$$

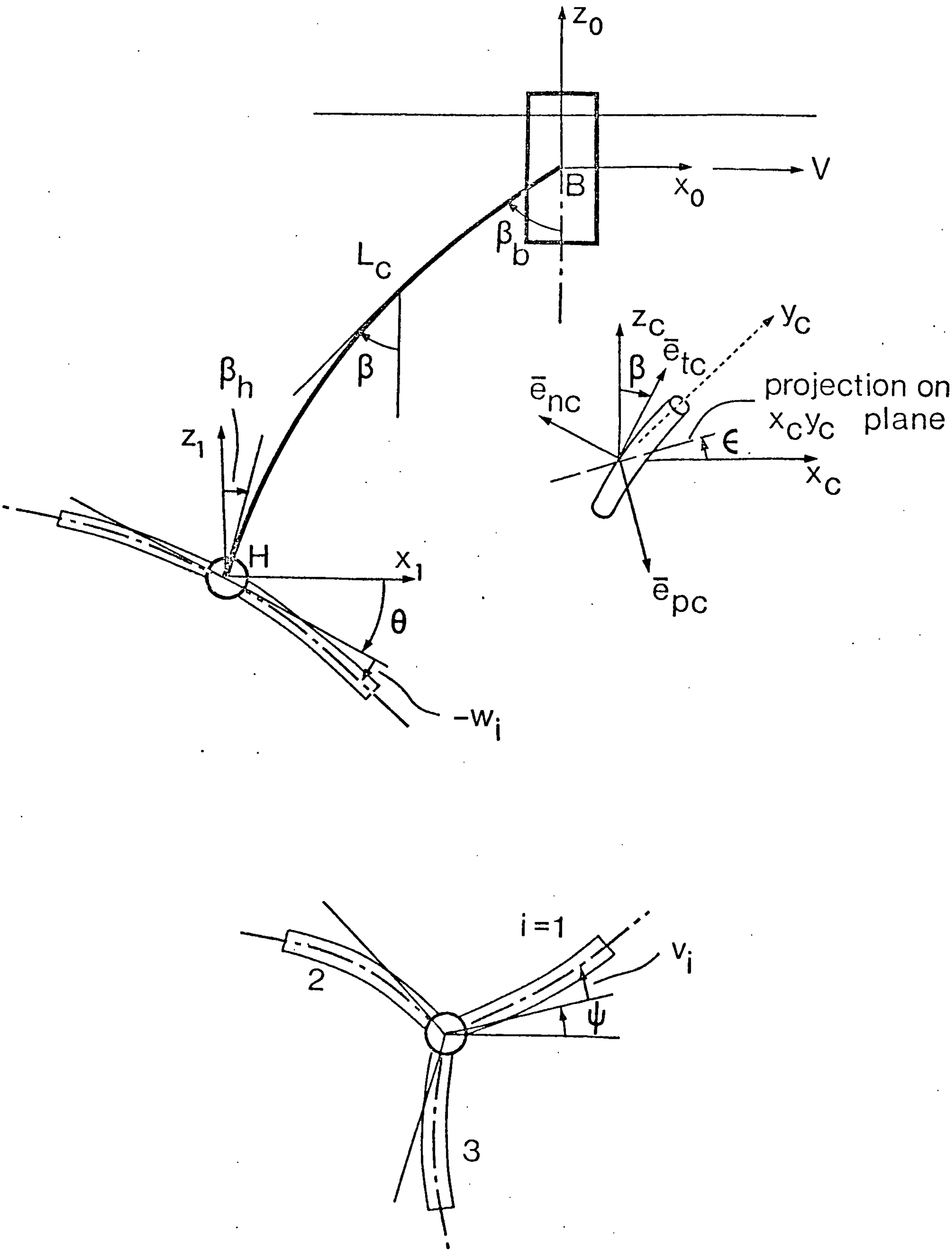

Figure 6-1 Geometry of drifting assembly with flexible legs

$$\bar{e}_{nc} = -\cos\beta\cos\varepsilon\bar{i}-\cos\beta\sin\varepsilon\bar{j}+\sin\beta\bar{k} \quad , \tag{6.2b}$$

$$\bar{e}_{pc} = \sin\varepsilon\bar{i}-\cos\varepsilon\bar{j} \quad , \tag{6.2c}$$

where $\bar{i}$, $\bar{j}$ and $\bar{k}$ are unit vectors in x_0, y_0 and z_0 directions, respectively. On the other hand, the angles β and ε are related to the Cartesian components of ds by

$$\sin\beta\cos\varepsilon = \frac{dx_1}{ds} \quad , \tag{6.3a}$$

$$\sin\beta\sin\varepsilon = \frac{dy_1}{ds} \quad , \tag{6.3b}$$

and

$$\cos\beta = \frac{dz_1}{ds} \quad . \tag{6.3c}$$

The velocity of this element is given by

$$\bar{V}_c = (\dot{x}_1-\dot{x}_{1b})\bar{i}+(\dot{y}_1-\dot{y}_{1b})\bar{j}+(\dot{z}_1-\dot{z}_{1b})\bar{k} \ . \tag{6.4}$$

The coordinate system x_1, y_1, z_1 is transformed to x, y, z axes by rotations θ of the plane of the array about y_1 axis and ψ in the plane of the array giving its final orientation. As observed in Chpater 3, for analysis in the small, two Eulerian rotations describe any arbitrary orientation. The flexural displacements, which are now superposed on these rotations, can be resolved into two components: v_i in the plane of the array and w_i perpendicular to it. Hence the co-ordinates of a point on the i^{th} leg at a distance $\xi L(0\leq\xi\leq 1)$ from the root are given by

$$x = \xi L\cos I_i - v_i\sin I_i \ , \tag{6.5a}$$

$$y = \xi L\sin I_i + v_i\cos I_i \ , \tag{6.5b}$$

$$z = w_i \ , \tag{6.5c}$$

where I_i is given by (3.3b).

The kinetic energy T of the system comprises of T_a of the array, T_h of the central head and T_c of the cable where

$$\begin{aligned}T_a = {} & (m/2)(1+C_m)[3(\dot{x}_{1b}^2+\dot{y}_{1b}^2+\dot{z}_{1b}^2)+\sum_{i=1}^{3}\int_0^1[\dot{\psi}^2(\xi^2L^2+v_i^2)+\dot{\theta}^2(\xi^2L^2\cos^2\psi_i \\ & +v_i^2\sin^2\psi_i-\xi Lv_i\sin 2\psi_i+w_i^2)-2\dot{\psi}\dot{\theta}w_i(\xi L\sin\psi_i+v_i\cos\psi_i) \\ & +2\dot{\theta}\{-\xi L\dot{w}_i\cos\psi_i+v_i\dot{w}_i\sin\psi_i-w_i\dot{v}_i\sin\psi_i-v_i\sin\psi_i(\dot{x}_{1b}\sin\theta+\dot{z}_{1b}\cos\theta) \\ & +w_i(-\dot{x}_{1b}\cos\theta+\dot{z}_{1b}\sin\theta)\}+2\dot{\psi}\{\xi L\dot{v}_i+v_i(\dot{x}_{1b}\cos\theta\cos\psi_i+\dot{y}_{1b}\sin\psi_i \\ & -\dot{z}_{1b}\sin\theta\cos\psi_i)\}-2\dot{v}_i(-\dot{x}_{1b}\cos\theta\sin\psi_i+\dot{y}_{1b}\cos\psi_i+\dot{z}_{1b}\sin\theta\sin\psi_i) \\ & -2\dot{w}_i(\dot{x}_{1b}\sin\theta+\dot{z}_{1b}\cos\theta)+(\dot{v}_i^2+\dot{w}_i^2)]d\xi] \ ,\end{aligned} \tag{6.6a}$$

$$T_h = (m_h/2)(1+C_{mh})(\dot{x}_{1b}^2+\dot{y}_{1b}^2+\dot{z}_{1b}^2)+(I_{xxa}\sin^2\psi+I_{yya}\cos^2\psi)(\dot{\theta}^2/2)$$

$$+I_{zza}\dot{\psi}^2/2 \quad , \tag{6.6b}$$

$$T_c = \int_{m_c}\{(\dot{x}_1-\dot{x}_{1b})^2+(\dot{y}_1-\dot{y}_{1b})^2+(\dot{z}_1-\dot{z}_{1b})^2\}(1+C_{mc})(dm_c/2), \tag{6.6c}$$

and ψ_i as obtained from (5.1). The above expressions include the kinetic energy associated with the apparent inertia.

To determine $\dot{x}_{1b}$, $\dot{y}_{1b}$ and $\dot{z}_{1b}$ appearing in the above expressions, the geometry of the cable must be known. It has been shown by Cannon[43] that the two dimensional steady state cable configuration is given by

$$\frac{d^2\beta}{ds^2} + f(\beta)\left(\frac{d\beta}{ds}\right)^2 = 0 \quad , \tag{6.7a}$$

where

$$f(\beta) = [2\rho_c g\cos\beta+(\rho_w/2)C_{Tc}d_cV^2\sin^2\beta+\rho_wC_{Nc}d_cV^2\sin\beta\cos\beta]/$$

$$[-\rho_c g\ \sin\beta+(\rho_w/2)C_{Nc}d_cV^2\cos^2\beta] \quad . \tag{6.7b}$$

Since the above equation is not tractable exactly, an approximate solution may be obtained by taking an average value for $f(\beta)$, say f. The solution of the equation can now be obtained as

$$\beta = \beta_h + (1/f)\ell n(1+fG_h s) \quad , \tag{6.8a}$$

where

$$\beta_h = (\beta)_{s=0} \quad \text{and} \quad G_h = \left(\frac{d\beta}{ds}\right)_{s=0} \quad .$$

Hence from Equation (6.3c)

$$z_1 = \int_0^s \cos\beta \, ds$$

$$= [(1+fG_h s)(f\cos\beta + \sin\beta) - (f\cos\beta_h + \sin\beta_h)]/G_h(1+f^2) \quad . \tag{6.8b}$$

If the curvature of the cable is assumed to be small, which is the case for most practical situations, $G_h = \left(\frac{d\beta}{ds}\right)_{s=0}$ is small, and its second and higher powers may be neglected. Hence from Equations (6.8a) and (6.8b)

$$\beta = \beta_h + G_h s \quad , \tag{6.9a}$$

and

$$z_1 = s\cos\beta_h - (1/2)G_h s^2 \sin\beta_h \quad . \tag{6.9b}$$

For the oscillating cable, it will be assumed that the functional relation between β and s remains approximately the same as that of a nonvibrating cable. However, the quantities β_h and G_h now become functions of time. The equations governing the behaviour of a cable in three dimensions being of similar form[43], the expressions for β and ε, similar to the two dimensional solution for β, would be logical initial choices in the general case. Moreover, the lateral motion being usually small,

$$\sin \varepsilon \simeq \varepsilon \ .$$

Accordingly,

$$\beta = \beta_h(t) + G_h(t)s \ , \tag{6.10a}$$

and

$$\varepsilon = \varepsilon_h(t) + k_h(t)s \ . \tag{6.10b}$$

From Equations (6.3) and (6.10), neglecting second and higher powers of G_h, ε_h and k_h,

$$x_1 = s \sin\beta_h + (1/2)G_h s^2 \cos\beta_h \ , \tag{6.11a}$$

$$y_1 = \{\varepsilon_h s + (1/2)k_h s^2\}\sin\beta_h \ , \tag{6.11b}$$

and

$$z_1 = s \cos\beta_h - (1/2)G_h s^2 \sin\beta_h \ . \tag{6.11c}$$

Noting that $x_{1b} = x_1(L_c)$, $y_{1b} = y_1(L_c)$ and $z_{1b} = z_1(L_c)$, substitution of (6.11) into (6.6) leads to

$$T = (\dot{\psi}^2/2)[m(1+C_m)(L^2+\sum_{i=1}^{3}\int_0^1 v_i^2 d\xi)+I_{zza}]+(\dot{\theta}^2/2)[m(1+C_m)\{(L^2/2)$$

$$+\sum_{i=1}^{3}(\sin^2\psi_i\int_0^1 v_i^2 d\xi+\int_0^1 w_i^2 d\xi-L\sin 2\psi_i\int_0^1 \xi v_i d\xi)\}+(I_{xxa}\sin^2\psi+I_{yya} \ *$$

$$\cos^2\psi)]+(m/2)(1+C_m)\sum_{i=1}^{3}\int_0^1(\dot{v}_i^2+\dot{w}_i^2)d\xi-m(1+C_m)\dot{\psi}\dot{\theta}\sum_{i=1}^{3}\{L\sin\psi_i\int_0^1\xi w_i d\xi$$

$$+\cos\psi_i\int_0^1 v_i w_i d\xi\}+m(1+C_m)\dot{\theta}\sum_{i=1}^{3}\int_0^1(-L\xi\dot{w}_i\cos\psi_i+v_i\dot{w}_i\sin\psi_i-w_i\dot{v}_i\sin\psi_i)d\xi$$

$$+m(1+C_m)L\dot{\psi}\sum_{i=1}^{3}\int_0^1\xi\dot{v}_i d\xi+m(1+C_m)L_c\dot{\theta}\dot{\beta}_h[\{\sin(\beta_h-\theta)+(G_h/2)\ *$$

$$L_c\cos(\beta_h-\theta)\}\sum_{i=1}^{3}\sin\psi_i\int_0^1 v_i d\xi-\{\cos(\beta_h-\theta)-(G_h/2)L_c\sin(\beta_h-\theta)\}\ *$$

$$\sum_{i=1}^{3}\int_0^1 w_i d\xi]+(m/2)(1+C_m)L_c^2\dot{\theta}\dot{G}_h[\sin(\beta_h-\theta)\sum_{i=1}^{3}\sin\psi_i\int_0^1 v_i d\xi$$

$$-\cos(\beta_h-\theta)\sum_{i=1}^{3}\int_0^1 w_i d\xi]+m(1+C_m)L_c\dot{\psi}\dot{\beta}_h\sum_{i=1}^{3}[\cos\psi_i\{\cos(\beta_h-\theta)-(G_h/2)L_c\ *$$

$$\sin(\beta_h-\theta)\}+\sin\psi_i\cos\beta_h(\varepsilon_h+k_hL_c/2)]\int_0^1 v_i d\xi+(m/2)(1+C_m)L_c^2\dot{\psi}\dot{G}_h\cos(\beta_h-\theta)*$$

$$\sum_{i=1}^{3}\cos\psi_i\int_0^1 v_i d\xi+m(1+C_m)L_c\dot{\psi}(\dot{\varepsilon}_h+\dot{k}_hL_c/2)\sin\beta_h\sum_{i=1}^{3}\sin\psi_i\int_0^1 v_i d\xi$$

$$+m(1+C_m)L_c\sum_{i=1}^{3}\int_0^1(X_{i1}\dot{v}_i+X_{i2}\dot{w}_i)d\xi+(X_3/2)L_c^2\ , \tag{6.12}$$

where

$$X_{i1} = \dot{\beta}_h[\sin\psi_i\{\cos(\beta_h-\theta)-(G_h/2)L_c\sin(\beta_h-\theta)\}-\cos\psi_i(\varepsilon_h+k_hL_c/2)\cos\beta_h]$$

$$+(\dot{G}_hL_c/2)\sin\psi_i\cos(\beta_h-\theta)-(\dot{\varepsilon}_h+\dot{k}_hL_c/2)\cos\psi_i\sin\beta_h\quad ,$$

$$X_{i2} = \dot{\beta}_h\{\sin(\beta_h-\theta)+(G_h/2)L_c\cos(\beta_h-\theta)\}+(\dot{G}_hL_c/2)\sin(\beta_h-\theta) \quad ,$$

and

$$\begin{aligned}X_3 = {} & \dot{\beta}_h^2[\{m_T+(m_{ca}/3)(1+\varepsilon_h^2\cos^2\beta_h)\}+\varepsilon_hk_hL_c\cos^2\beta_h(m_T+5m_{ca}/12) \\ & +(G_h^2+k_h^2)(L_c^2/4)(m_T+8m_{ca}/15)]+\dot{\varepsilon}_h^2[(m_T+m_{ca}/3)\sin^2\beta_h] \\ & +(\dot{G}_h^2+\dot{k}_h^2\sin^2\beta_h)(L_c^2/4)(m_T+8m_{ca}/15)+\dot{\beta}_h\dot{G}_hL_c(m_T+5m_{ca}/12) \\ & +2\dot{\beta}_h\dot{\varepsilon}_h\sin\beta_h\cos\beta_h[\varepsilon_h(m_T+m_{ca}/3)+(k_hL_c/2)(m_T+5m_{ca}/12)] \\ & +\dot{\beta}_h\dot{k}_hL_c\sin\beta_h\cos\beta_h[\varepsilon_h(m_T+5m_{ca}/12)+(k_hL_c/2)(m_T+8m_{ca}/15)] \\ & +\dot{\varepsilon}_h\dot{k}_hL_c\sin^2\beta_h(m_T+5m_{ca}/12) \quad .\end{aligned}$$

Here m_T and m_{ca} are the total apparent masses of the array and the cable, respectively.

The potential energy U of the system consists of the gravitational energy U_g and the strain energy U_e stored in the legs of the array and can be obtained to be

$$U = U_g+U_e = -m_h g z_{1b}+\int_0^{L_c}(z_1-z_{1b})g\rho_c ds+(EI/2L^3)\sum_{i=1}^{3}\int_0^1\left[\left\{\frac{\partial^2 v_i}{\partial\xi^2}\right\}^2+\left\{\frac{\partial^2 w_i}{\partial\xi^2}\right\}^2\right]d\xi$$

$$=-m_h g L_c\{\cos\beta_h-(G_h L_c/2)\sin\beta_h\}-m_c g L_c\{(1/2)\cos\beta_h-(1/3)G_h L_c\sin\beta_h\}$$

$$+(EI/2L^3)\sum_{i=1}^{3}\int_0^1\left[\left\{\frac{\partial^2 v_i}{\partial\xi^2}\right\}^2+\left\{\frac{\partial^2 w_i}{\partial\xi^2}\right\}^2\right]d\xi \quad . \tag{6.13}$$

The Lagrangian equations of motion can now be written as

$$\frac{d}{dt}\left(\frac{\partial T}{\partial \dot{q}_k}\right)-\frac{\partial T}{\partial q_j}+\frac{\partial U}{\partial q_j} = Q_j, \quad (q_j \equiv \beta_h, G_h, \varepsilon_h, k_h, \psi \text{ and } \theta) \tag{6.14a}$$

and

$$\frac{\partial}{\partial t}\left(\frac{\partial\hat{T}}{\partial\dot{q}_k}\right)-\frac{\partial\hat{T}}{\partial q_k}+\frac{\partial\hat{U}}{\partial q_k} = \hat{Q}_k, \quad (q_k \equiv v_k, w_k;\ k = 1,2,3) \ , \tag{6.14b}$$

where T and U are the kinetic and potential energy of the system given by (6.12) and (6.13) respectively, $\hat{T}$ and $\hat{U}$ the corresponding densities and Q_j and $\hat{Q}_k$ the generalized forces arising due to nonconservative forces acting on the system. Equations (6.14b) are valid for elastic legs, but can easily be modified for the viscoelastic case by replacing E with the appropriate modulus. It may be noticed that the motion of the system is described by a hybrid set of equations since Equations (6.14a) are ordinary differential equations while (6.14b) are partial differential equations.

The contributions to the generalized forces $Q_j(q_j \equiv \beta_h, G_h, \varepsilon_h, k_h, \psi$ and $\theta)$ comes from the hydrodynamic forces on the cable and legs of the array while $\hat{Q}_k(q_k \equiv v_k, w_k)$ results both from the hydrodynamic forces and the axial forces due to the internal pressure. The contribution due to the pressure forces is

$$\hat{Q}'_k = -(F_a/L^2)\,\frac{\partial^2 q_k}{\partial \xi^2}\ , \quad q_k \equiv v_k, w_k; \quad k=1,2,3 \ . \tag{6.15}$$

As before, the tangential and normal forces acting on an element ds of the cable can be written as

$$d\bar{F}_{Tc} = (\rho_w/2) C_{Tc} d_c (\bar{W}_c \cdot \bar{e}_{tc}) |\bar{W}_c \cdot \bar{e}_{tc}| \bar{e}_{tc}\ ds\ , \tag{6.16a}$$

and

$$d\bar{F}_{Nc} = -(\rho_w/2) C_{Nc} d_c \{\bar{W}_c - (\bar{W}_c \cdot \bar{e}_{tc})\bar{e}_{tc}\} |\bar{W}_c - (\bar{W}_c \cdot \bar{e}_{tc})\bar{e}_{tc}| ds\ , \tag{6.16b}$$

where $\bar{W}_c$ and $\bar{e}_{tc}$ are the relative velocity with respect to the fluid and unit tangential vector of the element, respectively and can be shown to be

$$\begin{aligned}\bar{W}_c = {} & [V + \dot{\beta}_h (s-L_c)\cos\beta_h + (\dot{G}_h \cos\beta_h - G_h \dot{\beta}_h \sin\beta_h)(s^2-L_c^2)/2]\bar{i} \\ & + [(\dot{\varepsilon}_h \sin\beta_h + \varepsilon_h \dot{\beta}_h \cos\beta_h)(s-L_c) + (\dot{k}_h \sin\beta_h + k_h \dot{\beta}_h \cos\beta_h) * \\ & (s^2-L_c^2)/2]\bar{j} + [-\dot{\beta}_h (s-L_c)\sin\beta_h - (\dot{G}_h \sin\beta_h + G_h \dot{\beta}_h \cos\beta_h) * \\ & (s^2-L_c^2)/2]\bar{k}\ ,\end{aligned} \tag{6.16c}$$

$$\bar{e}_{tc} = (\sin\beta_h + G_h s \cos\beta_h)\bar{i} + (\varepsilon_h + k_h s)\sin\beta_h \bar{j} + (\cos\beta_h - G_h s \sin\beta_h)\bar{k} \ . \tag{6.16d}$$

Similarly, the hydrodynamic forces acting on an element $Ld\xi$ of the i^{th} leg are given by

$$d\bar{F}_{iT} = (\rho_w/2)C_T Ld(\bar{W}_{\ell i}\cdot\bar{e}_{ti})|\bar{W}_{\ell i}\cdot\bar{e}_{ti}|\bar{e}_{ti}d\xi \ , \tag{6.17a}$$

$$d\bar{F}_{iN} = -(\rho_w/2)C_N Ld\{\bar{W}_{\ell i} - (\bar{W}_{\ell i}\cdot\bar{e}_{ti})\bar{e}_{ti}\}|\bar{W}_{\ell i} - (\bar{W}_{\ell i}\cdot\bar{e}_{ti})\bar{e}_{ti}| \tag{6.17b}$$

where

$$\begin{aligned}\bar{W}_{\ell i} = {} & [V - \dot{\beta}_h L_c \cos\beta_h - (\dot{G}_h \cos\beta_h - G_h \dot{\beta}_h \sin\beta_h)(L_c^2/2) + \dot{\theta}\{\sin\theta(-\xi L\cos\psi_i \\ & + v_i \sin\psi_i) + w_i \cos\theta\} - \dot{\psi}\cos\theta(\xi L \sin\psi_i + v_i \cos\psi_i) - \dot{v}_i \cos\theta \sin\psi_i \\ & + \dot{w}_i \sin\theta]\bar{i} + [-(\dot{\varepsilon}_h \sin\beta_h + \varepsilon_h \dot{\beta}_h \cos\beta_h)L_c - (\dot{k}_h \sin\beta_h + k_h \dot{\beta}_h \cos\beta_h)(L_c^2/2) \\ & + \dot{\psi}(\xi L \cos\psi_i - v_i \sin\psi_i) + \dot{v}_i \cos\psi_i]\bar{j} + [\dot{\beta}_h L_c \sin\beta_h + (\dot{G}_h \sin\beta_h + G_h \dot{\beta}_h \cos\beta_h) * \\ & (L_c^2/2) + \dot{\theta}\{\cos\theta(-\xi L \cos\psi_i + v_i \sin\psi_i) - w_i \sin\theta\} + \dot{\psi}\sin\theta(\xi L \sin\psi_i \\ & + v_i \cos\psi_i) + \dot{v}_i \sin\theta \sin\psi_i + \dot{w}_i \cos\theta]\bar{k} \ ,\end{aligned} \tag{6.17c}$$

and

$$\bar{e}_{ti} = (\cos\theta\cos\psi_i - \frac{1}{L}\frac{\partial v_i}{\partial\xi}\cos\theta\sin\psi_i + \frac{1}{L}\frac{\partial w_i}{\partial\xi}\sin\theta)\bar{i} + (\sin\psi_i$$

$$+ \frac{1}{L}\frac{\partial v_i}{\partial\xi}\cos\psi_i)\bar{j} + (-\sin\theta\cos\psi_i + \frac{1}{L}\frac{\partial v_i}{\partial\xi}\sin\theta\sin\psi_i + \frac{1}{L}\frac{\partial w_i}{\partial\xi}\cos\theta)\bar{k}. \tag{6.17d}$$

The above expressions can be used to determine the generalized forces.

6.2 Equilibrium Configurations

To obtain the equilibrium configurations (represented by subscript '0'), the time derivative terms must vanish. Hence from (6.14)

$$Q_{j0} = 0 , \quad (q_j \equiv \psi, \theta, \varepsilon_h, k_h) ,$$

$$gL_c[m_h\{\sin\beta_{h0} + (G_{h0}L_c/2)\cos\beta_{h0}\} + m_c\{(1/2)\sin\beta_{h0} + (G_{h0}L_c/3)\cos\beta_{h0}\}] = Q_{\beta h0},$$

$$gL_c^2[(m_h/2)+(m_c/3)]\sin\beta_{h0} = Q_{Gh0} ,$$

$$(EI/L^4)\frac{\partial^4 q_{k0}}{\partial\xi^4} - (F_a/L^2)\frac{\partial^2 q_{k0}}{\partial\xi^2} = \hat{Q}_{k0} , \quad (q_k \equiv v_k, w_k). \tag{6.18}$$

The above equations yield (Appendix I) the steady state solutions:

$$\psi_0 (= \psi_{i0} - I_i) = 0 \text{ or } \pi/3 , \tag{6.19a}$$

$$\theta = 0 \text{ or } \pi/2 , \tag{6.19b}$$

$$\eta_{i0} = v_{i0}/d \simeq -(\rho_w V^2 L^4/2EI)C_N|(1-\cos^2\theta_0\cos^2\psi_{i0})^{1/2}|\cos\theta_0\sin\psi_{i0}Y_0(\xi), \tag{6.19c}$$

$$\zeta_{i0} = w_{i0}/d \simeq (\rho_w V^2 L^4/2EI)C_N|(1-\cos^2\theta_0\cos^2\psi_{i0})^{1/2}|\sin\theta_0 Y_0(\xi), \tag{6.19d}$$

where

$$Y_0(\xi) = (1/P)[(1/P)\{\cosh\sqrt{P} - \cosh\sqrt{P}\,(1-\xi)\} - (\xi/\sqrt{P})\sinh\sqrt{P} + (\xi^2/2)],$$

and P is obtained from Equation (2.15). Only the orientation $\theta_0 = 0$ is of interest to us. Correspondingly,

$$\eta_{i0} \simeq -(\rho_w V^2 L^4/2EI)C_N|\sin\psi_{i0}|\sin\psi_{i0}Y_0(\xi), \tag{6.19c'}$$

and

$$\zeta_{i0} \simeq 0 \quad . \tag{6.19d'}$$

The cable shape is given by

$$\varepsilon_{h0} = k_{h0} = 0 \quad , \tag{6.19e}$$

$$\{m_h+(m_c/2)\}g\sin\beta_{h0}+\{(m_h/2)+(m_c/3)\}g(G_{h0}L_c)\cos\beta_{h0} = (\rho_w/2)V^2[\{C_N^* Ld$$
$$+C_{Nc}(L_c/2)d_c\cos\beta_{h0}\}\cos\beta_{h0}-\{C_N^*(L/2)d\sin\beta_{h0}+(L_c/6)d_c(C_{Nc}\sin 2\beta_{h0}$$
$$+C_{Tc}\sin^2\beta_{h0})\}(G_{h0}L_c)] \quad , \tag{6.19f}$$

$$\{(m_h/2)+(m_c/3)\}g\sin\beta_{h0} = (\rho_w/2)V^2[(1/2)\{C_N^*Ld+C_{Nc}(L_c/3)d_c\cos\beta_{h0}\} *$$

$$\cos\beta_{h0}-(L_c/8)d_c(C_{Nc}\sin 2\beta_{h0}+C_{Tc}\sin^2\beta_{h0})(G_{h0}L_c)] \ , \qquad (6.19g)$$

where

$$C_N^* = \sum_{i=1}^{3}\int_0^1[-C_T(\cos\psi_{i0}-\frac{1}{R}\frac{\partial\eta_{i0}}{\partial\xi}\sin\psi_{i0})^2|\cos\psi_{i0}-\frac{1}{R}\frac{\partial\eta_{i0}}{\partial\xi}\sin\psi_{i0}|$$

$$+C_N(\sin\psi_{i0}+\frac{1}{R}\frac{\partial\eta_{i0}}{\partial\xi}\cos\psi_{i0})^2|\sin\psi_{i0}+\frac{1}{R}\frac{\partial\eta_{i0}}{\partial\xi}\cos\psi_{i0}|]d\xi \ .$$

$$(6.19h)$$

Equations (6.19f) and (6.19g) can be solved simultaneously to determine β_{h0} and G_{h0} for a given set of system parameters.

6.3 Motion Around the Stable Equilibrium Configuration

The differential equations governing the motion of the system are coupled, highly nonlinear and not amenable to analytical methods due to their complexity. The numerical solution to these equations is likely to be very expensive in the light of the fact that a great amount of computer time was required even for the simplified model considered before. Hence the dynamics of the system is investigated by giving small disturbances to the steady state solution and studying the resulting linearized equations. While considerable amount of information can be obtained following this procedure, the analysis is vastly simplified since a set of linear differential equations describing a dynamical system can easily be converted to a set of algebraic equations. Thus the generalized co-ordinates are represented by

$$\psi_i = \psi_{i0}+\delta\psi, \quad \theta = \theta_0+\delta\theta, \quad \eta_i = \eta_{i0}+\delta\eta_i, \quad \zeta_i = \zeta_{i0}+\delta\zeta_i,$$

$$\beta_h = \beta_{h0}+\delta\beta_h, \quad G_h = G_{h0}+\delta G_h, \quad \varepsilon_h = \varepsilon_{h0}+\delta\varepsilon_h$$

and $$k_h = k_{h0}+\delta k_h \quad . \tag{6.20}$$

In the subsequent analysis, the second and higher powers of the variations $\delta\psi$ etc. are neglected. Similarly, the terms involving higher powers of $(1/R)$, where R is the length to diameter ratio of each arm, are also ignored. This is a reasonable assumption considering the fact that R is likely to be greater than 20.

The position vectors $\bar{r}_i$ and $\bar{r}_c$ with respect to the inertial co-ordinate system are now given by

$$\bar{r}_i = [-L_c\{\sin\beta_{h0}+(G_{h0}L_c/2)\cos\beta_{h0}\}-L_c\{\delta\beta_h+(L_c/2)\delta G_h\}\{\cos\beta_{h0}$$

$$-(G_{h0}L_c/2)\sin\beta_{h0}\}+L\{(\xi\cos\psi_{i0}-\eta_{i0}\sin\psi_{i0}/R)-\delta\psi(\xi\sin\psi_{i0}$$

$$+\eta_{i0}\cos\psi_{i0}/R)-\delta\eta_i\sin\psi_{i0}/R\}]\bar{i}+[-L_c\sin\beta_{h0}\{\delta\varepsilon_h+(L_c/2)\delta k_h\}$$

$$+L\{(\xi\sin\psi_{i0}+\eta_{i0}\cos\psi_{i0}/R)+\delta\psi(\xi\cos\psi_{i0}-\eta_{i0}\sin\psi_{i0}/R)$$

$$+\delta\eta_i\cos\psi_{i0}/R\}]\bar{j}+[-L_c\{\cos\beta_{h0}-(G_{h0}L_c/2)\sin\beta_{h0}\}+L_c\{\delta\beta_h$$

$$+(L_c/2)\delta G_h\}\{\sin\beta_{h0}+(G_{h0}L_c/2)\cos\beta_{h0}\}+L\{-(\xi\cos\psi_{i0}$$

$$-\eta_{i0}\sin\psi_{i0}/R)\delta\theta+\delta\zeta_i/R\}]\bar{k} \quad , \tag{6.21a}$$

and

$$\bar{r}_c = [\{(s-L_c)\sin\beta_{h0}+(G_{h0}/2)(s^2-L_c^2)\cos\beta_{h0}\}+\delta\beta_h\{(s-L_c)\cos\beta_{h0}$$

$$-(G_{h0}/2)(s^2-L_c^2)\sin\beta_{h0}\}+\delta G_h(1/2)(s^2-L_c^2)\cos\beta_{h0}]\bar{i}$$

$$+\sin\beta_{h0}[\delta\varepsilon_h(s-L_c)+(\delta k_h/2)(s^2-L_c^2)]\bar{j}+[\{(s-L_c)\cos\beta_{h0}$$

$$-(G_{h0}/2)(s^2-L_c^2)\sin\beta_{h0}\}-\delta\beta_h\{(s-L_c)\sin\beta_{h0}+(G_{h0}/2)(s^2$$

$$-L_c^2)\cos\beta_{h0}\}-\delta G_h(1/2)(s^2-L_c^2)\sin\beta_{h0}]\bar{k} \quad , \tag{6.21b}$$

while the relative velocities $\bar{W}_{\ell i}$ and $\bar{W}_c$ are obtained by differentiating the above equations with respect to the time and adding $\bar{i}V$ to it. The unit vectors $\bar{e}_{ti}$ and $\bar{e}_{tc}$ can be written as

$$\bar{e}_{ti} = [\{\cos\psi_{i0}-(1/R)\,\frac{\partial\eta_{i0}}{\partial\xi}\,\sin\psi_{i0}\}-\{\delta\psi+(1/R)\frac{\partial\delta\eta_i}{\partial\xi}\,\}\{\sin\psi_{i0}$$

$$+(1/R)\frac{\partial\eta_{i0}}{\partial\xi}\,\cos\psi_{i0}\}]\bar{i}+[\{\sin\psi_{i0}+(1/R)\,\frac{\partial\eta_{i0}}{\partial\xi}\,\cos\psi_{i0}\}$$

$$+\{\delta\psi+(1/R)\ \frac{\partial\delta\eta_i}{\partial\xi}\}\{\cos\psi_{i0}-(1/R)\ \frac{\partial\eta_{i0}}{\partial\xi}\ \sin\psi_{i0}\}]\bar{j}$$

$$+[-\delta\theta\{\cos\psi_{i0}-(1/R)\ \frac{\partial\eta_{i0}}{\partial\xi}\ \sin\psi_{i0}\}+(1/R)\ \frac{\partial\delta\zeta_i}{\partial\xi}\ ]\bar{k}\quad , \tag{6.21c}$$

and

$$\bar{e}_{tc} = [(\sin\beta_{h0}+G_{h0}s\cos\beta_{h0})+(\cos\beta_{h0}-G_{h0}s\ \sin\beta_{h0})\delta\beta_h+\delta G_h s\cos\beta_{h0}]\bar{i}$$

$$+(\delta\varepsilon_h+\delta k_h s)\bar{j}+[(\cos\beta_{h0}-G_{h0}s\ \sin\beta_{h0})-(\sin\beta_{h0}+G_{h0}s\cos\beta_{h0})\delta\beta_h$$

$$-\delta G_h s\ \sin\beta_{h0}]\bar{k}\quad . \tag{6.21d}$$

The generalized forces can now be determined using the principle of virtual work in conjunction with Equation (6.21).

Retaining upto the quadratic terms in the expressions for kinetic and potential energy (Equations 6.12 and 6.13, respectively) the Lagrangian equations of motion are

$$(1+I_z^*)\delta\psi''+(1/R)\sum_{i=1}^{3}\int_0^1\xi\delta\eta_i''d\xi+(R_\ell/R)(\delta\varepsilon_h''+\delta k_h''L_c/2)\sin\beta_{h0}I_\eta = Q_\psi^*\ , \tag{6.22a}$$

$$[\{(1/2)+(-1)^{N-1}(\sqrt{3}/R)\int_0^1\xi\eta_0 d\xi\}+I_x^*\sin^2\psi_0+I_y^*\cos^2\psi_0]\delta\theta''-(1/R)\quad *$$

$$\sum_{i=1}^{3}\cos\psi_{i0}\int_0^1 \xi\delta\zeta_i''d\xi+(R_\ell/R)[\{\sin\beta_{h0}+(G_{h0}L_c/2)\cos\beta_{h0}\}\delta\beta_h''$$

$$+\sin\beta_{h0}(L_c/2)\delta G_h'']I_\eta \quad = \quad Q_\theta^* \quad , \tag{6.22b}$$

$$(1/R)\{\sin\beta_{h0}+(G_{h0}L_c/2)\cos\beta_{h0}\}\{I_\eta\delta\theta''+\sum_{i=1}^{3}\int_0^1\delta\zeta_i''d\xi\}+(1/R)\{\cos\beta_{h0}$$

$$-(G_{h0}L_c/2)\sin\beta_{h0}\}\sum_{i=1}^{3}\sin\psi_{i0}\int_0^1\delta\eta_i''d\xi+(3+r_{h\ell}+r_{c\ell}/3)R_\ell\delta\beta_h''$$

$$+(3+r_{h\ell}+5r_{c\ell}/12)R_\ell(L_c/2)\delta G_h'' \quad = \quad Q_{\beta h}^* \tag{6.22c}$$

$$(1/R)\sin\beta_{h0}\{I_\eta\delta\theta''+\sum_{i=1}^{3}\int_0^1\delta\zeta_i''d\xi\}+(1/R)\cos\beta_{h0}\sum_{i=1}^{3}\sin\psi_{i0}\int_0^1\delta\eta_i''d\xi$$

$$+(3+r_{h\ell}+5r_{c\ell}/12)R_\ell\delta\beta_h''+(3+r_{h\ell}+8r_{c\ell}/15)R_\ell(L_c/2)\delta G_h'' \quad = \quad Q_{Gh}^*, \tag{6.22d}$$

$$(1/R)\{I_\eta\delta\psi''-\sum_{i=1}^{3}\cos\psi_{i0}\int_0^1\delta\eta_i''d\xi\}+(3+r_{h\ell}+r_{c\ell}/3)R_\ell\sin\beta_{h0}\delta\varepsilon_h''$$

$$+(3+r_{h\ell}+5r_{c\ell}/12)R_\ell\sin\beta_{h0}(L_c/2)\delta k_h'' \quad = \quad Q_{\varepsilon h}^* \quad , \tag{6.22e}$$

$$(1/R)\{I_\eta\delta\psi''-\sum_{i=1}^{3}\cos\psi_{i0}\int_0^1\delta\eta_i''d\xi\}+(3+r_{h\ell}+5r_{c\ell}/12)R_\ell\sin\beta_{h0}\delta\varepsilon_h''$$

$$+(3+r_{h\ell}+8r_{c\ell}/15)R_\ell\sin\beta_{h0}(L_c/2)\delta k_h'' \quad = \quad Q_{kh}^* \quad , \tag{6.22f}$$

$$\{\xi\delta\psi''+(1/R)\delta\eta_i''\}+R_\ell\sin\psi_{i0}[\{\cos\beta_{h0}-(G_{h0}L_c/2)\sin\beta_{h0}\}\delta\beta_h''$$

$$+\cos\beta_{h0}(L_c/2)\delta G_h'']-R_\ell\cos\psi_{i0}\sin\beta_{h0}\{\delta\varepsilon_h''+(L_c/2)\delta k_h''\} = Q^*_{\eta i} \;, \tag{6.22g}$$

$$[-\{\xi\cos\psi_{i0}-(1/R)\eta_{i0}\sin\psi_{i0}\}\delta\theta''+(1/R)\delta\zeta_i'']+R_\ell[\{\sin\beta_{h0}$$

$$+(G_{h0}L_c/2)\cos\beta_{h0}\}\delta\beta_h''+\sin\beta_{h0}(L_c/2)\delta G_h''] = Q^*_{\zeta i} \;, \quad i = 1,2,3; \tag{6.22h}$$

where prime denotes differentiation with respect to τ defined in Equation (5.11), $R_\ell = L_c/L$ and

$$I_\eta = \sqrt{3}\int_0^1 \eta_0 d\xi \quad .$$

N takes the values 1 and 2 for the equilibrium configurations $\psi_0 = 0$ and $\pi/3$, respectively. Here $\delta\eta_i$ and $\delta\zeta_i$ can be expressed in terms of a set of admissible functions $\Psi_j(\xi)$ (mode shapes with equivalent P) as follows:

$$\delta\eta_i = \sum_{j=1}^{\infty}\delta a_{ij}(\tau)\Psi_j(\xi)$$

$$\delta\zeta_i = \sum_{j=1}^{\infty}\delta b_{ij}(\tau)\Psi_j(\xi) \quad .$$

For convenience, the dimensionless generalized forces Q^*_ψ etc., shown in Appendix II, also include the potential forces. By assuming solutions of the form $\delta\psi = |\delta\psi| e^{\lambda\tau}$ etc., Equation (6.22) yields an eigenvalue problem of the form

$$[A]\,\{q\} = \lambda [B]\,\{q\}$$

which can be studied by matrix iteration method to determine the influence of different parameters on the system behaviour.

6.4 Results and Discussion

As seen from Equations (6.19a and b), there are four possible steady state orientations. However, the attention is focussed only on the stable one corresponding to the array remaining horizontal and the leading leg aligned in the direction of drifting ($\psi_0 = \theta_0 = 0$). There are no out of plane flexural displacements corresponding to this equilibrium configuration but the hydrodynamic forces acting on the arms produce some inplane deflections as given, approximately, by (6.19c'). Clearly, the arm oriented along the drifting velocity remains undeflected while the other two have equal bending deformations but in opposite directions. It may be pointed out that for large L and V, these deflections are likely to be substantial as the elastic modulus of the arm material is usually not very high (E for the sandwich material of polyethylene and mylar is of the order of 25×10^4 psi). Hence for large length to diameter ratio R, an expression slightly more accurate than

(6.19c'), was used to compute the deformations (Equation I.2e).

Due to the symmetry of the towed body, the cable lies in a plane in its steady state configuration. The corresponding slope and curvature at any given point can be characterized by β_{h0} and G_{h0}. Figure 6-2 shows the variation of β_{h0} and β_{b0} ($=\beta_{h0}+G_{h0}L_c$) with different system parameters. It may be noticed that the difference between β_{h0} and β_{b0} is not very large, which substantiates the assumption that the second and higher powers of G_{h0} may be neglected. For given cable dimensions, central head and R_ℓ, β_{h0} and β_{b0} are almost equal for small length to diameter ratio (R), i.e., the cable is essentially straight (Figure 6-2a). As R is increased, the difference between the two angles gradually increases making the cable appear convex when viewed from the buoy. The angles themselves are smaller for larger R since the drag forces acting on the array decrease with reduction in diameter. The cable remains closer to the vertical with its curvature reduced as the central head is made heavier. It is clear from Figure 6-2b that for a given cable length and leg diameter β_{h0} and β_{b0} at first increase, subsequently reducing with an increase in R_ℓ. This is because when the legs are shortened, the total drag initially increases due to a comparatively larger value of C_N^*. However, when the length of the legs are reduced further, the total drag drops because of a smaller projection area. The effect of making the diameter of the cable larger is to keep it closer to the vertical.

The eigenvalue problem described by (6.22) was analyzed to study the perturbations from the steady state configurations. From

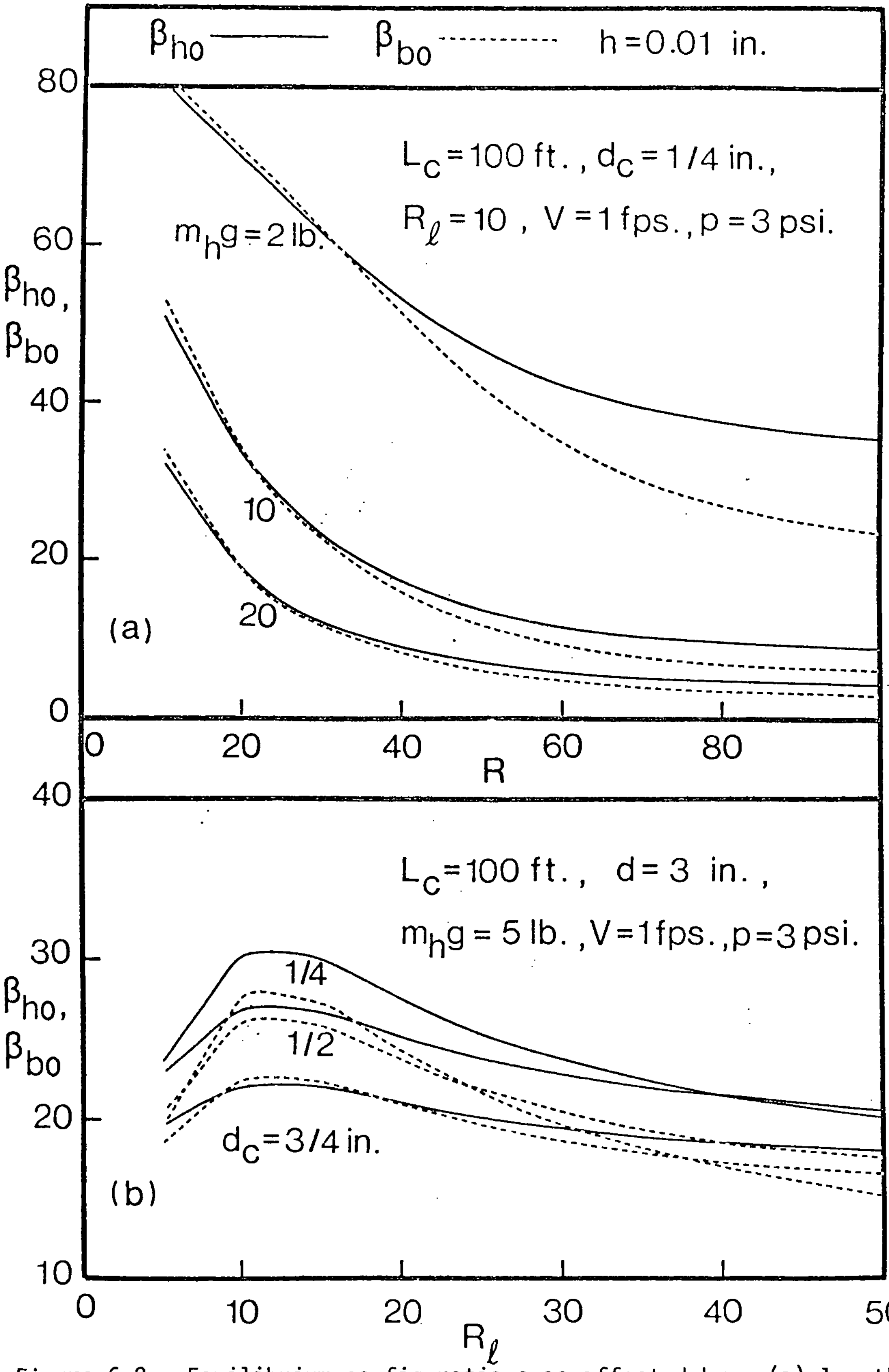

Figure 6-2 Equilibrium configurations as affected by: (a) length to diameter ratio (R) of a leg and the weight of the central head; (b) length ratio R_ℓ and the diameter of the cable

the eigenvectors obtained, it was observed that the lateral and longitudinal motions decouple, at least for the small motions under consideration. The former involves only $\delta\psi$, $\delta\varepsilon_h$, δk_h and $\delta\eta_i (i=1,2,3)$. The flexural vibrations are such that either $\delta\eta_2 = \delta\eta_3$ or $\delta\eta_1 = \delta\eta_2 + \delta\eta_3 = 0$. On the other hand, the latter involves only $\delta\theta$, $\delta\beta_h$, δG_h, $\delta\zeta_i$ and some inplane bending displacements under the constraints $\delta\eta_1 = 0$ and $\delta\eta_2 = -\delta\eta_3$. With this information Equations (6.22) can be divided into two sets which may be analyzed separately to study the lateral and longitudinal motions. This results in further saving of computer time required for matrix inversions. Furthermore, it was noticed that for small motions the sums $(\delta\beta_h+\delta G_h L_c/2)$ and $(\delta\varepsilon_h+\delta k_h L_c/2)$ can be treated essentially as distinct variables. The order of the eigenvalue problem depends on the number of admissible functions (mode shapes of a cantilever with equivalent P) taken in the expansions of $\delta\eta_i$ and $\delta\zeta_i$. In the actual computations only the first two modes were considered as they are likely to be the most important ones.

Three distinct sets of eigenvalues were obtained for both lateral and longitudinal motions:

(a) two pairs of eigenvalues describing the motion in which the rotation of the array and angular displacement of the cable are prominent;

(b) a set of frequencies corresponding to the first mode of the arms; and

(c) a set corresponding to the second mode.

The imaginary part of the eigenvalues in the set (a) may be zero or non-zero depending on the values of the parameters. On the other hand, the two sets (b) and (c) invariably contain non-zero imaginary parts and therefore involve oscillatory motion of the system. The effect of the flexibility becomes apparent if one recalls that in the rigid array analysis, the system was always overdamped. However, except for very small R_ℓ (i.e. long legs), the real parts of all the eigenvalues were found to be negative, signifying asymptotic stability.

The absolute values of the imaginary parts of the eigenvalues for both lateral and longitudinal motions have been plotted against R and R_ℓ in Figure 6-3. In general, the frequencies increase with R_ℓ (Figure 6-3a). For a particular mode of lateral motion in which the perturbation of ψ dominates, the eigenvalue has zero imaginary part except for very large values of R_ℓ. The corresponding transition for $\delta\theta$ in longitudinal motion takes place at smaller R_ℓ. The frequencies are comparatively less influenced by the length to diameter ratio R of the legs (Figure 6-3b) and show a slight increase with R for the longitudinal motion. On the other hand, in the lateral motion they at first increase, but subsequently reduce. The weight of the central head has negligible effect on the eigenvalues, but a shorter cable increases the possibility of oscillatory rotational motions (not shown).

In order to compare the damping rates for different system parameters, arbitrary perturbations of 0.2 radian were given to each rotational degree of freedom while the variables δa_{ij} and δb_{ij} were assigned the values 0.2 and 0.1 corresponding to the first and second mode, respectively. The time to damp within ±5 percent of the original disturbances was noted. The effect of a given parameter on

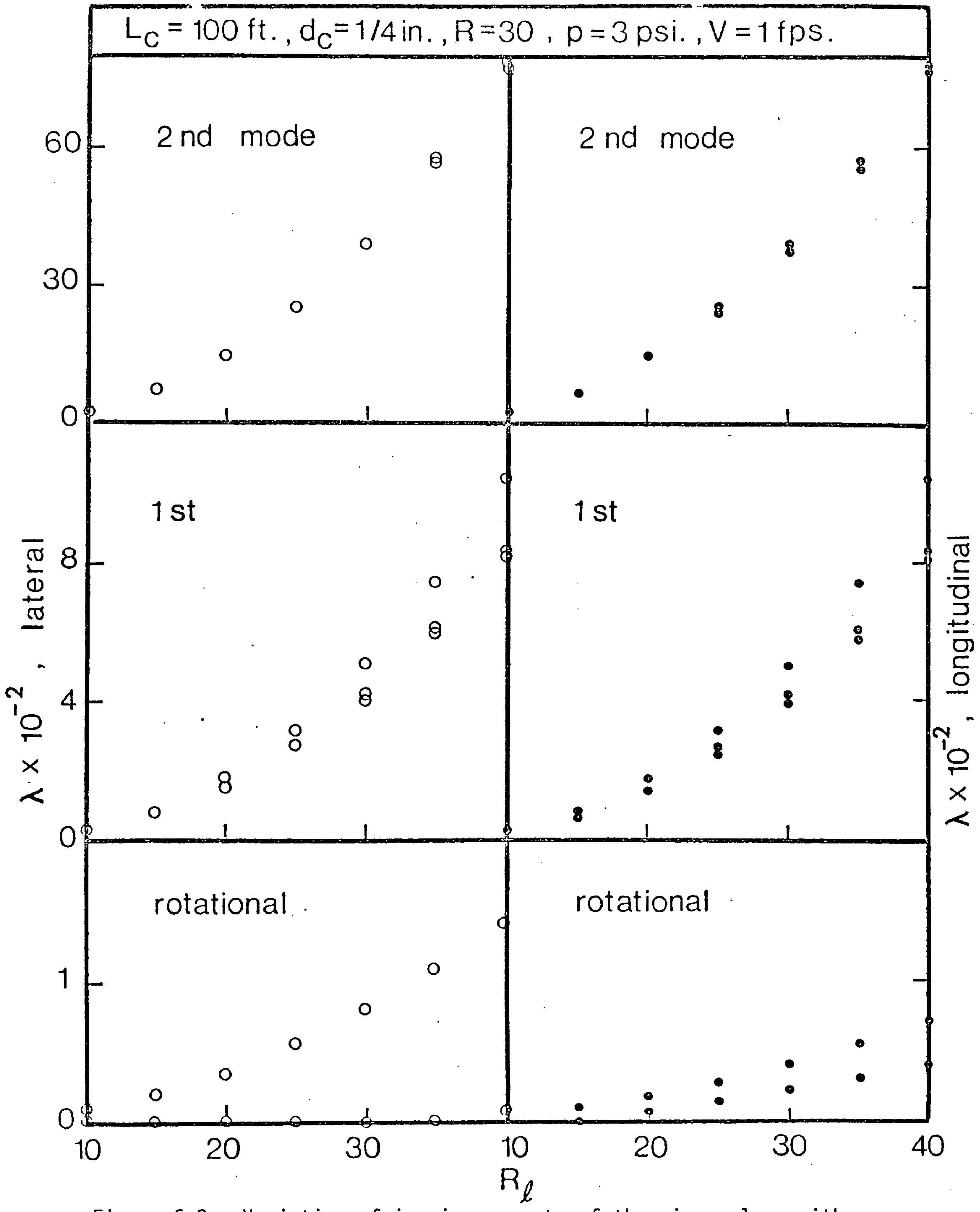

Figure 6-3 Variation of imaginary parts of the eigenvalues with:
(a) length ratio R_ℓ

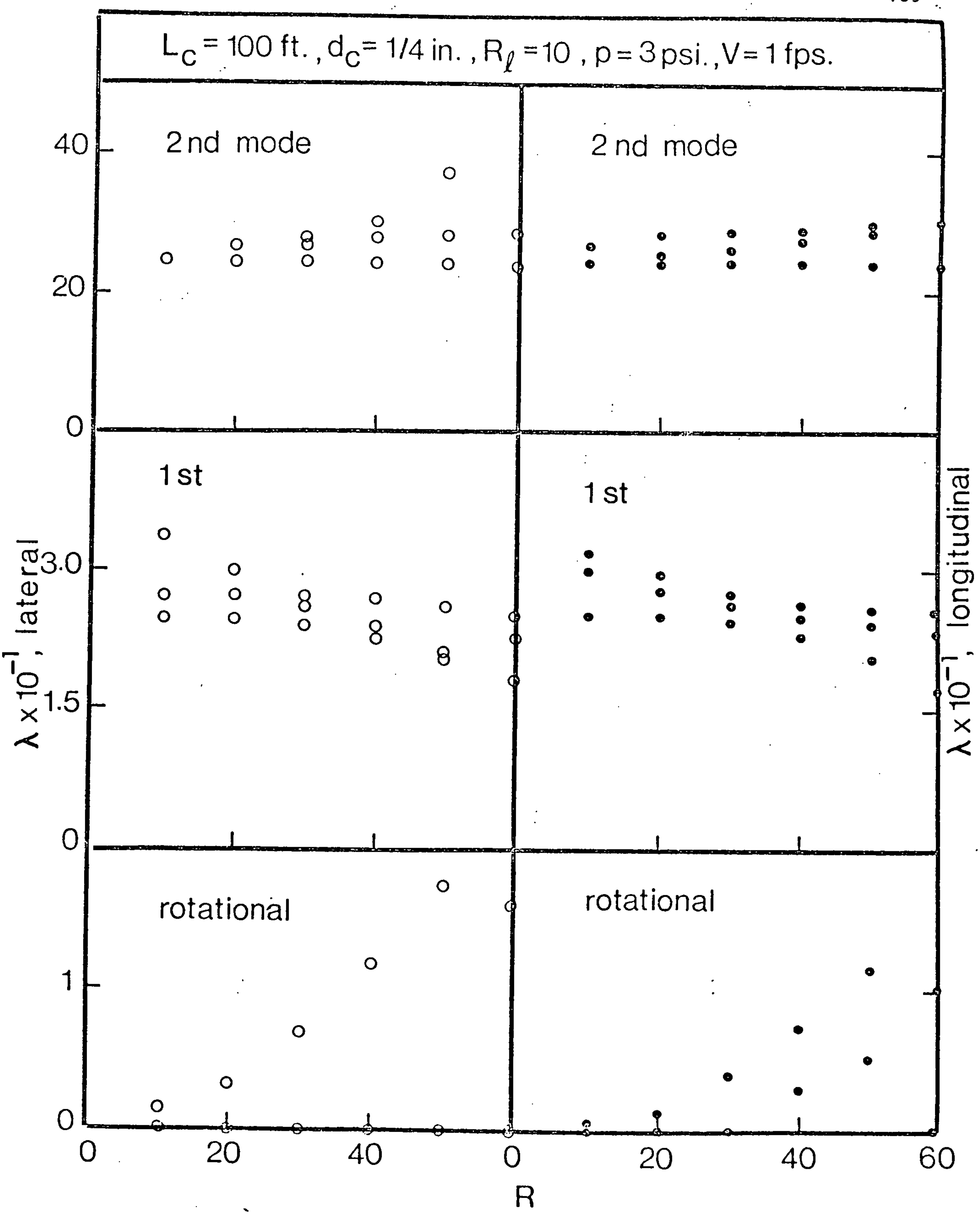

Figure 6-3 Variation of imaginary parts of the eigenvalues with: (b) length to diameter ratio (R) of a leg

the decay of lateral and longitudinal motion was observed to be similar (Figure 6-4). Note that an increase in R_ℓ improves the decay of the disturbances, suggesting the use of shorter arm lengths for a given cable. This is consistent with the conclusion of the rigid array analysis. However, a larger R does not reduce the damping times indefinitely as predicted by it. This is because of the increase in flexibility with reduction in the leg diameter. Above certain R (about 50 for the set of parameters considered), the motion appears to build-up instead of decaying. This may be partly due to the fact that the steady state bending deformations given by (6.19) are not accurate for large R. But the fact remains that the stability is reduced if R is increased indefinitely. A change in the weight of the central head has very little influence on the damping characteristics. On the other hand, a larger L_c tends to decay the cable oscillations faster.

6.5 Concluding Remarks

The above analysis leads to the following conclusions:

(i) The array lies in a horizontal plane, with its leading leg aligned in the direction of drifting, in the stable steady state configuration. There are no out of plane flexural displacements. The first (leading) leg has no inplane bending deformations either, but the other two undergo symmetrical flexure.

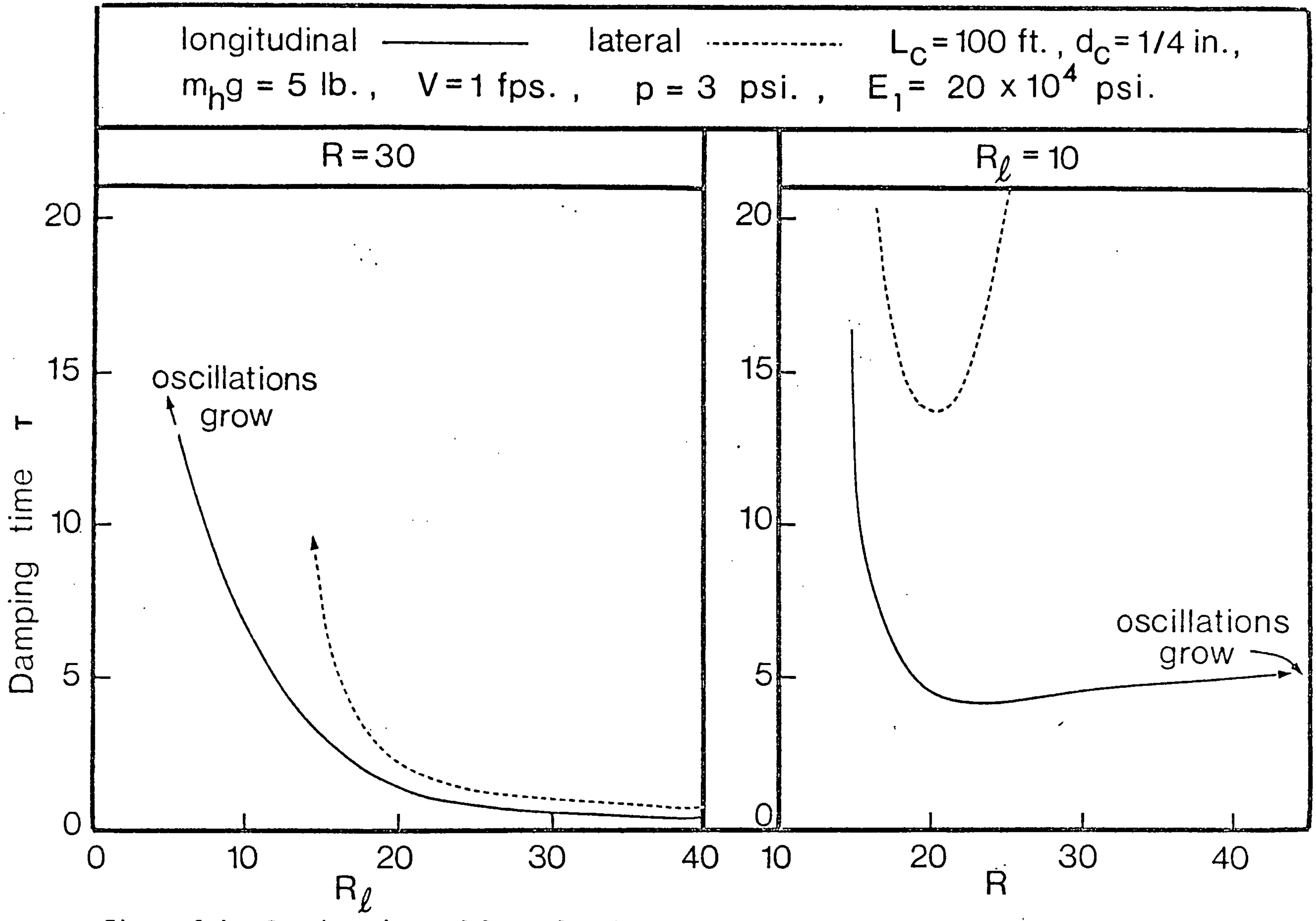

Figure 6-4 Damping times of lateral and longitudinal motion of the assembly as affected by length ratio R_ℓ and length to diameter ratio (R) of a leg

(ii) The cable lies in a plane in its equilibrium configuration. A heavier central head or smaller diameter of the arms keeps the cable closer to the vertical. The cable is essentially straight for larger arm diameters. As the length of the arms is decreased, β_{h0} and β_{b0} at first increase, reducing subsequently.

(iii) The system is asymptotically stable unless R_{ℓ} is very small, i.e. the legs are too long.

(iv) In accordance with the rigid array analysis, shorter arm length improves the decaying characteristics of the system. However, as pointed out before, the minimum acceptable length is determined from signal processing considerations and a compromise has to be made in the design.

(v) The damping time is initially reduced if length to diameter ratio R is increased. But above a certain R, the stability of the system decreases. Hence, for a given cable and arm length, there is an optimum diameter which must be used in the design.

7. CLOSING COMMENTS

7.1 Summary of Conclusions

As indicated at the outset, the main objective of this investigation has been to gain some insight to the statics and dynamics of submarine detection systems employing neutrally buoyant inflated structural members. The emphasis has been on the determination of trends rather than presenting massive data, specially in the cases involving considerable expenditure of computer time. Interest throughout has been in the development of approximate analytical procedures. The important conclusions based on the study can be summarized as follows:

(i) The inflatable members under consideration are made of materials exhibiting time dependent elastic properties which can be described with sufficient engineering accuracy by a three parameter solid model.

(ii) The dynamical analysis of each arm accounting for the hydrodynamic forces and axial tension due to the internal pressure, proves useful in the subsequent study of a more complex submarine detection system.

(iii) Investigation of the coupled motion of an array consisting of three legs and a central head yields the influence of different system parameters on the natural frequencies of its inplane and out of plane motions. For small values of inertia parameters, there is a possibility of unstable coupled motion above a certain magnitude of the pressure parameter.

(iv) The study of free vertical oscillation of the buoy-cable-array assembly yields two sets of repeated natural frequencies corresponding to the independent motion of the legs and a third set describing the coupled motion. During the coupled pure vertical motion, all the three legs move identically.

(v) The vertical oscillations of the leg tips can be reduced by using an elastic cable with small stiffness, legs having a large fundamental frequency or a heavier central head.

(vi) When the buoy-cable-array assembly is drifting with a uniform velocity, the stable steady state configuration corresponds to the array lying in a horizontal plane with its leading leg aligned in the direction of drifting. There are no flexural displacements of the leading leg, but the other two undergo symmetrical bending deformations. The equilibrium shape of the cable is confined to a plane due to the symmetry of the system. A heavier central head, smaller length or diameter of the arms keep the cable closer to the vertical.

(vii) The rigid array analysis shows that the drifting system is asymptotically stable in the range of practical interest. The disturbances damp out faster for shorter arms or smaller diameter.

(viii) For long arms or very small diameter, flexibility of the legs causes the perturbations from the steady state configurations to grow. Hence,for a given cable and arm length,there is an optimum diameter for the best decaying characteristics. Although smaller arms give greater stability to the system, they might create problems in signal processing due to a reduction in phase difference of the detected signals leading to a degree of compromise in the final design.

7.2 Recommendation for Future Work

There are numerous possibilities for extension of the present investigation. Only some of the important ones are mentioned below:

(i) In the analysis of the drifting system presented here, the buoy is assumed to move with a uniform velocity. This makes the expressions for kinetic energy comparatively less complex as the origin of the inertial co-ordinate system can be fixed to the centre of the buoy. However, in the actual practice, the drifting buoy is likely to undergo wave induced forward, up and down and/or rolling motions as well. An investigation taking this aspect of the problem into account is likely to be quite complex. Hence a first step might be to consider a rigid array, subsequently including the effect of flexibility.

(ii) Two rotations are sufficient to specify any orientation of the array only for small amplitude motions. A more general analysis of the drifting system should consider three Eulerian rotations.

(iii) There is a possibility of excessive flexural displacements for legs with very large L/d. A more accurate bending theory should be used under these circumstances as the slope is no longer negligible compared to unity.

(iv) In the present investigation, the cable was first approximated by two straight lines, a more accurate shape being considered subsequently. However, there is a scope of further improvement in the cable configuration by considering the set of partial differential equations governing its dynamics although the work involved may be enormous. Furthermore, the internal waves travelling along the cable, which are ignored here, may be considered.

(v) The current study deals with the motion of the system after it has attained its final shape. A study of its dynamics during inflation should constitute an interesting problem.

(vi) A systematic experimental program to determine the apparent mass coefficient, one of the uncertain parameters in the analysis, should prove quite useful. Prototype tests in the ocean would undoubtedly supplement the analyses.

BIBLIOGRAPHY

1. Brauer, K.O., "Present and Future Applications of Expandable Structures for Spacecraft and Space Experiments," Presented at the XXIInd International Astronautical Congress, Brussels, September 1971.

2. Leonard, R.W., Brooks, G.W., and McComb, H.G. (Jr), "Structural Considerations of Inflatable Reentry Vehicles," NASA TN D-457, September 1960.

3. Stein, M., and Hedgepeth, M.M., "Analysis of Partly Wrinkled Membranes," NASA TN D-813, July 1961.

4. Comer, R.L., and Levy, S., "Deflections of an Inflated Circular Cylindrical Cantilever Beam," AIAA Journal, Vol. 1, No. 7, July 1963, pp. 1652-1655.

5. Topping, A.D., "Shear Deflections and Buckling Characteristics of Inflated Members," Journal of Aircraft, Vol. 1, No. 5, September-October 1964, pp. 289-292.

6. Corneliussen, A.H., and R.T. Shield, "Finite Deformations of Elastic Membranes with Application to the Stability of an Inflated and Extended Tube," Archives of Rational Mechanical Analysis, Vol. 7, 1961, pp. 273-304.

7. Douglas, W.J., "Bending Stiffness of an Inflated Cylindrical Cantilever Beam," AIAA Journal, Vol. 7, No. 7, July 1969, pp. 1248-1253.

8. Koga, T., "Bending Rigidity of an Inflated Circular Cylindrical Membrane of Rubbery Materials," AIAA Journal, Vol. 10, No. 11, November 1972, pp. 1485-1489.

9. Morison, J.R., O'Brien, M.P., Johnson, J.W., and Schaaf, S.A., "The Forces Exerted by Surface Waves on Piles," Journal of Petroleum Technology, AIMME, Vol. 2, No. 5, May 1950, pp. 149-154.

10. Keulegan, G.H., and Carpenter, L.H., "Forces on Cylinders and Plates in an Oscillating Fluid," Journal of Research of the National Bureau of Standards, Vol. 60, No. 5, May 1958, pp. 423-440.

11. Laird, A.D.K., Johnson, C.A., and Walker, R.W., "Water Forces on Accelerated Cylinders," Journal of Waterways and Harbors, Vol. 85-WW1, March 1959, pp. 99-119.

12. Bishop, R.E.D., and Hassan, A.Y., "The Lift and Drag Forces on a Circular Cylinder Oscillating in a Flowing Fluid," Proceedings of the Royal Society, London, Series A, Vol. 277, 1964, pp. 32-75.

13. Toebes, G.H., and Ramamurthy, A.S., "Fluidelastic Forces on Circular Cylinders," Journal of Engineering Mechanics, Vol. 93-EM6, December 1967, pp. 1-20.

14. Protos, A., Goldschmidt, V.W., Toebes, G.H., "Hydroelastic Forces on Bluff Cylinders," Journal of Basic Engineering," Vol. 90, 1968, pp. 378-386.

15. Landweber, L., "Vibration in an Incompressible Fluid," IIHR Report, Contract Nonr. 3271 (01)(X), May 1963.

16. Landweber, L., "Vibration of a Flexible Cylinder in a Fluid," Journal of Ship Research, Vol. 11, No. 3, September 1967, pp. 143-150.

17. Warnock, R.G., "Added Masses of Vibrating Elastic Bodies," IIHR Report, Contract Nonr. 3271 (01)(X), February 1964.

18. Douglas, W.J., "Natural Vibrations of Finitely Deformable Structures," AIAA Journal, Vol. 5, No. 12, December 1967, pp. 2248-2253.

19. Choo, Y., and Casarella, M.J., "A Survey of Analytical Methods for Dynamic Simulation of Cable-Body Systems," Journal of Hydronautics, Vol. 7, No. 4, October 1973, pp. 137-144.

20. Relf, E.F., and Powell, E.H., "Tests on Smooth and Stranded Wires Inclined to the Wind Direction and a Comparison of Results on Stranded Wires in Air and Water," Great Britain Aeronautical Research Committee, R.&.M. No. 307, January 1917.

21. Hoerner, S.F., Fluid Dynamic Drag, Published by the Author, Midland Park, N.J., 1965.

22. Whicker, L.F., "The Oscillatory Motion of Cable-Towed Bodies," D. Eng. Thesis, University of California, Berkeley, June 1957.

23. Mustert, "Auftrieb und Widerstand von Schrag Angestromten Zylindrischen Korpchen," Aeronautical Research Institute, Gottingen, Germany, ZWB FB 1690, 1943.

24. Schneider, L., and Nickels, F., "Cable Equilibrium Trajectory in a Three Dimensional Flow Field," ASME Paper No 66-WA/UNT-12, July 1966.

25. Glauert, H., "The Stability of a Body Towed by a Light Wire," Great Britain Aeronautical Research Committee, R.&M. No. 1312, February 1930.

26. Glauert, H., "The Form of a Heavy Flexible Cable Used for Towing a Heavy Body below an Aeroplane," Great Britain Aeronautical Research Committee, R.&M. No. 1592, February 1934.

27. Bryant, L.W., Brown, W.S., and Sweeting, N.E., "Collected Researches on the Stability of Kites and Towed Gliders," Great Britain Aeronautical Research Council, R.&M. No. 2303, February 1942.

28. Mitchell, K., and Beach, C., "The Stability Derivatives of Glider Towing Cables, with a Method for Determining the Flying Conditions of the Glider," Great Britain Aeronautical Research Council, Report No. 6151, July 1942.

29. O'Hara, F., "Extension of Glider Tow Cable Theory to Elastic Cables Subject to Air Forces of a Generalized Form," Great Britain Aeronautical Research Council, R.&M. No. 2334, 1945.

30. Söhne, W., "Directional Stability of Towed Airplanes," NACA, TM No. 1401, January 1956.

31. Shanks, R.E., "Investigation of the Dynamic Stability and Controllability of a Towed Model of a Modified Halfcone Reentry Vehicle," NASA TN D-2517, February 1965.

32. Etkin, B., and Mackworth, J.C., "Aerodynamic Instability of Non-Lifting Bodies Towed Beneath an Aircraft," UTIA TN No. 65, Institute of Aerophysics, University of Toronto, January 1956.

33. Landweber, L., and Protter, M.H., "The Shape and Tension of a Light Flexible Cable in a Uniform Current," Journal of Applied Mechanics, Vol. 14, No. 2, June 1947, pp. 121-126.

34. Pode, L., "Tables for Computing the Equilibrium Configuration of a Flexible Cable in a Uniform Stream," David Taylor Model Basin, Report No. 687, March 1951.

35. Dominguez, R.F., "The Static and Dynamic Analysis of Discretely Represented Moorings and Cables by Numerical Means," Ph.D. Thesis, Oregon State University, Corvallis, Oregon, 1971.

36. Hicks, J.B., and Clark, L.B., "On the Dynamic Response of Buoy-Supported Cables and Pipes to Currents and Waves," Proceedings of the Offshore Technology Conference, Houston, Texas, Paper No. OTC 1556, April 1972.

37. Strandhagen, A.G., and Thomas, C.F., "Dynamics of Towed Underwater Vehicles, Navy Mine Defence Lab., Report No. 219, November 1963.

38. Morgan, B.J., "The Finite Element Method and Cable Dynamics," Proceedings of the Symposium on Ocean Engineering, University of Pennsylvania, Philadelphia, Paper No. 3C, November 1970.

39. Paul, B., and Soler, A.I., "Cable Dynamics and Optimum Towing Strategies for Submersibles," Marine Technology Society Journal, Vol. 6, No. 2, March-April 1972, pp. 34-42.

40. Phillips, W.H., "Theoretical Analysis of a Towed Cable," NACA TN No. 1796, January 1949.

41. Schram, J.W., "A Three Dimensional Analysis of a Towed System," Ph.D. Thesis, Rutgers University, New Brunswick, N.J., January 1968.

42. Huffman, R.R., and Genin, J., "The Dynamical Behaviour of an Extensible Flexible Cable in a Uniform Flow Field," Aeronautical Quarterly, Vol. 22, Part 2, May 1971, pp. 183-195.

43. Cannon, T.C., "A Three Dimensional Study of Towed Cable Dynamics," Ph.D. Thesis, Purdue University, Lafayette, Indiana, August 1970.

44. Flügge, W., Viscoelasticity, Blaisdell Publishing Company, Waltham, Massachusetts, 1967, pp. 32-50.

45. Bogoliubov, N.N., and Mitropolsky, Y.A., Asymptotic Methods in the Theory of Nonlinear Oscillations, Hindustan Publishing Corporation, India, 1961, p. 52.

46. Nayfeh, A.H., Perturbation Methods, John Wiley & Sons, New York, 1973, pp. 228-243.

47. Anderson, J.M., and King, W.W., "Vibration of a Cantilever Subjected to a Tensile Follower Force," AIAA Journal, Vol. 7, No. 4, April 1969, pp. 741-742.

48. Paidoussis, M.P., "Dynamics of Flexible Slender Cylinders in Axial Flow," Journal of Fluid Mechanics, Vol. 26, Part 4, 1966, pp. 717-736.

49. Lifshitz, J.M., and Kolsky, H., "Nonlinear Viscoelastic Behaviour of Polyethylene," International Journal of Solids and Structures, 1967, Vol. 3, pp. 383-397.

50. Findley, W.N., and Khosla, G., "An Equation for Tension Creep of Three Unfilled Thermoplastics," Society of Plastic Engineers Journal, 12, No. 12, December 1956, pp. 20-25.

51. Kalinnikov, A.E., "Creep and Aftereffect of PET Films Under Conditions of Uniaxial Stress," Mekhanika Polimerov, Vol. 1, No. 2, 1965, pp. 59-63.

52. Bolotin, V.V., Nonconservative Problems of the Theory of Elastic Stability, Pergamon Press, Oxford, England, 1963, p. 91.

53. Meirovitch, L., Analytical Methods in Vibrations, The Macmillan Co., New York, 1967, p. 49.

54. Wiegel, R.L., Oceanographical Engineering, Prentice-Hall, Englewood Cliffs, N.J., 1964, pp. 11-21.

APPENDIX I

STEADY STATE ORIENTATIONS OF THE ARRAY

In the steady state,

$$Q_{\psi 0} = (C_T/R)\sum_{i=1}^{3}\cos\theta_0\cos\psi_{i0}|\cos\theta_0\cos\psi_{i0}|\int_0^1(\xi\frac{\partial\eta_{i0}}{\partial\xi}-\eta_{i0})d\xi$$

$$+(C_N/R)\sum_{i=1}^{3}|(1-\cos^2\theta_0\cos^2\psi_{i0})^{1/2}|\int_0^1\xi[\cos\theta_0\sin\psi_{i0}+(1/R)\ *$$

$$\frac{\partial\eta_{i0}}{\partial\xi}\cos\theta_0\cos\psi_{i0}\{1+\cos^2\theta_0\sin^2\psi_{i0}/(1-\cos^2\theta_0\cos^2\psi_{i0})\}$$

$$-(1/R)\frac{\partial\zeta_{i0}}{\partial\xi}\cos\theta_0\cos\psi_{i0}\{\sin\theta_0\cos\theta_0\sin\psi_{i0}/(1-$$

$$-\cos^2\theta_0\cos^2\psi_{i0})\}]d\xi = 0 \quad , \qquad \text{(I.1a)}$$

$$Q_{\theta 0} = -(C_T/R)\sum_{i=1}^{3}\cos\theta_0\cos\psi_{i0}|\cos\theta_0\cos\psi_{i0}|\int_0^1(\xi\frac{\partial\zeta_{i0}}{\partial\xi}-\zeta_{i0})\cos\psi_{i0}d\xi$$

$$+(C_N/R)\sum_{i=1}^{3}|(1-\cos^2\theta_0\cos^2\psi_{i0})^{1/2}|\int_0^1[\xi\cos\psi_{i0}\{\sin\theta_0+(1/R)*$$

$$\frac{\partial\eta_{i0}}{\partial\xi}\cos\theta_0\cos\psi_{i0}(\sin\theta_0\cos\theta_0\sin\psi_{i0})/(1-\cos^2\theta_0\cos^2\psi_{i0})$$

$$-(1/R)\frac{\partial\zeta_{i0}}{\partial\xi}\cos\theta_0\cos\psi_{i0}(1+\sin^2\theta_0/(1-\cos^2\theta_0\cos^2\psi_{i0}))\}$$

$$-(1/R)\sin\psi_{i0}(\eta_{i0}\sin\theta_0+\zeta_{i0}\cos\theta_0\sin\psi_{i0})]d\xi = 0 \quad , \qquad \text{(I.1b)}$$

$$\frac{\partial^4 \eta_{i0}}{\partial \xi^4} - P\frac{\partial^2 \eta_{i0}}{\partial \xi^2} = (\rho_w V^2 L^4/2EI)[C_T \cos\theta_0 \cos\psi_{i0} |\cos\theta_0 \cos\psi_{i0}| (1/R) *$$

$$\frac{\partial \eta_{i0}}{\partial \xi} + C_N |(1-\cos^2\theta_0 \cos^2\psi_{i0})^{1/2}| \{\cos\theta_0 \sin\psi_{i0} + (1/R)\frac{\partial \eta_{i0}}{\partial \xi} \cos\theta_0 *$$

$$\cos\psi_{i0}(1+(\cos^2\theta_0 \sin^2\psi_{i0})/(1-\cos^2\theta_0\cos^2\psi_{i0})) - (1/R)\frac{\partial \zeta_{i0}}{\partial \xi} \cos\theta_0 *$$

$$\cos\psi_{i0}(\sin\theta_0 \cos\theta_0 \sin\psi_{i0})/(1-\cos^2\theta_0 \cos^2\psi_{i0})\}] , \qquad (I.1c)$$

$$\frac{\partial^4 \zeta_{i0}}{\partial \xi^4} - P\frac{\partial^2 \zeta_{i0}}{\partial \xi^2} = (\rho_w V^2 L^4/2EI)[C_T \cos\theta_0 \cos\psi_{i0} |\cos\theta_0 \cos\psi_{i0}| (1/R) *$$

$$\frac{\partial \zeta_{i0}}{\partial \xi} - C_N |(1-\cos^2\theta_0 \cos^2\psi_{i0})^{1/2}| \{\sin\theta_0 + (1/R)\frac{\partial \eta_{i0}}{\partial \xi} \cos\theta_0 \cos\psi_{i0} *$$

$$(\sin\theta_0 \cos\theta_0 \sin\psi_{i0})/(1-\cos^2\theta_0 \cos^2\psi_{i0}) - (1/R)\frac{\partial \zeta_{i0}}{\partial \xi} \cos\theta_0 \cos\psi_{i0} *$$

$$(1+\sin^2\theta_0/(1-\cos^2\theta_0 \cos^2\psi_{i0}))\}]. \qquad (I.1d)$$

Examination of the above equations yields

$$\psi_{i0} = I_i \quad \text{or} \quad I_i + \pi/3 \quad , \tag{I.2a}$$

$$\theta_0 = 0 \quad \text{or} \quad \pi/2 \quad . \tag{I.2b}$$

Only the orientation $\theta_0 = 0$ is of interest to us. Correspondingly,

$$\zeta_{i0} = 0 \quad , \tag{I.2c}$$

and η_{i0} satisfies the equation

$$\frac{\partial^4 \eta_{i0}}{\partial \xi^4} - P \frac{\partial^2 \eta_{i0}}{\partial \xi^2} = (\rho_w V^2 L^4/2EI)[A_i + B_i (1/R) \frac{\partial \eta_{i0}}{\partial \xi}] \quad , \tag{I.2d}$$

where

$$A_i = C_N |\sin\psi_{i0}| \sin\psi_{i0} \quad ,$$

and

$$B_i = \{C_T |\cos\psi_{i0}| + 2C_N |\sin\psi_{i0}|\} \cos\psi_{i0} \quad ,$$

with the boundary conditions

$$\eta_{i0}(0) = \frac{\partial \eta_{i0}}{\partial \xi}(0) = \frac{\partial^2 \eta_{i0}}{\partial \xi^2}(1) = \frac{\partial^3 \eta_{i0}}{\partial \xi^3}(1) = 0 \quad .$$

If the slope is not very large, the second term on the right hand side of (I.2d) may be neglected compared to the first, as the former is multiplied by $(1/R)$. The solution to (I.2d) can now be written as

$$\eta_{i0} = -(\rho_w V^2 L^4/2EI)C_N|\sin\psi_{i0}|\sin\psi_{i0}(1/P)[(1/P)\{\cosh\sqrt{P} -\cosh\sqrt{P}(1-\xi)\}-(\xi/\sqrt{P})\sinh\sqrt{P}+(\xi^2/2)] \quad . \tag{I.2d'}$$

If the slope is large, the second term on the right hand side cannot be neglected in Equation (I.2d) and the solution is obtained in the form

$$\frac{\partial\eta_{i0}}{\partial\xi} = \sum_{r=1}^{3} D_{ir}\exp(\alpha_{ir}\xi)-RA_i/B_i \quad , \tag{I.2e}$$

where $\alpha_{ir}(r=1,2,3)$ are the roots of the cubic equation

$$\alpha_{ir}^3-P\alpha_{ir}-(\rho_w V^2 L^4/2EI)(1/R)B_i = 0 \quad . \tag{I.2f}$$

The constants D_{ir} are evaluated using the last three boundary conditions. η_{i0} may be obtained by integrating (I.2e) with the help of the condition $\eta_{i0}(0) = 0$.

APPENDIX II

GENERALIZED FORCES

$$Q_\psi^* = Rr_1[C_T \sum_{i=1}^{3} |\cos\psi_{i0}^*| \cos\psi_{i0}^* \int_0^1 \xi\{\delta\psi+(1/R)\ \frac{\partial\delta\eta_i}{\partial\xi}\}d\xi + C_N \sum_{i=1}^{3} \int_0^1 |\sin\psi_{i0}^*|$$

$$[\{\delta\psi+(1/R)\ \frac{\partial\delta\eta_i}{\partial\xi}\}\{2\xi\cos\psi_{i0}^* - (1/R)(\xi\frac{\partial\eta_{i0}}{\partial\xi} - \eta_{i0})\sin\psi_{i0}\} + 20\xi\{\delta\beta_h'$$

$$+(L_c/2)\delta G_h'\}\cos\beta_{h0}^*\sin\psi_{i0}^* + 20\xi\{\delta\varepsilon_h' + (L_c/2)\delta k_h'\}\sin\beta_{h0}\cos\psi_{i0}^*$$

$$-(20/R_\ell)\xi^2\delta\psi' - (20/RR_\ell)\xi\delta\eta_i']d\xi]$$

$$Q_\theta^* = Rr_1[C_T \sum_{i=1}^{3} |\cos\psi_{i0}^*| \cos\psi_{i0}^* \int_0^1 \xi\cos\psi_{i0}\{\delta\theta\cos\psi_{i0} - (1/R)\ \frac{\partial\delta\zeta_i}{\partial\xi}\}d\xi$$

$$+C_N \sum_{i=1}^{3} \int_0^1 |\sin\psi_{i0}^*| \{\xi\cos\psi_{i0} - (1/R)\eta_{i0}\sin\psi_{i0}\}[\cos\psi_{i0}^*\{\delta\theta\cos\psi_{i0}^*$$

$$-(1/R)\ \frac{\partial\delta\zeta_i}{\partial\xi}\} + 10\{\delta\beta_h' + (L_c/2)\delta G_h'\}\sin\beta_{h0}^* - (10/R_\ell)\{\xi\cos\psi_{i0}$$

$$-(1/R)\eta_{i0}\sin\psi_{i0}\} + (10/RR_\ell)\delta\zeta_i']d\xi]$$

$$Q^{*}_{\beta h} = Rr_1[-r_{hd}[\{(\cos\beta_{h0}-G_{h0}L_c\sin\beta_{h0}/2)+r_{ch}(\cos\beta_{h0}/2$$

$$-G_{h0}L_c\sin\beta_{h0}/3)\}\delta\beta_h+\cos\beta_{h0}(1+2r_{ch}/3)(L_c/2)\delta G_h]$$

$$+C_T R_\ell \sum_{i=1}^{3} |\cos\psi^{*}_{i0}|[3\cos\beta^{*}_{h0}\sin\psi^{*}_{i0}\cos\psi^{*}_{i0}\{\delta\psi+(1/R)$$

$$\frac{\partial\delta\eta_i}{\partial\xi}\}-\sin\beta^{*}_{h0}\cos\psi^{*}_{i0}\{\delta\theta\cos\psi^{*}_{i0}-(1/R)\frac{\partial\delta\zeta_i}{\partial\xi}\}+10\cos\beta^{*}_{h0}\cos\psi^{*}_{i0}$$

$$\{(\delta\beta_h'+\delta G_h'L_c/2)\cos\psi^{*}_{i0}\cos\beta^{*}_{h0}+(\delta\varepsilon_h'+\delta k_h'L_c/2)\sin\psi^{*}_{i0}\sin\beta_{h0}$$

$$-(1/RR_\ell)\delta\psi'(\xi\frac{\partial\eta_{i0}}{\partial\xi}-\eta_{i0})\}]d\xi+C_N R_\ell \sum_{i=1}^{3}\int_0^1 |\sin\psi^{*}_{i0}|[3\cos\beta^{*}_{h0}$$

$$\sin\psi^{*}_{i0}\cos\psi^{*}_{i0}\{\delta\psi+(1/R)\ \frac{\partial\delta\eta_i}{\partial\xi}\}-\sin\beta^{*}_{h0}\cos\psi^{*}_{i0}\{\delta\theta\cos\psi^{*}_{i0}$$

$$-(1/R)\frac{\partial\delta\zeta_i}{\partial\xi}\}-10\{\delta\beta_h'+(L_c/2)\delta G_h'\}(2\cos^2\beta^{*}_{h0}\sin^2\psi_{i0}+\sin^2\beta^{*}_{h0})$$

$$+20\sin\beta_{h0}\cos\beta^{*}_{h0}\sin\psi^{*}_{i0}\cos\psi^{*}_{i0}\{\delta\varepsilon_h'+(L_c/2)\delta k_h'\}-(20/R_\ell)\cos\beta^{*}_{h0}\sin\psi^{*}_{i0}$$

$$\{\xi\delta\psi'+(1/R)\delta\eta_i'\}+(10/R_\ell)\sin\beta^{*}_{h0}\{\delta\theta'(\xi\cos\psi_{i0}-\eta_{i0}\sin\psi_{i0}/R)$$

$$-(1/R)\delta\zeta_i'\}]d\,\xi-C_{Tc}R_d R_\ell^2|\sin\beta_{h0}|\sin\beta_{h0}(1/2)(\delta\beta_h+\delta G_h/3)$$

$$-C_{Nc}R_d R_\ell^2[\{\sin\beta_{h0}\cos\beta_{h0}-G_{h0}(L_c/6)(3\sin^2\alpha_{h0}-1)\}\delta\beta_h$$

$$+\delta G_h(L_c/3)\sin\beta_{h0}\cos\beta_{h0}-(20/3)\{(\cos\beta_{h0}-G_{h0}L_c\sin\beta_{h0}/4)\delta\beta_h'$$

$$+(5\cos\beta_{h0}/4-7G_{h0}L_c\sin\beta_{h0}/20)\delta G_h'(L_c/2)\}]]$$

$$Q_{Gh}^* = Rr_1(L_c/2)R_\ell[C_T\sum_{i=1}^{3}\int_0^1|\cos\psi_{i0}^*|[3\cos\beta_{h0}\sin\psi_{i0}^*\cos\psi_{i0}^*\{\delta\psi+(1/R)\frac{\partial\delta\eta_i}{\partial\xi}\}$$

$$-\sin\beta_{h0}\cos\psi_{i0}^*\{\delta\theta\cos\psi_{i0}^*-(1/R)\frac{\partial\delta\zeta_i}{\partial\xi}\}+10\cos\psi_{i0}^*\{\cos\beta_{h0}\cos\psi_{i0}^*(\delta\beta_h'\cos\beta_{h0}^*$$

$$+\delta G_h'\cos\beta_{h0}L_c/2)+\sin\beta_{h0}\cos\beta_{h0}\sin\psi_{i0}^*(\delta\varepsilon_h'+\delta k_h'L_c/2)-(1/RR_\ell)(\xi\frac{\partial\eta_{i0}}{\partial\xi}$$

$$-\eta_{i0})\cos\beta_{h0}\}]d\xi+C_N\sum_{i=1}^{3}\int_0^1|\sin\psi_{i0}^*|[3\cos\beta_{h0}\sin\psi_{i0}^*\cos\psi_{i0}^*\{\delta\psi+(1/R)\frac{\partial\delta\eta_i}{\partial\xi}\}$$

$$-\sin\beta_{h0}\cos\psi_{i0}^*\{\delta\theta\cos\psi_{i0}^*-(1/R)\frac{\partial\delta\zeta_i}{\partial\xi}\}-10\{(2\cos\beta_{h0}^*\cos\beta_{h0}\sin^2\psi_{i0}^*$$

$$+\sin\beta_{h0}^*\sin\beta_{h0})\delta\beta_h'+(2\cos^2\beta_{h0}\sin^2\psi_{i0}^*+\sin^2\beta_{h0})\delta G_h'(L_c/2)\}$$

$$+20\sin\beta_{h0}\cos\beta_{h0}\sin\psi_{i0}^*\cos\psi_{i0}^*\{\delta\varepsilon_h'+(L_c/2)\delta k_h'\}-(20/R_\ell)\cos\beta_{h0}$$

$$\sin\psi_{i0}^*(\xi\delta\psi'+\delta\eta_i'/R)+(10/R_\ell)\sin\beta_{h0}\{\delta\theta'(\xi\cos\psi_{i0}-\eta_{i0}\sin\psi_{i0}/R)$$

$$-(1/R)\delta\zeta_i'\}]d\xi - C_{Tc}R_dR_\ell|\sin\beta_{h0}|\sin\beta_{h0}(2\delta\beta_h/3+\delta G_hL_c/4)$$

$$-C_{Nc}R_dR_\ell[\{(4/3)\sin\beta_{h0}\cos\beta_{h0}+(L_c/4)G_{h0}(5\cos^2\beta_{h0}-2)\}\delta\beta_h$$

$$-\sin\beta_{h0}\cos\beta_{h0}\delta G_h(L_c/2)-(20/3)\{(5\cos\beta_{h0}/4-7G_{h0}L_c\sin\beta_{h0}/20)\delta\beta_h'$$

$$+(8\cos\beta_{h0}/5-G_{h0}L_c\sin\beta_{h0}/2)\delta G_h'(L_c/2)\}]]$$

$$Q_{\varepsilon h}^* = Rr_1R_\ell[-C_T\sum_{i=1}^{3}\int_0^1 \mathrm{sgn}(\cos\psi_{i0}^*)[(\cos^2\psi_{i0}^*-\sin^2\psi_{i0}^*)\{\delta\psi+(1/R)\frac{\partial\delta\eta_i}{\partial\xi}\}$$

$$-10\sin\psi_{i0}^*\{\cos\beta_{h0}^*\cos\psi_{i0}^*(\delta\beta_h'+\delta G_h'L_c/2)+\sin\beta_{h0}\sin\psi_{i0}^*(\delta\varepsilon_h'$$

$$+\delta k_h'L_c/2)-(1/RR_\ell)\delta\psi'(\xi\frac{\partial\eta_{i0}}{\partial\xi}-\eta_{i0})\}]d\xi - C_N\sum_{i=1}^{3}\int_0^1|\sin\psi_{i0}^*|[(3\cos^2\psi_{i0}^*$$

$$-1)\{\delta\psi+(1/R)\frac{\partial\delta\eta_i}{\partial\xi}\}-20\cos\psi_{i0}^*\{\cos\beta_{h0}^*\sin\psi_{i0}^*(\delta\beta_h'+\delta G_h'L_c/2)$$

$$-\sin\beta_{h0}\cos\psi_{i0}^*(\delta\varepsilon_h'+\delta k_h'L_c/2)+(1/R_\ell)(\xi\delta\psi'+\delta\eta_i'/R)\}]d\xi$$

$$-C_{Tc}R_dR_\ell\sin^3\beta_{h0}(1/2)(\delta\varepsilon_h+\delta k_hL_c/3)-C_{Nc}R_dR_\ell\cos\beta_{h0}\sin\beta_{h0}$$

$$\{(1/2)\sin\beta_{h0}(\delta\varepsilon_h+\delta k_h L_c/3)-(10/3)(\delta\varepsilon_h'+5\delta k_h' L_c/8)\}]$$

$$Q^*_{kh} = Q^*_{\varepsilon h}(L_c/2)+Rr_1(L_c/2)R_d R_\ell^2[C_{Tc}|\sin\beta_{h0}|\sin^2\beta_{h0}(1/6)(\delta\varepsilon_h$$

$$-\delta k_h L_c/2)+C_{Nc}\sin\beta_{h0}\cos\beta_{h0}\{-(1/6)(\delta\varepsilon_h+\delta k_h L_c/2)-(10/12)(\delta\varepsilon_h'$$

$$+7\delta k_h' L_c/10)\}]$$

$$Q^*_{\eta i} = Rr_1[-(2EI/\rho_w V^2 L^4)(\frac{\partial^4\delta\eta_i}{\partial\xi^4} -P \frac{\partial^2\delta\eta_i}{\partial\xi^2})+C_T|\cos\psi_{i0}|\cos\psi_{i0}\{\delta\psi$$

$$+(1/R) \frac{\partial\delta\eta_i}{\partial\xi}\}+C_N|\sin\psi^*_{i0}|[\{2\cos\psi_{i0}-(3/R)\sin\psi_{i0} \frac{\partial\eta_{i0}}{\partial\xi}\}\{\delta\psi$$

$$+(1/R) \frac{\partial\delta\eta_i}{\partial\xi}\}-20\{\sin\psi^*_{i0}(\delta\beta_h'+\delta G_h' L_c/2)\cos\beta^*_{h0}-\cos\psi^*_{i0}(\delta\varepsilon_h'+\delta k_h' L_c/2)$$

$$\sin\beta_{h0}\}-(20/R_\ell)\{\xi\delta\psi'+(1/R)\delta\eta_i'\}]]$$

$$Q^*_{\zeta i} = Rr_1[-(2EI/\rho_w V^2 L^4)(\frac{\partial^4\delta\zeta_i}{\partial\xi^4} -P \frac{\partial^2\delta\zeta_i}{\partial\xi^2})-C_T|\cos\psi_{i0}|\cos\psi_{i0}\{\delta\theta$$

$$\cos\psi_{i0}-(1/R)\ \frac{\partial\delta\zeta_i}{\partial\xi}\}-C_N|\sin\psi^*_{i0}|[\cos\psi^*_{i0}\{\delta\theta\cos\psi^*_{i0}-(1/R)\ \frac{\partial\delta\zeta_i}{\partial\xi}\}$$

$$+10\sin\beta^*_{h0}(\delta\beta'_h+\delta G'_h L_c/2)-(10/R_\ell)\{\delta\theta'(\xi\cos\psi_{i0}-\eta_{i0}\sin\psi_{i0}/R)$$

$$-(1/R)\delta\zeta'_i\}]] \quad ,$$

where

$$\psi^*_{i0} = \cos^{-1}\{\cos\psi_{i0}-(1/R)\ \frac{\partial\eta_{i0}}{\partial\xi}\ \sin\psi_{i0}\} \quad ,$$

and

$$\beta^*_{h0} = \cos^{-1}\{\cos\beta_{h0}-(G_{h0}L_c/2)\sin\beta_{h0}\} \quad .$$